이학박사 학위논문

Mixed-Reference Spin-Flip Time-Dependent Density Functional Theory (MRSF-TDDFT): An accurate and efficient method of calculating electronic excited states for studying light-energy conversion mechanisms

혼합기준 스핀젖힘 시간의존 밀도범함수 이론:
빛 에너지 전환 메커니즘 연구를 위한 정확하고
효율적인 전자 전이상태 계산 방법

2019년 8월

서울대학교 대학원
화 학 부
이 승 훈

Mixed-Reference Spin-Flip Time-Dependent Density Functional Theory (MRSF-TDDFT): An accurate and efficient method of calculating electronic excited states for studying light-energy conversion mechanisms

지도 교수 이 상 엽

이 논문을 이학박사 학위논문으로 제출함

2019년 8월

서울대학교 대학원

화학부 물리화학전공

이 승 훈

이승훈의 이학박사 학위논문을 인준함

2019년 8월

위 원 장 _____ (인)

부위원장 _____ (인)

위 원 _____ (인)

위 원 _____ (인)

위 원 _____ (인)

감사의 글

어느 새 5년 반의 박사과정을 마치고 학위 논문을 제출하게 되었습니다. 많은 분들의 도움 덕분에 즐겁게 연구하며 졸업할 수 있었습니다. 학위 논문을 마치며 감사의 말씀을 전합니다.

한 없이 부족했던 제가 한걸음씩 성장해 나갈 수 있도록 인내심을 갖고 지도해 주시고, 항상 저를 믿고 아낌없이 지원 해주신 이상엽 교수님, 최철호 교수님께 진심으로 감사 인사 드립니다.
Many thanks to Dr. Michael and Dr. Hiroya for your kind help.
또한 따뜻한 격려와 조언을 해주신 석차옥 교수님, 정연준 교수님 그리고 성재영 교수님께도 감사 드립니다.

박사과정 동안 얻은 가장 큰 선물은 사랑하는 은지와 결혼한 것과 세상에서 가장 귀여운 아들 상백이가 태어난 것 입니다. 덕분에 너무 행복한 나날을 지낼 수 있었습니다. 감사합니다.
말로 표현을 많이 못해 드렸지만, 엄마 아빠 장모님 장인어른 항상 너무 감사하고 사랑합니다.

ABSTRACT

The mixed-reference spin-flip time-dependent density functional theory (MRSF-TDDFT) is proposed, which is derived from linear response formalism for the time-dependent Kohn-Sham equation by the use of mixed reference. Linear response from the mixed reference, which combines M_S = + 1 and −1 components of triplet state, generates additional configurations in the realm of TDDFT. Resultantly, MRSF-TDDFT eliminates the erroneous spin-contamination of the SF-TDDFT. Analytic energy gradients of the response states with respect to nuclear coordinates are also derived and implemented. The computational overhead of singlet or triplet states for MRSF-TDDFT is nearly identical to that of SF-TDDFT. The resulting MRSF-TDDFT computational scheme has several advantages before the conventional SF-TDDFT. Linear-response equations for the singlet and triplet responses are clearly separated. This considerably simplifies the identification of the excited states, especially in the ``black-box'' type applications, such as the automatic geometry optimization, reaction path following, or molecular dynamics simulations of the targeted states. Accuracy of MRSF-TDDFT has been tested and verified in various ways including vertical-excitation energy, singlet-triplet energy gap, adiabatic-excitation energy, optimized structure, minimum energy conical intersection, nonadiabatic coupling term, and

nonadiabatic molecular dynamic simulation. Therefore, it is highly expected that the MRSF-TDDFT has advantages over SF-TDDFT in terms of both practicality and accuracy.

Keyword: Photochemistry, Spin-flip time-dependent density functional theory, Spin contamination problem, Conical intersection, Nonadiabatic coupling matrix term, Nonadiabatic molecular dynamics.

Student Number: 2014-21231

TABLE OF CONTENTS

LIST OF FIGURES

LIST OF TABLES

INTRODUCTION

Proper and efficient descriptions of electronic excited states have become more important than ever, as the theoretical studies of emerging sciences, such as photovoltaics,[1, 2] molecular rotor[3] are heavily dependent on them. A widely used methodology for studying molecular excited states is the linear-response time-dependent density functional theory (LR-TDDFT).[4-10] It is based on the time-dependent Kohn-Sham (TD-KS) equation with the linear-response formalism using a singlet ground state as a reference state. In this approach, a fictitious noninteracting system is introduced whose density is equal to that of the real interacting system.[11, 12] A wave function of the noninteracting system is assumed to be described by a single Slater determinant, which is referred to as an idempotency of reduced density matrix in terms of the density matrix.[13, 14]

Contrasting to its popularity, well-known failures of this methodology exist, in describing the energy of long-range charge transfer excitations,[15-19] excited states with substantial double excitation character,[20-23] excited states of molecules undergoing bond breaking,[23-25] and real and avoided crossings between the ground and excited states of molecules.[26-29] Some of these

drawbacks, in particular, the incorrect description of the S_1/S_0 conical intersections and the poor description of multi-reference electronic states, can be corrected to some extent by the spin-flip (SF)-TDDFT,[30-32] which employs an Ms = +1 component of triplet ground state *e.g.*, $|\alpha\alpha\rangle$, as a reference state instead of the closed-shell reference of the LR-TDDFT. However, the use of only one component of the degenerate triplet state leads to considerable spin contamination of the resulting excited electronic states, except in a few low-lying excited states.[33] The spin contamination of SF-TDDFT is different from that of the unrestricted Hatree-Fock (UHF) wavefunction come from orbital asymmetries. On the other hand, in SF-TDDFT, the main source of spin contamination is due to spin incompleteness of an excited set of configurations. Therefore, a key solution for this problem is to expand the response space of SF-TDDFT such that it can include the missing configurations.

Within the same contexts, several approaches have been developed to tackle the spin-contamination problem of the SF configuration interaction with single excitations (CIS),[33-37] which is a wave function version of SF-TDDFT. However, unlike SF-CIS, a considerable challenge remains with respect to TDDFT when going beyond the adiabatic approximation to account for more than single

excitations.[38, 39] Because of this difficulty, only a few methods have been developed to address the spin-contamination problem of the SF-TDDFT. One means of adding more responses is to use a higher excitation operator.[38] Without the TD-KS equation being utilized, on the other hand, tensor equation-of-motion (TEOM) approaches achieved considerable progress, yielding a series of SA-SF-DFT methodologies.[36, 40, 41] These approaches can produce correct spin eigenstates by applying tensor operators to a tensor reference. However, the matrix elements of TEOM are evaluated using the Wigner-Eckart theorem, which is not satisfied by the approximate density functionals. Thus, the SA-SF-DFT formalism[36] requires an *a posteriori* DFT correction to the SA-SF-CIS equations. Due to the complexity of TEOM, the analytic energy gradient for the SA-SF-DFT has yet to be derived.

Rather than using a high excitation operator[38] or using a tensor operator with a tensor reference,[36] a means of expanding the response space by linear response from more than one reference[42] is shown in this thesis. In *THEORETICAL BACKGROUND* section, a brief review of derivation for linear response equation from time-dependent Kohn-Sham equation is described. In addition, SF-TDDFT is introduced and its advantages

and disadvantages are summarized. In *MIXED-REFERENCE SPIN-FLIP TDDFT* section, mixed-reference spin-flip (MRSF)-TDDFT is proposed which eliminate spin-contamination problem of SF-TDDFT while maintaining its advantages. Linear response equation of MRSF-TDDFT is derived and *a posteriori* coupling, which is referred as spin-pairing coupling, is introduced. In *ANALYTIC ENERGY GRADIENT OF MIXED-REFERENCE SPIN-FLIP TDDFT* section, analytic energy gradient is derived by the Lagrangian of MRSF-TDDFT. In *NUMERICAL RESULTS* section, accuracy of MRSF-TDDFT has been tested and verified in various ways including vertical-excitation energy, adiabatic-excitation energy, optimized structure, minimum energy conical intersection, nonadiabatic coupling term, and nonadiabatic molecular dynamic simulation.

It is noted that this thesis reorganizes the contents of three papers published in international journals and those of papers in preparation.

MIXED-REFERENCE SPIN-FLIP TDDFT

S. Lee, M. Filatov, S. Lee, C.H. Choi, J. Chem. Phys. **149**, 104101 (2018)

ANALYTIC ENERGY GRADIENT OF MIXED-REFERENCE SPIN-FLIP TDDFT

S. Lee, E.E. Kim, H. Nakata, S. Lee, C.H. Choi, J. Chem. Phys. **150**, 184111 (2019)

NUMERICAL RESULTS

1. Vertical excitation energy

S. Lee, M. Filatov, S. Lee, C.H. Choi, J. Chem. Phys. **149**, 104101 (2018)

Y. Horbatenko and S. Lee, M. Filatov, C.H. Choi submitted for publication

2. Singlet-triplet energy gap

Y. Horbatenko and S. Lee, M. Filatov, C.H. Choi submitted for publication

3. Geometry-optimization structure

S. Lee, E.E. Kim, H. Nakata, S. Lee, C.H. Choi, J. Chem. Phys. **150**, 184111 (2019)

3. Adiabatic excitation energy

S. Lee, E.E. Kim, H. Nakata, S. Lee, C.H. Choi, J. Chem. Phys. **150**, 184111 (2019)

4. Conical intersection

S. Lee, E.E. Kim, H. Nakata, S. Lee, C.H. Choi, J. Chem. Phys. **150**, 184111 (2019)

S. Lee and S. Shostak, M. Filatov, C.H. Choi, submitted for publication

5. Non-adiabatic coupling matrix elements

S. Lee, E.E. Kim, S. Lee, C.H. Choi, J. Chem. Theory Comput. **15**, 882 (2019)

6. Non-adiabatic molecular dynamics

S. Lee, E.E. Kim, M. Filatov, S. Lee, C.H. Choi, in prepararation

THEORETICAL BACKGROUND

1. Idempotency of reduced density matrix

The essence of time-dependent density functional theory (TDDFT) is the determination of the exact density in a time domain or in a frequency domain from which any many-particle observable can be obtained.[4-10] In this paper we shall only consider the density of electrons. Based on the Runge-Gross theorem, the fictitious non-interacting Kohn-Sham (KS) system is defined.[11, 12] In this system, there is no interaction between electrons but all potentials are described as one-particle operators. An one-electron wave function of non-interacting KS system, $\left|\psi_i^{\sigma_i}(t,x)\right\rangle$, is referred as KS molecular orbital (MO). The i and σ_i stand for index of the spatial part and that of spin part for the ith occupied KS MO, respectively, and x denotes both position and spin of the electron, $x=(r,\sigma)$. A many-electron wave function of the non-interacting system, $\left|\Psi[\rho](t)\right\rangle$, is usually restricted to be a normalized single Slater determinant. Then, the reduced density matrix (RDM) of the $\left|\Psi[\rho](t)\right\rangle$ can be represented as

$$\rho(t,x,x')=\sum_{i\sigma_i}^{\text{occ}}\left|\psi_i^{\sigma_i}(t,x)\right\rangle\left\langle\psi_i^{\sigma_i}(t,x')\right|, \qquad (1)$$

where the summation index of $i\sigma_i$ denotes a summation over occupied MOs. It can be rewritten with the time-independent KS MO, $\left|\phi_p^{\sigma_p}(x)\right\rangle$, (which is the solution of the usual time-independent KS equation) as

$$\rho(t,x,x') = \sum_{p\sigma_p q\sigma_q} P_{p\sigma_p q\sigma_q}(t)\left|\phi_p^{\sigma_p}(x)\right\rangle\left\langle\phi_q^{\sigma_q}(x')\right| \tag{2}$$

where summation indices of $p\sigma_p$ and $q\sigma_q$ represent summations over whole MOs, and $P_{p\sigma_p q\sigma_q}(t)$ is the discrete representation of the RDM; denoted as the density matrix, in the following. The diagonal part of the RDM is the density of the non-interacting system,

$$\rho(t,x) = \rho(t,x,x), \tag{3}$$

which is assumed to be equal to the density of the corresponding real system. In this paper, we shall only consider a case of systems consisting of even-number ($2n$) electrons,

$$\mathrm{Tr}\rho(t,x,x) = 2n. \tag{4}$$

Due to the restriction of single Slater determinant of $\left|\Psi[\rho](t)\right\rangle$, the RDM is idempotent,

$$\rho(t,x,x') = \int \rho(t,x,x'')\rho(t,x'',x')dx'', \tag{5}$$

which can be rewritten for the density matrix as

$$P_{p\sigma_p q\sigma_q}(t) = \sum_{t\sigma_t} P_{p\sigma_p t\sigma_t}(t)P_{t\sigma_t q\sigma_q}(t), \qquad \forall p\sigma_p, q\sigma_q. \tag{6}$$

2. Time-dependent Kohn-Sham equation

The TD density can be determined by the TD-KS equation which will be discussed in this subsection. First, let us consider the Dirac action:

$$A[\rho] = \int_0^{t_2} \left\langle \Psi[\rho](t) \middle| i\frac{\partial}{\partial t} - H(t) \middle| \Psi[\rho](t) \right\rangle dt. \tag{7}$$

The stationary action principle with respect to the KS MO, $\delta A[\rho] \Big/ \delta \left\langle \psi_i^{\sigma_i}(t,x) \right| = 0$, leads to the TD-KS equations,[43]

$$i\frac{\partial}{\partial t}\left| \psi_i^{\sigma_i}(t,x) \right\rangle = F[\rho(t)] \left| \psi_i^{\sigma_i}(t,x) \right\rangle, \qquad i\sigma_i \in \text{occupied MO.} \tag{8}$$

In terms of the RDM, the TD-KS equation can be rewritten as

$$i\frac{\partial}{\partial t}\rho = F\rho - \rho F, \tag{9}$$

which become

$$i\frac{\partial}{\partial t} P_{p\sigma_p q\sigma_q} = \sum_{t\sigma_t} \left(F_{p\sigma_p t\sigma_t} P_{t\sigma_t q\sigma_q} - P_{p\sigma_p t\sigma_t} F_{t\sigma_t q\sigma_q} \right), \qquad p\sigma_p, q\sigma_q \in \text{whole MO.} \tag{10}$$

where

$$F_{p\sigma_p q\sigma_q} = \int \phi_p^{\sigma_p *}(x) \left(-\frac{1}{2}\nabla^2 - \sum_A \frac{Z_A}{|r - R_A|} + \int \frac{\rho(t,x')}{|r' - r|} dx' + \frac{\delta A^{XC}[\rho]}{\delta\rho(t,x)} \right) \phi_q^{\sigma_q}(x) dx. \tag{11}$$

Within the adiabatic approximation, the exchange-correlation (XC) part A^{XC} of the action functional is replaced by the XC functional of time-independent DFT evaluated with the density ρ_t at time t, $\delta A^{XC}[\rho] / \delta\rho(t,x) \cong \delta E^{XC}[\rho_t] / \delta\rho_t(x)$. In the case of approximate hybrid XC

functionals, the Fock matrix, $F_{p\sigma_p q\sigma_q}$, becomes

$$
\begin{aligned}
F_{p\sigma_p q\sigma_q} = & \int \phi_p^{\sigma_p *}(x)\left(-\frac{1}{2}\nabla^2 - \sum_A \frac{Z_A}{|r-R_A|}\right)\phi_q^{\sigma_q}(x)dx \\
& + (1-c_H)\int \phi_p^{\sigma_p *}(x)\frac{\delta E^{XC}[\rho_t]}{\delta \rho_t(x)}\phi_q^{\sigma_q}(x)dx \\
& + \sum_{r\sigma_r s\sigma_s} P_{r\sigma_r s\sigma_s}(t)\int\int \phi_p^{\sigma_p *}(x)\phi_s^{\sigma_s *}(x')\frac{(1-c_H\hat{P}(x,x'))}{|r'-r|}\phi_r^{\sigma_r}(x')\phi_q^{\sigma_q}(x)dxdx',
\end{aligned}
\tag{12}
$$

where $\hat{P}(x,x')$ is the permutation (exchange) operator and c_H is the mixing coefficient for the exact (Hartree-Fock, HF) exchange; c_H = 0 or 1 recovers the pure DFT or pure HF limits, respectively.

3. Linear-response theory

A way to solve the density-matrix formulation of TD-KS equation in Eq. (10) within linear-response formalism is suggested by using the idempotency of RDM in Eq. (6).[13] In this subsection, a review of the derivation of linear-response equation is presented starting from the Volterra expansion.

3.1 Volterra expansion

Suppose a time-dependent one-electron external perturbation, *e.g.*, a time-dependent electric field, with a frequency Ω and a strength λ

$$v^{\text{ext}}_{p\sigma_p q\sigma_q}(t) = \lambda h_{p\sigma_p q\sigma_q} e^{-i\Omega t} + \text{c.c.} \tag{13}$$

is applied to a reference system at time 0, whose density can be determined by the usual time-independent DFT. Here, c.c. denotes complex conjugate of the preceding term. Then, the density matrix, $P_{p\sigma_p q\sigma_q}(t)$, and the Fock matrix, $F_{p\sigma_p q\sigma_q}(t)$, can be expanded in powers of λ as

$$P_{p\sigma_p q\sigma_q}(t) = P^{(0)}_{p\sigma_p q\sigma_q} + \lambda P^{(1)}_{p\sigma_p q\sigma_q}(t) + O(\lambda^2), \tag{14}$$

$$F_{p\sigma_p q\sigma_q}(t) = F^{(0)}_{p\sigma_p q\sigma_q} + \lambda F^{(1)}_{p\sigma_p q\sigma_q}(t) + O(\lambda^2). \tag{15}$$

If the reference system is described by a single Slater determinant, the zeroth-order density and Fock matrices are given in

$$P^{(0)}_{p\sigma_p q\sigma_q} = \begin{cases} \delta_{pq}\delta_{\sigma_p\sigma_q}, & \text{for } p\sigma_p, q\sigma_q \in \text{occupied MO}, \\ \text{otherwise, } 0 \end{cases} \tag{16}$$

$$\begin{aligned} F^{(0)}_{p\sigma_p q\sigma_q} &= \int \phi_p^{\sigma_p *}(x)\left(-\frac{1}{2}\nabla^2 - \sum_A \frac{Z_A}{|r-R_A|}\right)\phi_q^{\sigma_q}(x)dx \\ &+(1-c_H)\int \phi_p^{\sigma_p *}(x)\frac{\delta E^{XC}[\rho_0]}{\delta\rho_0(x)}\phi_q^{\sigma_q}(x)dx \\ &+\sum_{i\sigma_i}^{\text{occ}}\int\int \phi_p^{\sigma_p *}(x)\phi_i^{\sigma_i *}(x')\frac{(1-c_H\hat{P}(x,x'))}{|r'-r|}\phi_i^{\sigma_i}(x')\phi_q^{\sigma_q}(x)dxdx', \end{aligned} \tag{17}$$

The first-order density and Fock matrices can be represented by

$$P^{(1)}_{p\sigma_p q\sigma_q}(t) = d_{p\sigma_p q\sigma_q} e^{-i\Omega t} + \text{c.c.}, \tag{18}$$

$$F^{(1)}_{p\sigma_p q\sigma_q}(t) = v^{\text{ext}}_{p\sigma_p q\sigma_q}(t) + \sum_{r\sigma_r s\sigma_s} \frac{\partial F_{p\sigma_p q\sigma_q}}{\partial P_{r\sigma_r s\sigma_s}} P^{(1)}_{r\sigma_r s\sigma_s}(t). \tag{19}$$

The matrix, $d_{p\sigma_p q\sigma_q}$ in Eq. (18), represent amplitudes of linear

response of density. The first and the second terms of Eq. (19) are the external perturbation potential and the response of the Fock matrix to the density variation, respectively.

3.2 Connection between linear response of density and one-electron excitation

Substituting expansion of density matrix of Eq. (14) into the idempotency relation of Eq. (6) yields the idempotency relations for the zeroth- and first-order density matrices, respectively,

$$\sum_{t\sigma_t} P^{(0)}_{p\sigma_p t\sigma_t} P^{(0)}_{t\sigma_t q\sigma_q} = P^{(0)}_{p\sigma_p q\sigma_q}, \tag{20}$$

$$\sum_{t\sigma_t} \left(P^{(1)}_{p\sigma_p t\sigma_t} P^{(0)}_{t\sigma_t q\sigma_q} + P^{(0)}_{p\sigma_p t\sigma_t} P^{(1)}_{t\sigma_t q\sigma_q} \right) = P^{(1)}_{p\sigma_p q\sigma_q}, \qquad \forall p\sigma_p, q\sigma_q. \tag{21}$$

The former relation of Eq. (20) satisfied with the condition in Eq. (16) enable to define projection matrices onto the subspace of the occupied MOs, $P^{(0)}_{i\sigma_i i\sigma_i}$, and onto the unoccupied MOs, $\delta_{a\sigma_a a\sigma_a} - P^{(0)}_{a\sigma_a a\sigma_a}$. The orbital index convention used in this section is *i, j* for occupied MOs, *a, b* for virtual MOs, *p, q, r, s, t* for MOs in general.

Meanwhile, substituting the first-order density matrix of Eq. (18) into the first-order idempotency relation of Eq. (21) yields

$$\sum_{t\sigma_t} \left(d_{p\sigma_p t\sigma_t} P^{(0)}_{t\sigma_t q\sigma_q} + P^{(0)}_{p\sigma_p t\sigma_t} d_{t\sigma_t q\sigma_q} \right) = d_{p\sigma_p q\sigma_q}, \tag{22}$$

from which the amplitude matrix $d_{p\sigma_p q\sigma_q}$ can be represented as

$$d_{p\sigma_p q\sigma_q} = X_{p\sigma_p q\sigma_q} + Y_{p\sigma_p q\sigma_q}, \tag{23}$$

where

$$X_{p\sigma_p q\sigma_q} = \sum_{r\sigma_r s\sigma_s} (\delta_{p\sigma_p r\sigma_r} - P^{(0)}_{p\sigma_p r\sigma_r}) M_{r\sigma_r s\sigma_s} P^{(0)}_{s\sigma_s q\sigma_q}, \tag{24}$$

$$Y_{p\sigma_p q\sigma_q} = \sum_{r\sigma_r s\sigma_s} P^{(0)}_{p\sigma_p r\sigma_r} M_{r\sigma_r s\sigma_s} (\delta_{s\sigma_s q\sigma_q} - P^{(0)}_{s\sigma_s q\sigma_q}). \tag{25}$$

Here $M_{r\sigma_r s\sigma_s}$ is an arbitrary matrix. $X_{p\sigma_p q\sigma_q}$ has non-zero elements between the unoccupied $p\sigma_p$ and occupied $q\sigma_q$ MOs and corresponds to one-electron excitations, whereas the matrix $Y_{p\sigma_p q\sigma_q}$ has non-zero elements for the occupied $p\sigma_p$ and unoccupied $q\sigma_q$ MOs and corresponds to one-electron de-excitations. It is emphasized that the first-order density matrix can be represented in terms of MOs of reference system, and these can be interpreted as one-electron excitation and de-excitation from the Eqs. (24) and (25).

In this paper we shall use Tamm-Dancoff approximation (TDA)[44, 45] in which the excitation amplitude, $X_{p\sigma_p q\sigma_q}$, is only considered and the de-excitation amplitude $Y_{p\sigma_p q\sigma_q}$ is ignored.

3.3 Linear response equation

Substituting expansion of density and Fock matrices of Eqs. (14) and (15) into the TD-KS equation of Eq. (10) yields equation of motions for the *n*th-order density matrix. These for the zeroth- and the first-order density matrix are given by

$$0 = \sum_{t\sigma_t} \left(F^{(0)}_{p\sigma_p t\sigma_t} P^{(0)}_{t\sigma_t q\sigma_q} - P^{(0)}_{p\sigma_p t\sigma_t} F^{(0)}_{t\sigma_t q\sigma_q} \right), \tag{26}$$

$$i\frac{\partial}{\partial t} P^{(1)}_{p\sigma_p q\sigma_q} = \sum_{t\sigma_t} \left(F^{(0)}_{p\sigma_p t\sigma_t} P^{(1)}_{t\sigma_t q\sigma_q} - P^{(1)}_{p\sigma_p t\sigma_t} F^{(0)}_{t\sigma_t q\sigma_q} + F^{(1)}_{p\sigma_p t\sigma_t} P^{(0)}_{t\sigma_t q\sigma_q} - P^{(0)}_{p\sigma_p t\sigma_t} F^{(1)}_{t\sigma_t q\sigma_q} \right). \tag{27}$$

The former relation of Eq. (26) is already satisfied with a condition in Eq. (16), while the latter relation of Eq. (27) will determine linear-response of density. Substituting the first-order density and Fock matrice of Eqs. (18) and (19) into the the latter relation yields

$$\begin{aligned} \Omega d_{p\sigma_p q\sigma_q} = & \sum_{t\sigma_t} \left(h_{p\sigma_p t\sigma_t} P^{(0)}_{t\sigma_t q\sigma_q} - P^{(0)}_{p\sigma_p t\sigma_t} h_{t\sigma_t q\sigma_q} \right) \\ & + \sum_{t\sigma_t} \left(F^{(0)}_{p\sigma_p t\sigma_t} d_{t\sigma_t q\sigma_q} - d_{p\sigma_p t\sigma_t} F^{(0)}_{t\sigma_t q\sigma_q} \right. \\ & \left. + \sum_{r\sigma_r s\sigma_s} \frac{\partial F_{p\sigma_p t\sigma_t}}{\partial P_{r\sigma_r s\sigma_s}} d_{r\sigma_r s\sigma_s} P^{(0)}_{t\sigma_t q\sigma_q} - P^{(0)}_{p\sigma_p t\sigma_t} \sum_{r\sigma_r s\sigma_s} \frac{\partial F_{t\sigma_t q\sigma_q}}{\partial P_{r\sigma_r s\sigma_s}} d_{r\sigma_r s\sigma_s} \right). \end{aligned} \tag{28}$$

Within TDA, the right-multiplication of all terms in Eq. (28) by projection matrices on occupied MO space, $P^{(0)}_{q\sigma_q i\sigma_i}$, and the left-multiplication by projection matrices on virtual MO space, $\delta_{a\sigma_q p\sigma_p} - P^{(0)}_{a\sigma_q p\sigma_p}$, gives

$$-h_{a\sigma_a i\sigma_i} = \sum_{b\sigma_b j\sigma_j} \left(A_{a\sigma_a i\sigma_i, b\sigma_b j\sigma_j} - \Omega\delta_{ij}\delta_{\sigma_i\sigma_j}\delta_{ab}\delta_{\sigma_a\sigma_b} \right) X_{b\sigma_b j\sigma_j}, \tag{29}$$

where orbital Hessian matrix is

$$A_{a\sigma_a i\sigma_i, b\sigma_b j\sigma_j} = F^{(0)}_{a\sigma_a b\sigma_b}\delta_{ij}\delta_{\sigma_i\sigma_j} - F^{(0)}_{i\sigma_i j\sigma_j}\delta_{ab}\delta_{\sigma_a\sigma_b} + \sum_{j\sigma_j b\sigma_b} \frac{\partial F_{a\sigma_a i\sigma_i}}{\partial P_{b\sigma_b j\sigma_j}}. \tag{30}$$

3.4 Electronic excitation energy

Electronic excitation energies can be obtained from the linear-response amplitude of density by analysis of the poles of the polarizability suggested by M. E. Casida.[5] Within the sum-over-states (SOS) approach, the dynamic polarizability is represented as

$$\alpha_{xy} = \sum_I \frac{\mu_x^{\text{ref}\,I}\,\mu_y^{I\,\text{ref}}}{\Omega_I - \Omega} + \sum_I \frac{\mu_x^{\text{ref}\,I}\,\mu_y^{I\,\text{ref}}}{\Omega_I + \Omega}, \tag{31}$$

where $\mu_r^{\text{ref}\,I} = \langle \Psi_{\text{ref}} | r | \Psi_I \rangle$ and Ω_I are transition dipole moments in the r direction and the excitation energy, respectively, from the reference state to the Ith excited state, and Ω is frequency of the external perturbation.

Meanwhile, a linear-response amplitude of the dipole moment in x direction, $\delta\mu_x$, can be represented as

$$\delta\mu_x = -2 \sum_{p\sigma_p q\sigma_q} x_{q\sigma_q p\sigma_p} d_{p\sigma_p q\sigma_q}. \tag{32}$$

Thus, an element of polarizability is given by

$$\alpha_{xy} = \frac{\delta\mu_x}{\mathscr{E}_y} = -2 \sum_{p\sigma_p q\sigma_q} x_{q\sigma_q p\sigma_p} \frac{d_{p\sigma_p q\sigma_q}}{\mathscr{E}_y}. \quad (33)$$

where $\mathscr{E}_y$ is the TD perturbed electric field in y direction. As mentioned in a previous section, amplitude of linear-response density, $d_{p\sigma_p q\sigma_q}$, is equal to the excitation amplitude, $X_{p\sigma_p q\sigma_q}$, within TDA.

With Eq. (29), it can be rewritten as

$$\alpha_{xy} = 2 \sum_{p\sigma_p q\sigma_q} \sum_{r\sigma_r s\sigma_s} x_{q\sigma_q p\sigma_p} \left(A_{p\sigma_p q\sigma_q, r\sigma_r s\sigma_s} - \Omega\delta_{ij}\delta_{\sigma_i\sigma_j}\delta_{ab}\delta_{\sigma_a\sigma_b} \right)^{-1} y_{r\sigma_r s\sigma_s}. \quad (34)$$

The first term on the right-hand side of Eq. (31) has poles at excitation energies, Ω_I, and the second term has poles at de-excitation energies, $-\Omega_I$. Therefore, the excitation energy can be obtained by comparing the first term of Eq. (31) and Eq. (34) within TDA.[44, 45] It follows that the excitation energies are the solutions of the eigenvalue problem,

$$A_{p\sigma_p q\sigma_q, r\sigma_r s\sigma_s} X^I_{r\sigma_r s\sigma_s} = \Omega_I X^I_{p\sigma_p q\sigma_q}. \quad (35)$$

The final resulting equation is called as the linear-response equation or the Casida equation.

4. Spin-flip TDDFT

If the zeroth-order (reference) density matrix for the Volterra expansion in Eq. (16) satisfy that of the closed-shell ground singlet state, the linear-response equation of Eq. (35) is the conventional linear-response TDDFT with TDA. Meanwhile, for the spin-flip (SF)-TDDFT utilize the density matrix of the triplet open-shell reference[30, 31] shown in upper panel of Fig. 1.

For consistency's sake of describing SF-TDDFT and mixed-reference (MR) SF-TDDFT, notations used in this rest of thesis are redefined. Indices for doubly and singly occupied KS spin molecular orbitals (MOs) of reference states are labeled as i, j and x, y, respectively, whereas those of the virtual KS spin MOs are labeled as a, b. Those for arbitrary (occupied or virtual) KS spin MOs are written as p, q, r, s, t, u, and four Greek indices (μ, ν, κ, λ) denote atomic orbitals. The σ and τ denote the index for the spin function of the MO. In addition, the closed, open, and virtual orbital spaces are denoted as C, O and V, respectively. The number of electrons is $2n$, thus the nth and the (n+1)th MOs representing the two orbitals in O space. Indices of O1 and O2 are used instead of n and n+1 for these two specific orbitals. To prevent

repeated equations, the O1 and O2 are usually represented as Om (m=1, 2) or On (n=1, 2), respectively. The singlet and triplet states are denoted as S and T, respectively, and the index for these is labeled as k (k=S, T). All two-electron integrals are written in chemist notation.

Then, the density matrix of the M_S = +1 triplet reference can be represented as

$$P^{(0)}_{i\sigma_i i\sigma_i} = 1, \quad P^{(0)}_{\mathrm{O1}\alpha\mathrm{O1}\alpha} = 1, \quad P^{(0)}_{\mathrm{O2}\alpha\mathrm{O2}\alpha} = 1, \quad \text{otherwise } 0. \tag{36}$$

The SF-TDDFT usually utilize TDA and collinear approximation for exchange-correlation kernel. Thus, the linear-response equation of SF-TDDFT is given by

$$\sum_{rs} A_{p\beta q\alpha, r\beta s\alpha} X^I_{r\beta s\alpha} = \sum_{rs} \Omega_I \delta_{pr} \delta_{qs} X^I_{r\beta s\alpha}, \tag{37}$$

with

$$A_{p\beta q\alpha, r\beta s\alpha} = F^{(0)}_{p\beta r\beta} \delta_{sq} - F^{(0)}_{s\alpha q\alpha} \delta_{pr} - c_H \left(pr \mid sq \right). \tag{38}$$

Schematic diagram describing electronic configurations by one-electron spin-flip excitation (linear response) from the triplet reference is shown with black full arrows in Fig. 1. The configurations are categorized by different initial and final MOs of a spin-flip excitation for four types: TYPE I (O→O), TYPE II (C→O), TYPE III (O→V), TYPE IV (C→V). The configurations shown by the gray dashed arrows are missing in SF-TDDFT. Hence, the excitation space defined

by SF-TDDFT is incomplete and spin-contaminated, as the individual configurations shown in Fig. 1 are not eigenfunctions of the total spin S^2.

SF-TDDFT is known to have great advantages in describing single-bond breaking or single-bond twisting systems.[30, 33] Two features of SF-TDDFT can be supported this statement. One is that triplet reference can well-describe two degenerate open-shell MOs, which frequently occur when a bond is breaking or twisted. In other word, SF-TDDFT can take into account static correlation. In addition, since all singlet states are described as response states, there exists coupling between ground and excited states.[46] It has been found that there is a great advantage in describing avoided crossing or conical intersection topology correctly.[27, 46] Despite of such many advantages, severe spin-contamination of response states except for few of low-lying excited states makes it difficult to use SF-TDDFT practically.

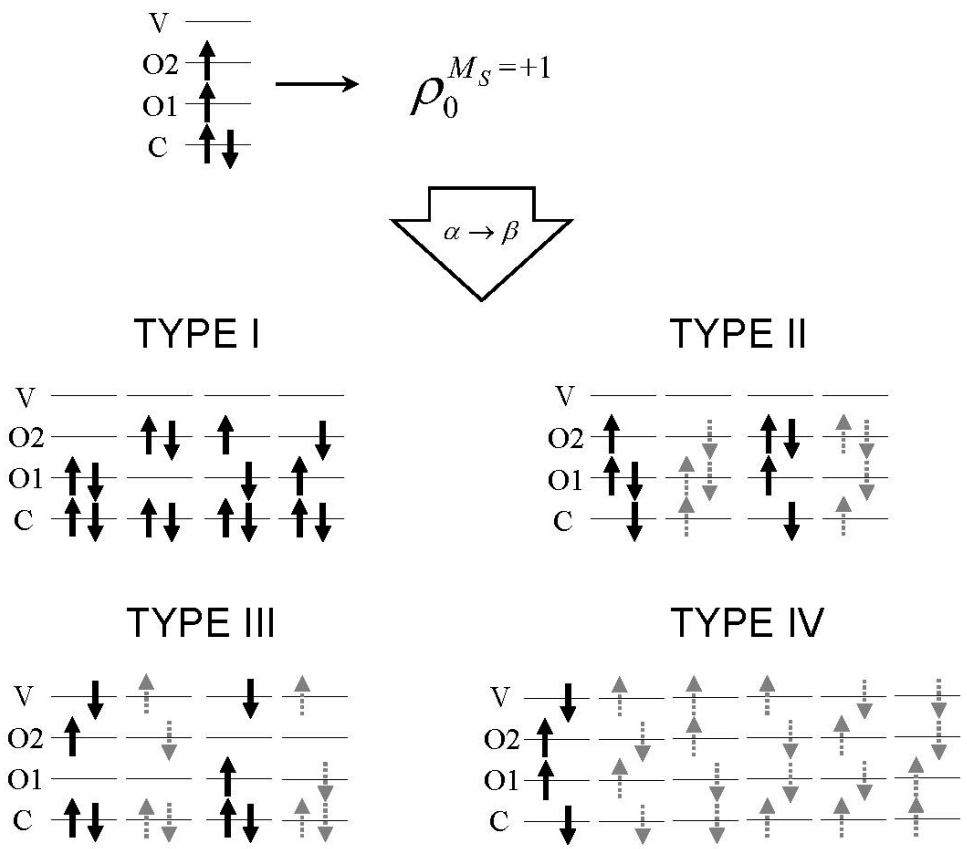

Figure. 1. A schematic diagram of SF-TDDFT. *The upper panel depicts the high-spin triplet reference and the corresponding zeroth-order RDM. In the lower pannel, a complete set of electronic configurations considered in SF-TDDFT is given. Electronic configurations which can be generated by SF linear responses (SF one-electron transitions) from the zeroth-order RDM are given by black arrows in four types. Configurations unable to be obtained in the linear responses of SF-TD-DFT are given by gray dashed arrows.*

MIXED-REFERENCE SPIN-FLIP TDDFT

The main sources of spin-contamination in SF-TDDFT is the missing electronic configurations (and the respective amplitudes) shown by the gray arrows as type II, III and IV in Fig. 1. In this thesis, the new mixed zeroth-order RDM is introduced[42] as an equiensemble of the M_S = +1 and -1 components of the triplet state in the first subsection of *Mixed-reference reduced density matrix*. As shown in Fig. 2, the use of the mixed-reference reduced density matrix (MR-RDM) includes many of the electronic configurations missing in SF-TDDFT. Linear-response equation with the MR-RDM is derived in the second subsection of in the second subsection of *Linear-response equation of mixed-reference spin-flip TDDFT*. *A posteriori* coupling between configurations originating from M_S = +1 and -1 are introduced in the next subsection of *Spin-pairing coupling*. Furthermore, expectation value of S^2 operator is evaluated for the response states of MRSF-TDDFT in the last subsection of *Expectation value of S^2 operator*. From this, it is proved that the spin-contamination of SF-TDDFT is nearly eliminated in MRSF-TDDFT.[42]

It is noteworthy that not all of the electronic configurations shown in Fig. 2 can be recovered by the use of the MR-RDM. Thus, four out of

six type IV configurations (four configurations shown with the gray arrows in Fig. 2) are still unencountered. Typically, these configurations represent high lying excited states and make insignificant contributions to the low lying states of molecules. Hence, the effect of the missing configurations for the spin-contamination of the SF-TDDFT response states is expected to be relatively small.

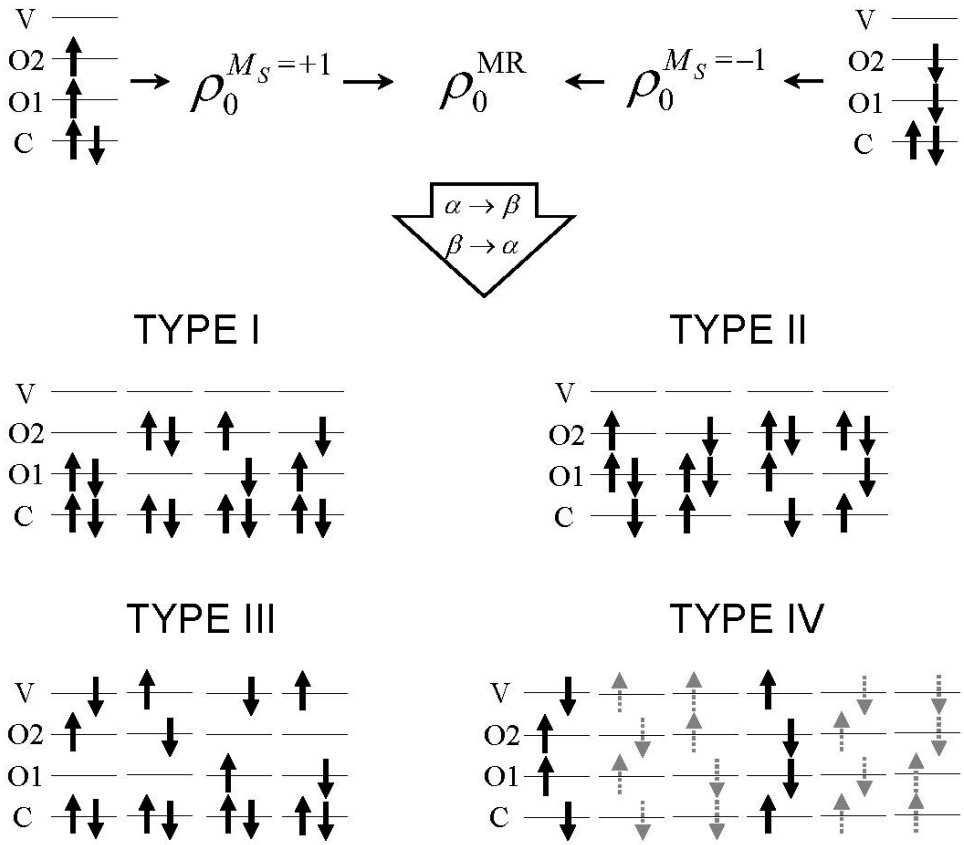

Figure. 2. A schematic diagram of MRSF-TDDFT. *The upper panel shows the zeroth-order MR-RDM which is a combination of M_S = + 1 and -1 RDMs. In the lower pannel, electronic configurations which can be generated by spin-flip linear responses from the MR-RDM are given by black arrows in four types. Configurations unable to be obtained in the linear responses of MR-SF-TD-DFT are given by gray dashed arrows.*

1. Mixed-reference reduced density matrix

1.1 Definition of mixed-reference reduced density matrix

The proposed mixed-reference reduced density matrix (MR-RDM) is

$$\rho_0^{\mathrm{MR}}(x,x') = \frac{1}{2}\left\{\rho_0^{\mathrm{Ms=+1}}(x,x') + \rho_0^{\mathrm{Ms=-1}}(x,x')\right\}. \tag{39}$$

In terms of the zeroth-order Kohn-Sham (KS) molecular orbital (MO), it is represented by

$$\begin{aligned}\rho_0^{MR}(x,x') = &\sum_{i\sigma_i}\phi_i^{\sigma_i}(x)\phi_i^{\sigma_i *}(x') + \frac{1}{2}\phi_{\mathrm{O1}}^{\alpha}(x)\phi_{\mathrm{O1}}^{\alpha *}(x') + \frac{1}{2}\phi_{\mathrm{O1}}^{\beta}(x)\phi_{\mathrm{O1}}^{\beta *}(x') \\ &+\frac{1}{2}\phi_{\mathrm{O2}}^{\alpha}(x)\phi_{\mathrm{O2}}^{\alpha *}(x') + \frac{1}{2}\phi_{\mathrm{O2}}^{\beta}(x)\phi_{\mathrm{O2}}^{\beta *}(x'),\end{aligned} \tag{40}$$

where the first term on the right hand side of the equation represents the RDM of the C space, the remaining terms – the RDM of the O space. The zeroth-order MR-RDM is a diagonal matrix with the elements

$$P_{i\sigma_i i\sigma_i}^{(0)MR} = 1,\ P_{\mathrm{O1}\alpha\mathrm{O1}\alpha}^{(0)MR} = \frac{1}{2},\ P_{\mathrm{O1}\beta\mathrm{O1}\beta}^{(0)MR} = \frac{1}{2},\ P_{\mathrm{O2}\alpha\mathrm{O2}\alpha}^{(0)MR} = \frac{1}{2},\ P_{\mathrm{O2}\beta\mathrm{O2}\beta}^{(0)MR} = \frac{1}{2},\ \mathrm{otherwise}\ 0, \tag{41}$$

and its trace satisfy the number of electrons:

$$\sum_{p\sigma_p} P_{p\sigma_p p\sigma_p}^{(0)\mathrm{MR}} = 2n. \tag{42}$$

1.2 Molecular orbital of mixed-reference reduced density matrix

According to the ensemble DFT,[47, 48] the energy of MR-RDM of

Eq. (39) is given by

$$E[\rho_0^{\mathrm{MR}}] = \frac{1}{2}\Big(E[\rho_0^{M_S=+1}] + E[\rho_0^{M_S=-1}] \Big), \tag{43}$$

where $E[\rho_0^{M_S=+1}]$ and $E[\rho_0^{M_S=-1}]$ are energies of $M_S = +1$ and -1 references, respectively. Since the energies of $M_S = +1$ and -1 references are same, the energy of MR-RDM and those of references are same as

$$E[\rho_0^{\mathrm{MR}}] = E[\rho_0^{M_S=+1}] = E[\rho_0^{M_S=-1}]. \tag{44}$$

By the ensemble DFT, the spatial part of MOs consisting MR-RDM, $\{\phi_k\}$, can be obtained with two conditions as

$$\frac{\delta}{\delta\phi_k}\left\{ E[\rho_0^{\mathrm{MR}}] + \sum_{pq} F_{pq}\left(\delta_{qp} - \langle \phi_q | \phi_p \rangle\right) \right\} = 0, \tag{45a}$$

$$F_{pq} = F_{qp}^*, \tag{45b}$$

where F_{pq} is the Lagrange multiplier. Substituting Eq. (44) into Eq. (45a) yield

$$\frac{\delta}{\delta\phi_k}\left\{ E[\rho_0^{M_S=+1}] + \sum_{pq} F_{pq}\left(\delta_{qp} - \langle \phi_q | \phi_p \rangle\right) \right\} = 0, \tag{46a}$$

$$F_{pq} = F_{qp}^*. \tag{46b}$$

The conditions of Eqs. (46a) and (46b) are those of restricted open-shell Kohn-Sham method for $M_S = +1$ reference which is the way to obtain the spatial part of MOs in SF-TDDFT. Therefore, one can use same spatial part of MOs of SF-TDDFT in MRSF-TDDFT.

1.3 Restoring idempotency of the mixed-reference reduced density matrix

The proposed MR-RDM does not satisfy the idempotency conditions as in Eq. (20); *e.g.*, an open-shell RDM of the new MR-RDM, $P^{(0)\mathrm{MR}}_{O1\alpha O1\alpha}$ (as well as $P^{(0)\mathrm{MR}}_{O1\beta O1\beta}$, $P^{(0)\mathrm{MR}}_{O2\alpha O2\alpha}$, and $P^{(0)\mathrm{MR}}_{O2\beta O2\beta}$), violates the condition

$$\sum_{t\sigma_t} P^{(0)\mathrm{MR}}_{\mathrm{O1}\alpha t\sigma_t} P^{(0)\mathrm{MR}}_{t\sigma_t \mathrm{O1}\alpha} = P^{(0)\mathrm{MR}}_{\mathrm{O1}\alpha \mathrm{O1}\alpha} P^{(0)\mathrm{MR}}_{\mathrm{O1}\alpha \mathrm{O1}\alpha} = \frac{1}{2} P^{(0)\mathrm{MR}}_{\mathrm{O1}\alpha \mathrm{O1}\alpha} \neq P^{(0)\mathrm{MR}}_{\mathrm{O1}\alpha \mathrm{O1}\alpha}, \tag{47}$$

thus precluding straightforward derivation of the linear-response equation. As follows from Eqs. (40) and (41), the non-idempotency of the RDM of Eq. (47) originates from half-integer populations of the zeroth-order open-shell KS orbitals $\phi^{\sigma}_{\mathrm{O1}}$ and $\phi^{\sigma}_{\mathrm{O2}}$, $\sigma = \alpha, \beta$. To resolve this difficulty and to restore idempotency of the respective RDM, we replace the original spin-orbitals (with the α or β spin) by the orbitals of mixed spin, labeled in the following by s_1 and s_2, obtained by the application of a unitary transformation $\mathbf{U}$

$$\mathbf{U}^{\dagger} = \begin{pmatrix} \langle \alpha | s_1 \rangle & \langle \alpha | s_2 \rangle \\ \langle \beta | s_1 \rangle & \langle \beta | s_2 \rangle \end{pmatrix} = \frac{1}{2} \begin{pmatrix} 1+i & 1-i \\ 1-i & 1+i \end{pmatrix}, \tag{48}$$

which leads to the new mixed spin functions of the O space

$$s_1 = \frac{(1+i)\alpha + (1-i)\beta}{2}, \; s_2 = \frac{(1-i)\alpha + (1+i)\beta}{2}. \tag{49}$$

The new mixed spin O orbitals $\phi^{s_m}_{\mathrm{O}k}$, $k, m = 1, 2$ are orthonormal among themselves and with respect to the C and V orbitals.

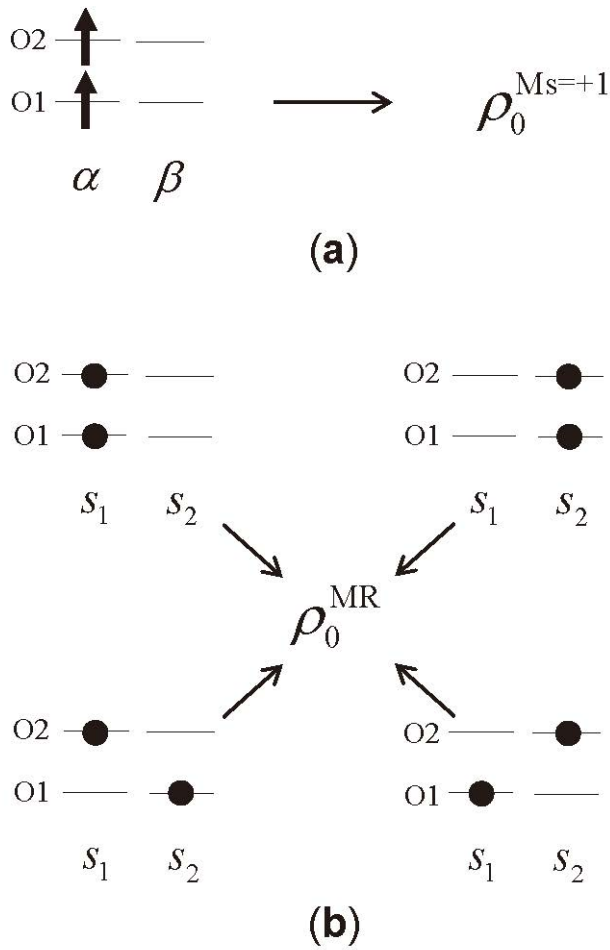

Figure. 3. Occupation of open-shell orbitals in a single KS determinant and its relationship with the respective zeroth-order RDM. *A single KS determinant shown in subfigure (a) represents the RDM of the SF-TDDFT method. Subfigure (b) shows equivalence between four possible occupation patterns of the mixed spin-orbitals s_1 and s_2, which all yield the same zeroth order RDM. Populations of the conventional α spin-orbitals are shown with upward pointing arrows and of the mixed spin-orbitals are shown with dots.*

There exist four possible choices for populating the new mixed spin-orbitals, as shown in Fig. 3b. As all the four population patterns result in the same RDM, for convenience, the configuration in Fig. 3b with both s_1 mixed spin-orbitals occupied is selected. With this choice of occupations, the RDM becomes

$$\rho_0^{\mathrm{MR}}(x,x') = \sum_{i\sigma_i} \phi_i^{\sigma_i}(x)\phi_i^{\sigma_i *}(x') + \phi_{\mathrm{O1}}^{s_1}(x)\phi_{\mathrm{O1}}^{s_1 *}(x') + \phi_{\mathrm{O2}}^{s_1}(x)\phi_{\mathrm{O2}}^{s_1 *}(x') \quad (50)$$

$$P_{i\sigma_i j\sigma_j}^{(0)\mathrm{MR}} = \delta_{ij}\delta_{\sigma_i\sigma_j},\ P_{\mathrm{O1}s_1\mathrm{O1}s_1}^{(0)\mathrm{MR}} = 1,\ P_{\mathrm{O2}s_1\mathrm{O2}s_1}^{(0)\mathrm{MR}} = 1,\ \text{otherwise } 0. \quad (51)$$

With spatial part of MOs described by real function, the redefined RDM of Eq. (50) is identical to Eq. (40), as can be easily seen by expanding the open-shell contributions as, *e.g.*,

$$\begin{aligned}
&\phi_{\mathrm{O1}}^{((1+i)\alpha+(1-i)\beta)/2}(x)\phi_{\mathrm{O1}}^{((1+i)\alpha+(1-i)\beta)/2 *}(x') \\
&= \frac{1}{2}\left\{\phi_{\mathrm{O1}}^{\alpha}(x)\phi_{\mathrm{O1}}^{\alpha *}(x') + \phi_{\mathrm{O1}}^{\beta}(x)\phi_{\mathrm{O1}}^{\beta *}(x') + i\phi_{\mathrm{O1}}^{\alpha}(x)\phi_{\mathrm{O1}}^{\beta *}(x') - i\phi_{\mathrm{O1}}^{\beta}(x)\phi_{\mathrm{O1}}^{\alpha *}(x')\right\} \quad (52) \\
&= \frac{1}{2}\left\{\phi_{\mathrm{O1}}^{\alpha}(x)\phi_{\mathrm{O1}}^{\alpha *}(x') + \phi_{\mathrm{O1}}^{\beta}(x)\phi_{\mathrm{O1}}^{\beta *}(x')\right\}
\end{aligned}$$

and a similar expression for the other open-shell contribution to Eq. (50). Replacing the old spin parts of the O spin-orbitals (represented by the α and β spin functions) by the mixed spin functions s_1 and s_2, while keeping the α and β spin functions for the C and V orbitals and using Eq. (51), lets one to show that the overall idempotency relation

$$\sum_{t\sigma_t} P_{p\sigma_p t\sigma_t}^{(0)\mathrm{MR}} P_{t\sigma_t q\sigma_q}^{(0)\mathrm{MR}} = P_{p\sigma_p q\sigma_q}^{(0)\mathrm{MR}}. \quad (53)$$

holds for the redefined density matrix.

2. Linear-response equation of mixed-reference spin-flip TDDFT

As described by previous section, the idempotency of the zeroth-order density matrix can be recovered by the introduced spin rotation. Following same steps described in subsection 3 of the first *THEORETICAL BACKGROUND* section one can straightforwardly obtain a linear-response equation of MR-RDM. However, linear responses from each of M_S = +1 and -1 references should appear mixed in the linear responses from the MR-RDM. Therefore, one need to disentangle the mixed responses which is described in subsection 2.1 of *Definition of separated excitation amplitude* and subsection 2.2 of *Disentangling different M_S response*. In addition, type I (O→O) configurations shown in Fig. 2 can be generated by both M_S = +1 and -1 reference. Due to the unmatching of configuration from different reference, additional rearrangement is required and it is presented in subsection 2.3 of *Recovery of one-to-one relation between configuration and excitation amplitude*. With these procedure, one can obtain clearly separated linear-response equation for singlet and triplet states, which is described in the next subsection 2.4 of *Separating matrix equations for singlet and triplet response states*. With dimensional transformation matrix introduced in the last

subsection 2.5 of *Dimensional transformation matrix*, the linear-response equation for the singlet and triplet states can be described succinctly with a single form. Furthermore, this concept is useful for the implementation of MRSF-TDDFT with a little modification of code of SF-TDDFT.

SF-TDDFT				MRSF-TDDFT				
$M_S = +1$ reference		$M_S = -1$ reference		Mixed amplitude		Separated amplitude		
$X^{I}_{O_\beta C_\alpha}$	+	$X^{I}_{O_\alpha C_\alpha}$	$\rightarrow$	$X^{\mathrm{MR},I}_{O_{s_2} C_\alpha}$	$\rightarrow$	$X^{M_S=0,I}_{O_{s_2} C_\alpha}$	+	$X^{M_S=-1,I}_{O_{s_2} C_\alpha}$
$X^{I}_{O_\beta C_\beta}$	+	$X^{I}_{O_\alpha C_\beta}$	$\rightarrow$	$X^{\mathrm{MR},I}_{O_{s_2} C_\beta}$	$\rightarrow$	$X^{M_S=0,I}_{O_{s_2} C_\beta}$	+	$X^{M_S=+1,I}_{O_{s_2} C_\beta}$
$X^{I}_{V_\beta O_\alpha}$	+	$X^{I}_{V_\beta O_\beta}$	$\rightarrow$	$X^{\mathrm{MR},I}_{V_\beta O_{s_1}}$	$\rightarrow$	$X^{M_S=0,I}_{V_\beta O_{s_1}}$	+	$X^{M_S=-1,I}_{V_\beta O_{s_1}}$
$X^{I}_{V_\alpha O_\alpha}$	+	$X^{I}_{V_\alpha O_\beta}$	$\rightarrow$	$X^{\mathrm{MR},I}_{V_\alpha O_{s_1}}$	$\rightarrow$	$X^{M_S=0,I}_{V_\alpha O_{s_1}}$	+	$X^{M_S=+1,I}_{V_\alpha O_{s_1}}$
$X^{I}_{V_\beta C_\alpha}$	+	$X^{I}_{V_\beta C_\alpha}$	$\rightarrow$	$X^{\mathrm{MR},I}_{V_\beta C_\alpha}$	$\rightarrow$	$X^{M_S=0,I}_{V_\beta C_\alpha}$	+	$X^{M_S=-2,I}_{V_\beta C_\alpha}$
$X^{I}_{V_\alpha C_\beta}$	+	$X^{I}_{V_\alpha C_\beta}$	$\rightarrow$	$X^{\mathrm{MR},I}_{V_\alpha C_\beta}$	$\rightarrow$	$X^{M_S=0,I}_{V_\alpha C_\beta}$	+	$X^{M_S=+2,I}_{V_\alpha C_\beta}$
$X^{I}_{O_\beta O_\alpha}$	+	$X^{I}_{O_\alpha O_\beta}$	$\rightarrow$	$X^{\mathrm{MR},I}_{O_{s_2} O_{s_1}}$	$\rightarrow$	$X^{M_S=0,I}_{O_{s_2} O_{s_1}}$	+	$X^{\mathrm{Redun},I}_{O_{s_2} O_{s_1}}$
$X^{I}_{V_\alpha C_\alpha}$	+	$X^{I}_{V_\alpha C_\alpha}$	$\rightarrow$	$X^{\mathrm{MR},I}_{V_\alpha C_\alpha}$				
$X^{I}_{V_\beta C_\beta}$	+	$X^{I}_{V_\beta C_\beta}$	$\rightarrow$	$X^{\mathrm{MR},I}_{V_\beta C_\beta}$				

Table 1. Connection between the excitation amplitudes of the SF-TDDFT from each $M_S = +1$ or -1 reference, and the new excitation amplitudes of the MRSF-TDDFT from the mixed reference.

2.1 Definition of separated excitation amplitude

As shown in Tab. 1, it is natural to think that total eighteen types of independent excitation amplitudes $X^{I}_{p\sigma_p q\sigma_q}$ from $M_S = +1$ or $M_S = -1$ reference, are entangled in the nine types of new excitation amplitudes $X^{\mathrm{MR},I}_{p\sigma_p q\sigma_q}$; for each row, two $X^{I}_{p\sigma_p q\sigma_q}$ are entangled in $X^{\mathrm{MR},I}_{p\sigma_p q\sigma_q}$. It is noted that $X^{\mathrm{MR},I}_{\mathrm{O}_{S2}\mathrm{O}_{S1}}$ on the 7th row has a redundant part since the configurations are same generated by O→O excitations from two different references.

The starting point for separating these entangled excitation amplitudes can be found in the general expression of the summation $\sum_{r\sigma_r s\sigma_s}\left(\partial F_{p\sigma_p q\sigma_q}/\partial P_{r\sigma_r s\sigma_s}\right) X^{\mathrm{MR},I}_{r\sigma_r s\sigma_s}$ in the matrix equation. For any index $p\sigma_p$ and $q\sigma_q$, the summation index $r\sigma_r$ and $s\sigma_s$ can be expanded into the 7 types of Tab. 1 as

$$\sum_{r\sigma_r s\sigma_s}\frac{\partial F_{p\sigma_p q\sigma_q}}{\partial P_{r\sigma_r s\sigma_s}} X^{\mathrm{MR},I}_{r\sigma_r s\sigma_s} =$$

$$+\left\{\sum_{wj}\frac{1}{\sqrt{2}}\frac{\partial F_{p\sigma_p q\sigma_q}}{\partial P_{w\beta j\alpha}}\frac{1+i}{\sqrt{2}} X^{\mathrm{MR},I}_{ws_2 j\alpha}+\sum_{wj}\frac{1}{\sqrt{2}}\frac{\partial F_{p\sigma_p q\sigma_q}}{\partial P_{w\alpha j\alpha}}\frac{1-i}{\sqrt{2}} X^{\mathrm{MR},I}_{ws_2 j\alpha}\right\} \tag{54a}$$

$$+\left\{\sum_{wj}\frac{1}{\sqrt{2}}\frac{\partial F_{p\sigma_p q\sigma_q}}{\partial P_{w\alpha j\beta}}\frac{1-i}{\sqrt{2}} X^{\mathrm{MR},I}_{ws_2 j\beta}+\sum_{wj}\frac{1}{\sqrt{2}}\frac{\partial F_{p\sigma_p q\sigma_q}}{\partial P_{w\beta j\beta}}\frac{1+i}{\sqrt{2}} X^{\mathrm{MR},I}_{ws_2 j\beta}\right\} \tag{54b}$$

$$+\left\{\sum_{bz}\frac{1}{\sqrt{2}}\frac{\partial F_{p\sigma_p q\sigma_q}}{\partial P_{b\beta z\alpha}}\frac{1-i}{\sqrt{2}} X^{\mathrm{MR},I}_{bzs_1}+\sum_{bz}\frac{1}{\sqrt{2}}\frac{\partial F_{p\sigma_p q\sigma_q}}{\partial P_{b\beta z\beta}}\frac{1+i}{\sqrt{2}} X^{\mathrm{MR},I}_{bzs_1}\right\} \tag{54c}$$

$$+\left\{\sum_{bz}\frac{1}{\sqrt{2}}\frac{\partial F_{p\sigma_p q\sigma_q}}{\partial P_{b\alpha z\beta}}\frac{1+i}{\sqrt{2}}X^{MR,I}_{b\alpha zs_1}+\sum_{bz}\frac{1}{\sqrt{2}}\frac{\partial F_{p\sigma_p q\sigma_q}}{\partial P_{b\alpha z\alpha}}\frac{1-i}{\sqrt{2}}X^{MR,I}_{b\alpha zs_1}\right\} \quad (54d)$$

$$+\left\{\sum_{bj}\frac{1}{\sqrt{2}}\frac{\partial F_{p\sigma_p q\sigma_q}}{\partial P_{b\beta j\alpha}}\frac{1}{\sqrt{2}}X^{MR,I}_{b\beta j\alpha}+\sum_{bj}\frac{1}{\sqrt{2}}\frac{\partial F_{p\sigma_p q\sigma_q}}{\partial P_{b\beta j\alpha}}\frac{1}{\sqrt{2}}X^{MR,I}_{b\beta j\alpha}\right\} \quad (54e)$$

$$+\left\{\sum_{bj}\frac{1}{\sqrt{2}}\frac{\partial F_{p\sigma_p q\sigma_q}}{\partial P_{b\alpha j\beta}}\frac{1}{\sqrt{2}}X^{MR,I}_{b\alpha j\beta}+\sum_{bj}\frac{1}{\sqrt{2}}\frac{\partial F_{p\sigma_p q\sigma_q}}{\partial P_{b\alpha j\beta}}\frac{1}{\sqrt{2}}X^{MR,I}_{b\alpha j\beta}\right\} \quad (54f)$$

$$+\left\{\sum_{wz}\frac{1}{2}\left(\frac{\partial F_{p\sigma_p q\sigma_q}}{\partial P_{w\beta z\alpha}}+\frac{\partial F_{p\sigma_p q\sigma_q}}{\partial P_{w\alpha z\beta}}\right)X^{MR,I}_{ws_2zs_1}+\sum_{wz}\frac{1}{2}\left(\frac{\partial F_{p\sigma_p q\sigma_q}}{\partial P_{w\alpha z\alpha}}-\frac{\partial F_{p\sigma_p q\sigma_q}}{\partial P_{w\beta z\beta}}\right)iX^{MR,I}_{ws_2zs_1}\right\}. \quad (54g)$$

In each of Eqs. (54a)-(54f), two terms are given come from M_S = + 1 and −1 references. The excitation amplitude in the left term corresponds to a configuration with M_S = 0, and that in the right term corresponds to a configuration with $M_S \neq 0$. While, in Eq. (54g), the left term come from both M_S = + 1 and −1 references, and the right term is the redundant term. From this fact, the separated excitation amplitudes can be defined as in Tab. 2.

$M_S = 0$ amplitudes	$M_S \neq 0$ amplitudes	
$X_{us_2i\alpha}^{M_S=0,I} \equiv \frac{1+i}{\sqrt{2}} X_{us_2i\alpha}^{MR,I}$	$X_{us_2i\alpha}^{M_S=-1,I} \equiv \frac{1-i}{\sqrt{2}} X_{us_2i\alpha}^{MR,I}$	$X_{us_2i\alpha}^{M_S=0,I} = iX_{us_2i\alpha}^{M_S=-1,I}$
$X_{us_2i\beta}^{M_S=0,I} \equiv \frac{1-i}{\sqrt{2}} X_{us_2i\beta}^{MR,I}$	$X_{us_2i\beta}^{M_S=+1,I} \equiv \frac{1+i}{\sqrt{2}} X_{us_2i\beta}^{MR,I}$	$X_{us_2i\beta}^{M_S=0,I} = -iX_{us_2i\beta}^{M_S=+1,I}$
$X_{a\beta vs_1}^{M_S=0,I} \equiv \frac{1-i}{\sqrt{2}} X_{a\beta vs_1}^{MR,I}$	$X_{a\beta vs_1}^{M_S=-1,I} \equiv \frac{1+i}{\sqrt{2}} X_{a\beta vs_1}^{MR,I}$	$X_{a\beta vs_1}^{M_S=0,I} = -iX_{a\beta vs_1}^{M_S=-1,I}$
$X_{a\alpha vs_1}^{M_S=0,I} \equiv \frac{1+i}{\sqrt{2}} X_{a\alpha vs_1}^{MR,I}$	$X_{a\alpha vs_1}^{M_S=+1,I} \equiv \frac{1-i}{\sqrt{2}} X_{a\alpha vs_1}^{MR,I}$	$X_{a\alpha vs_1}^{M_S=0,I} = iX_{a\alpha vs_1}^{M_S=+1,I}$
$X_{a\beta i\alpha}^{M_S=0,I} \equiv \frac{1}{\sqrt{2}} X_{a\beta i\alpha}^{MR,I}$	$X_{a\beta i\alpha}^{M_S=-2,I} \equiv \frac{1}{\sqrt{2}} X_{a\beta i\alpha}^{MR,I}$	$X_{a\beta i\alpha}^{M_S=0,I} = X_{a\beta i\alpha}^{M_S=-2,I}$
$X_{a\alpha i\beta}^{M_S=0,I} \equiv \frac{1}{\sqrt{2}} X_{a\alpha i\beta}^{MR,I}$	$X_{a\alpha i\beta}^{M_S=+2,I} \equiv \frac{1}{\sqrt{2}} X_{a\alpha i\beta}^{MR,I}$	$X_{a\alpha i\beta}^{M_S=0,I} = X_{a\alpha i\beta}^{M_S=+2,I}$
$X_{us_2vs_1}^{M_S=0,I} \equiv X_{us_2vs_1}^{MR,I}$	$X_{us_2vs_1}^{Redun,I} \equiv iX_{us_2vs_1}^{MR,I}$	$X_{us_2vs_1}^{M_S=0,I} = -iX_{us_2vs_1}^{Redun,I}$

Table 2. Detailed connection between the new excitation amplitudes and their respective separated contributions. *The M_S value represented at superscript of a newly defined excitation amplitude denotes the value of a corresponding configuration.*

After substituting amplitude matrices defined in Tab. 2, the equation 54a-g becomes

$$\sum_{r\sigma_r s\sigma_s} \frac{\partial F_{p\sigma_p q\sigma_q}}{\partial P_{r\sigma_r s\sigma_s}} X^{\mathrm{MR},I}_{r\sigma_r s\sigma_s} =$$

$$+\left\{\sum_{wj}\frac{1}{\sqrt{2}}\frac{\partial F_{p\sigma_p q\sigma_q}}{\partial P_{w\beta j\alpha}} X^{M_S=0,I}_{ws_2 j\alpha} + \sum_{wj}\frac{1}{\sqrt{2}}\frac{\partial F_{p\sigma_p q\sigma_q}}{\partial P_{w\alpha j\alpha}} X^{M_S=-1,I}_{ws_2 j\alpha}\right\} \tag{55a}$$

$$+\left\{\sum_{wj}\frac{1}{\sqrt{2}}\frac{\partial F_{p\sigma_p q\sigma_q}}{\partial P_{w\alpha j\beta}} X^{M_S=0,I}_{ws_2 j\beta} + \sum_{wj}\frac{1}{\sqrt{2}}\frac{\partial F_{p\sigma_p q\sigma_q}}{\partial P_{w\beta j\beta}} X^{M_S=+1,I}_{ws_2 j\beta}\right\} \tag{55b}$$

$$+\left\{\sum_{bz}\frac{1}{\sqrt{2}}\frac{\partial F_{p\sigma_p q\sigma_q}}{\partial P_{b\beta z\alpha}} X^{M_S=0,I}_{b\beta zs_1} + \sum_{bz}\frac{1}{\sqrt{2}}\frac{\partial F_{p\sigma_p q\sigma_q}}{\partial P_{b\beta z\beta}} X^{M_S=-1,I}_{b\beta zs_1}\right\} \tag{55c}$$

$$+\left\{\sum_{bz}\frac{1}{\sqrt{2}}\frac{\partial F_{p\sigma_p q\sigma_q}}{\partial P_{b\alpha z\beta}} X^{M_S=0,I}_{b\alpha zs_1} + \sum_{bz}\frac{1}{\sqrt{2}}\frac{\partial F_{p\sigma_p q\sigma_q}}{\partial P_{b\alpha z\alpha}} X^{M_S=+1,I}_{b\alpha zs_1}\right\} \tag{55d}$$

$$+\left\{\sum_{bj}\frac{1}{\sqrt{2}}\frac{\partial F_{p\sigma_p q\sigma_q}}{\partial P_{b\beta j\alpha}} X^{M_S=0,I}_{b\beta j\alpha} + \sum_{bj}\frac{1}{\sqrt{2}}\frac{\partial F_{p\sigma_p q\sigma_q}}{\partial P_{b\beta j\alpha}} X^{M_S=-2,I}_{b\beta j\alpha}\right\} \tag{55e}$$

$$+\left\{\sum_{bj}\frac{1}{\sqrt{2}}\frac{\partial F_{p\sigma_p q\sigma_q}}{\partial P_{b\alpha j\beta}} X^{M_S=0,I}_{b\alpha j\beta} + \sum_{bj}\frac{1}{\sqrt{2}}\frac{\partial F_{p\sigma_p q\sigma_q}}{\partial P_{b\alpha j\beta}} X^{M_S=+2,I}_{b\alpha j\beta}\right\} \tag{55f}$$

$$+\left\{\sum_{wz}\frac{1}{2}\left(\frac{\partial F_{p\sigma_p q\sigma_q}}{\partial P_{w\beta z\alpha}} + \frac{\partial F_{p\sigma_p q\sigma_q}}{\partial P_{w\alpha z\beta}}\right) X^{M_S=0,I}_{ws_2 zs_1} + \sum_{wz}\frac{1}{2}\left(\frac{\partial F_{p\sigma_p q\sigma_q}}{\partial P_{w\alpha z\alpha}} - \frac{\partial F_{p\sigma_p q\sigma_q}}{\partial P_{w\beta z\beta}}\right) X^{\mathrm{Redun},I}_{ws_2 zs_1}\right\}. \tag{55g}$$

2.2 Disentangling different M_S response

Using the newly defined separated excitation amplitudes in Tab. 2, one can separate equations of motion (EOM) into EOMs with different M_S values. Of the nine types of the $X^{MR,I}_{p\sigma_p q\sigma_q}$ amplitudes shown in Tab. 1, the last two amplitudes, $X^{MR,I}_{V_\alpha C_\alpha}$ and $X^{MR,I}_{V_\beta C_\beta}$, do not include the $M_S = 0$ amplitudes and they are dropped in the EOM. For the remaining seven types, the $M_S = \pm 1$ contributions shown of the light gray background in the last column of Tab. 1 and the $M_S = \pm 2$ contributions (dark gray background) are removed from the EOM of the $M_S = 0$ amplitudes as described in the following.

Removal of the contributions with $M_S \neq 0$ from the response equations is illustrated by the example of the $X^{MR,I}_{us_2 i\alpha}$ amplitude matrix. The EOM are first pre-multiplied by $(1+i)/\sqrt{2}$ and then transformed according to Eq. (55) to yield

$$\frac{1}{2}\left\{\omega_I X^{M_S=0,I}_{us_2 i\alpha} + i\omega_I X^{M_S=-1,I}_{us_2 i\alpha}\right\}$$

$$= \frac{1}{2}\left\{\sum_{wj}\left(F^{(0)}_{u\beta w\beta}\delta_{ij} - F^{(0)}_{j\alpha i\alpha}\delta_{uw} + \frac{\partial F_{u\beta i\alpha}}{\partial P_{w\beta j\alpha}}\right) X^{M_S=0,I}_{ws_2 j\alpha}\right.$$

$$\left. + i\sum_{wj}\left(F^{(0)}_{u\alpha w\alpha}\delta_{ij} - F^{(0)}_{j\alpha i\alpha}\delta_{uw} + \frac{\partial F_{u\alpha i\alpha}}{\partial P_{w\alpha j\alpha}} X^{M_S=-1,I}_{ws_2 j\alpha} + \frac{\partial F_{u\alpha i\alpha}}{\partial P_{w\beta j\beta}} X^{M_S=+1,I}_{ws_2 j\beta}\right)\right\} \quad (56a)$$

$$+ \frac{1}{2}\left\{\sum_{bz}\frac{\partial F_{u\beta i\alpha}}{\partial P_{b\beta z\alpha}} X^{M_S=0,I}_{b\beta zs_1} + i\sum_{bz}\left(\frac{\partial F_{u\alpha i\alpha}}{\partial P_{b\alpha z\alpha}} X^{M_S=+1,I}_{b\alpha zs_1} + \frac{\partial F_{u\alpha i\alpha}}{\partial P_{b\beta z\beta}} X^{M_S=-1,I}_{b\beta zs_1}\right)\right\} \quad (56b)$$

$$+\frac{1}{2}\left\{\sum_{bj}\left(F^{(0)}_{u\beta b\beta}\delta_{ij}+\frac{\partial F_{u\beta i\alpha}}{\partial P_{b\beta j\alpha}}\right)X^{M_S=0,I}_{b\beta j\alpha}+\sum_{bj}\left(F^{(0)}_{u\beta b\beta}\delta_{ij}+\frac{\partial F_{u\beta i\alpha}}{\partial P_{b\beta j\alpha}}\right)X^{M_S=-2,I}_{b\beta j\alpha}\right\} \tag{56c}$$

$$+\frac{1}{2\sqrt{2}}\left\{\sum_{wz}\left(-F^{(0)}_{z\alpha i\alpha}\delta_{uw}+\frac{\partial F_{u\beta i\alpha}}{\partial P_{w\beta z\alpha}}\right)X^{M_S=0,I}_{ws_2zs_1}+i\sum_{wz}\left(-F^{(0)}_{z\alpha i\alpha}\delta_{uw}+\frac{\partial F_{u\alpha i\alpha}}{\partial P_{w\alpha z\alpha}}-\frac{\partial F_{u\alpha i\alpha}}{\partial P_{w\beta z\beta}}\right)X^{\mathrm{Redun},I}_{ws_2zs_1}\right\}. \tag{56d}$$

In Eqs. (56a) and (56b), the $M_S=\pm1$ amplitudes make purely imaginary contributions into the response equations and are dropped from the equations for the $M_S=0$ amplitudes; the same is true for the redundant part of the O→O transitions, see Eq. (56d). Although the $M_S=-2$ amplitude, Eq. (56c), is coupled with the $M_S=0$ contributions, its amplitude is neglected in the final response equation; this is similar to the assumptions behind the standard SF-TDDFT formalism. Hence, keeping only the $M_S=0$ amplitudes the response equations read

$$\omega_I\mathbf{X}^{M_S=0,I}_{\mathrm{O}_{s_2}\mathrm{C}_\alpha}=\mathbf{A}_{11}\mathbf{X}^{M_S=0,I}_{\mathrm{O}_{s_2}\mathrm{C}_\alpha}+\mathbf{A}_{12}\mathbf{X}^{M_S=0,I}_{\mathrm{V}_\beta\mathrm{O}_{s_1}}+\mathbf{A}_{13}\mathbf{X}^{M_S=0,I}_{\mathrm{V}_\beta\mathrm{C}_\alpha}+\mathbf{A}_{14}\mathbf{X}^{M_S=0,I}_{\mathrm{O}_{s_2}\mathrm{O}_{s_1}}, \tag{57}$$

where amplitude vectors are $(\mathbf{X}^{M_S=0,I}_{\mathrm{O}_{s_2}\mathrm{C}_\alpha})_{wj}=X^{M_S=0,I}_{ws_2j\alpha}$, $(\mathbf{X}^{M_S=0,I}_{\mathrm{V}_\beta\mathrm{O}_{s_1}})_{bz}=X^{M_S=0,I}_{b\beta zs_1}$, $(\mathbf{X}^{M_S=0,I}_{\mathrm{V}_\beta\mathrm{C}_\alpha})_{bj}=X^{M_S=0,I}_{b\beta j\alpha}$, $(\mathbf{X}^{M_S=0,I}_{\mathrm{O}_{s_2}\mathrm{O}_{s_1}})_{wz}=X^{M_S=0,I}_{ws_2zs_1}$, and the coupling block matrices are $(\mathbf{A}_{11})_{ui,wj}\equiv F^{(0)}_{u\beta w\beta}\delta_{ij}-F^{(0)}_{j\alpha i\alpha}\delta_{uw}+\frac{\partial F_{u\beta i\alpha}}{\partial P_{w\beta j\alpha}}$, $(\mathbf{A}_{12})_{ui,bz}\equiv\frac{\partial F_{u\beta i\alpha}}{\partial P_{b\beta z\alpha}}$, $(\mathbf{A}_{13})_{ui,bj}\equiv F^{(0)}_{u\beta b\beta}\delta_{ij}+\frac{\partial F_{u\beta i\alpha}}{\partial P_{b\beta j\alpha}}$ and $(\mathbf{A}_{14})_{ui,wz}\equiv\frac{1}{\sqrt{2}}(-F^{(0)}_{z\alpha i\alpha}\delta_{uw}+\frac{\partial F_{u\beta i\alpha}}{\partial P_{w\beta z\alpha}})$.

It is noted that all the zeroth-order Fock matrices in Eq. (56) are

originated from M_S = +1 reference. Those from from M_S = −1 reference will be represented with a tilde as $\tilde{F}^{(0)}_{p\sigma_p q\sigma_q}$, and these satisfy following equalities

$$F^{(0)}_{p\alpha q\alpha} = \tilde{F}^{(0)}_{p\beta q\beta}, \quad F^{(0)}_{p\beta q\beta} = \tilde{F}^{(0)}_{p\alpha q\alpha}. \tag{58}$$

The response equations for the M_S = 0 amplitudes of the other six types also can be obtained in a similar way, and collecting all these equations can form a matrix equation as

$$\begin{pmatrix} \mathbf{A}_{11} & \mathbf{A}_{12} & \mathbf{A}_{13} & \mathbf{A}_{14} & \mathbf{0} & \mathbf{0} & \mathbf{0} \\ \mathbf{A}_{21} & \mathbf{A}_{22} & \mathbf{A}_{23} & \mathbf{A}_{24} & \mathbf{0} & \mathbf{0} & \mathbf{0} \\ \mathbf{A}_{31} & \mathbf{A}_{32} & \mathbf{A}_{33} & \mathbf{A}_{34} & \mathbf{0} & \mathbf{0} & \mathbf{0} \\ \mathbf{A}_{41} & \mathbf{A}_{42} & \mathbf{A}_{43} & \mathbf{A}_{44} & \mathbf{A}_{45} & \mathbf{A}_{46} & \mathbf{A}_{47} \\ \mathbf{0} & \mathbf{0} & \mathbf{0} & \mathbf{A}_{54} & \mathbf{A}_{55} & \mathbf{A}_{56} & \mathbf{A}_{57} \\ \mathbf{0} & \mathbf{0} & \mathbf{0} & \mathbf{A}_{64} & \mathbf{A}_{65} & \mathbf{A}_{66} & \mathbf{A}_{67} \\ \mathbf{0} & \mathbf{0} & \mathbf{0} & \mathbf{A}_{74} & \mathbf{A}_{75} & \mathbf{A}_{76} & \mathbf{A}_{77} \end{pmatrix} \begin{pmatrix} \mathbf{X}^{M_S=0,I}_{O_{s_2}C_\alpha} \\ \mathbf{X}^{M_S=0,I}_{V_\beta O_{s_1}} \\ \mathbf{X}^{M_S=0,I}_{V_\beta C_\alpha} \\ \mathbf{X}^{M_S=0,I}_{O_{s_2}O_{s_1}} \\ \mathbf{X}^{M_S=0,I}_{V_\alpha C_\beta} \\ \mathbf{X}^{M_S=0,I}_{V_\alpha O_{s_1}} \\ \mathbf{X}^{M_S=0,I}_{O_{s_2}C_\beta} \end{pmatrix} = \omega_I \begin{pmatrix} \mathbf{X}^{M_S=0,I}_{O_{s_2}C_\alpha} \\ \mathbf{X}^{M_S=0,I}_{V_\beta O_{s_1}} \\ \mathbf{X}^{M_S=0,I}_{V_\beta C_\alpha} \\ \mathbf{X}^{M_S=0,I}_{O_{s_2}O_{s_1}} \\ \mathbf{X}^{M_S=0,I}_{V_\alpha C_\beta} \\ \mathbf{X}^{M_S=0,I}_{V_\alpha O_{s_1}} \\ \mathbf{X}^{M_S=0,I}_{O_{s_2}C_\beta} \end{pmatrix}, \tag{59}$$

where the amplitude vectors are $(\mathbf{X}^{M_S=0,I}_{V_\alpha C_\beta})_{bj} = X^{M_S=0,I}_{b\alpha j\beta}$, $(\mathbf{X}^{M_S=0,I}_{V_\alpha O_{s_1}})_{bz} = X^{M_S=0,I}_{b\alpha z s_1}$, and $(\mathbf{X}^{M_S=0,I}_{O_{s_2}C_\beta})_{wj} = X^{M_S=0,I}_{w s_2 j\beta}$, and $\mathbf{0}$ is the zero matrix block. Complete specifications of the block matrices $\mathbf{A}_{km}$ ($k,m = 1 \sim 7$) are given in the Tab. 3.

By spin symmetry, the block-coupling matrices from the $M_S = +1$ component are identical to the respective matrices from $M_S = -1$. Hence, the matrix elements of A satisfy

$$\mathbf{A}_{km} = \mathbf{A}_{(8-k)(8-m)}, \quad k,m = 1,2,3. \tag{60}$$

In addition, $\mathbf{A}$ is a symmetric matrix ($\mathbf{A} = \mathbf{A}^T$), see Tab. 3.

$$\left(\mathbf{A}_{11}\right)_{ui,wj} \equiv F^{(0)}_{u\beta w\beta}\delta_{ij} - F^{(0)}_{j\alpha i\alpha}\delta_{uw} + \frac{\partial F_{u\beta i\alpha}}{\partial P_{w\beta j\alpha}} \qquad \left(\mathbf{A}_{12}\right)_{ui,bz} \equiv \frac{\partial F_{u\beta i\alpha}}{\partial P_{b\beta z\alpha}}$$

$$\left(\mathbf{A}_{13}\right)_{ui,bj} \equiv F^{(0)}_{u\beta b\beta} + \delta_{ij}\frac{\partial F_{u\beta i\alpha}}{\partial P_{b\beta j\alpha}}, \qquad \left(\mathbf{A}_{14}\right)_{ui,wz} \equiv \frac{1}{\sqrt{2}}\left(-F^{(0)}_{z\alpha i\alpha}\delta_{uw} + \frac{\partial F_{u\beta i\alpha}}{\partial P_{w\beta z\alpha}}\right)$$

$$\left(\mathbf{A}_{21}\right)_{av,wj} \equiv \frac{\partial F_{a\beta v\alpha}}{\partial P_{w\beta j\alpha}} \qquad \left(\mathbf{A}_{22}\right)_{av,bz} \equiv F^{(0)}_{a\beta b\beta}\delta_{vz} - F^{(0)}_{z\alpha v\alpha}\delta_{ab} + \frac{\partial F_{a\beta v\alpha}}{\partial P_{b\beta z\alpha}},$$

$$\left(\mathbf{A}_{23}\right)_{av,bj} \equiv -F^{(0)}_{j\alpha v\alpha}\delta_{ab} + \frac{\partial F_{a\beta v\alpha}}{\partial P_{b\beta j\alpha}} \qquad \left(\mathbf{A}_{24}\right)_{av,wz} \equiv \frac{1}{\sqrt{2}}\left(F^{(0)}_{a\beta w\beta}\delta_{vz} + \frac{\partial F_{a\beta v\alpha}}{\partial P_{w\beta z\alpha}}\right)$$

$$\left(\mathbf{A}_{31}\right)_{ai,wj} \equiv F^{(0)}_{a\beta w\beta}\delta_{ij} + \frac{\partial F_{a\beta i\alpha}}{\partial P_{w\beta j\alpha}} \qquad \left(\mathbf{A}_{32}\right)_{ai,bz} \equiv -F^{(0)}_{j\alpha i\alpha}\delta_{ab} + \frac{\partial F_{a\beta i\alpha}}{\partial P_{b\beta z\alpha}}$$

$$\left(\mathbf{A}_{33}\right)_{ai,bj} \equiv F^{(0)}_{a\beta b\beta}\delta_{ij} - F^{(0)}_{j\alpha i\alpha}\delta_{ab} + \frac{\partial F_{a\beta i\alpha}}{\partial P_{b\beta j\alpha}} \qquad \left(\mathbf{A}_{34}\right)_{ai,wz} \equiv \frac{1}{\sqrt{2}}\frac{\partial F_{a\beta i\alpha}}{\partial P_{w\beta z\alpha}}$$

$$\left(\mathbf{A}_{41}\right)_{uv,wj} \equiv \frac{1}{\sqrt{2}}\left(-F^{(0)}_{j\alpha v\alpha}\delta_{uw} + \frac{\partial F_{u\beta v\alpha}}{\partial P_{w\beta j\alpha}}\right) \qquad \left(\mathbf{A}_{42}\right)_{uv,bz} \equiv \frac{1}{\sqrt{2}}\left(F^{(0)}_{u\beta b\beta}\delta_{vz} + \frac{\partial F_{u\beta v\alpha}}{\partial P_{b\beta z\alpha}}\right)$$

$$\left(\mathbf{A}_{43}\right)_{uv,bj} \equiv \frac{1}{\sqrt{2}}\frac{\partial F_{u\beta v\alpha}}{\partial P_{b\beta j\alpha}} \qquad \left(\mathbf{A}_{45}\right)_{uv,wj} \equiv \frac{1}{\sqrt{2}}\left(-\tilde{F}^{(0)}_{j\beta v\beta}\delta_{uw} + \frac{\partial F_{u\alpha v\beta}}{\partial P_{w\alpha j\beta}}\right)$$

$$\left(\mathbf{A}_{44}\right)_{uv,wz} \equiv \frac{1}{2}\left(F^{(0)}_{u\beta w\beta}\delta_{vz} - F^{(0)}_{z\alpha v\alpha}\delta_{uw} + \frac{\partial F_{u\beta v\alpha}}{\partial P_{w\beta z\alpha}}\right) + \frac{1}{2}\left(\tilde{F}^{(0)}_{u\alpha w\alpha}\delta_{vz} - \tilde{F}^{(0)}_{z\beta v\beta}\delta_{uw} + \frac{\partial F_{u\alpha v\beta}}{\partial P_{w\alpha z\beta}}\right)$$

$$\left(\mathbf{A}_{46}\right)_{uv,bz} \equiv \frac{1}{\sqrt{2}}\left(\tilde{F}^{(0)}_{u\alpha b\alpha}\delta_{vz} + \frac{\partial F_{u\alpha v\beta}}{\partial P_{b\alpha z\beta}}\right) \qquad \left(\mathbf{A}_{47}\right)_{uv,bj} \equiv \frac{1}{\sqrt{2}}\frac{\partial F_{u\alpha v\beta}}{\partial P_{b\alpha j\beta}}$$

$$\left(\mathbf{A}_{54}\right)_{ai,wz} \equiv \frac{1}{\sqrt{2}}\frac{\partial F_{a\alpha i\beta}}{\partial P_{w\alpha z\beta}} \qquad \left(\mathbf{A}_{55}\right)_{ai,bj} \equiv \tilde{F}^{(0)}_{a\alpha b\alpha}\delta_{ij} - \tilde{F}^{(0)}_{j\beta i\beta}\delta_{ab} + \frac{\partial F_{a\alpha i\beta}}{\partial P_{b\alpha j\beta}}$$

$$\left(\mathbf{A}_{56}\right)_{ai,bz} \equiv -\tilde{F}^{(0)}_{z\beta i\beta}\delta_{ab} + \frac{\partial F_{a\alpha i\beta}}{\partial P_{b\alpha z\beta}} \qquad \left(\mathbf{A}_{57}\right)_{ai,wj} \equiv \tilde{F}^{(0)}_{a\alpha w\alpha}\delta_{ij} + \frac{\partial F_{a\alpha i\beta}}{\partial P_{w\alpha j\beta}}$$

$$\left(\mathbf{A}_{64}\right)_{av,wz} \equiv \frac{1}{\sqrt{2}}\left(\tilde{F}^{(0)}_{a\alpha w\alpha}\delta_{vz} + \frac{\partial F_{a\alpha v\beta}}{\partial P_{w\alpha z\beta}}\right) \qquad \left(\mathbf{A}_{65}\right)_{av,bj} \equiv -\tilde{F}^{(0)}_{j\beta v\beta}\delta_{ab} + \frac{\partial F_{a\alpha v\beta}}{\partial P_{b\alpha j\beta}}$$

$$\left(\mathbf{A}_{66}\right)_{av,bz} \equiv \tilde{F}^{(0)}_{a\alpha b\alpha}\delta_{vz} - \tilde{F}^{(0)}_{z\beta v\beta}\delta_{ab} + \frac{\partial F_{a\alpha v\beta}}{\partial P_{b\alpha z\beta}} \qquad \left(\mathbf{A}_{67}\right)_{av,wj} \equiv \frac{\partial F_{a\alpha v\beta}}{\partial P_{w\alpha j\beta}}$$

$$\left(\mathbf{A}_{74}\right)_{ui,wz} \equiv \frac{1}{\sqrt{2}}\left(-\tilde{F}^{(0)}_{z\beta i\beta}\delta_{uw} + \frac{\partial F_{u\alpha i\beta}}{\partial P_{w\alpha z\beta}}\right) \qquad \left(\mathbf{A}_{75}\right)_{ui,bj} \equiv \tilde{F}^{(0)}_{u\alpha b\alpha}\delta_{ij} + \frac{\partial F_{u\alpha i\beta}}{\partial P_{b\alpha j\beta}}$$

$$\left(\mathbf{A}_{76}\right)_{ui,bz} \equiv \frac{\partial F_{u\alpha i\beta}}{\partial P_{b\alpha z\beta}} \qquad \left(\mathbf{A}_{77}\right)_{ui,wj} \equiv \tilde{F}^{(0)}_{u\alpha w\alpha}\delta_{ij} - \tilde{F}^{(0)}_{j\beta i\beta}\delta_{uw} + \frac{\partial F_{u\alpha i\beta}}{\partial P_{w\alpha j\beta}}$$

Table 3. Details of the block-coupling matrices. *The zeroth-order Fock matrix without a tilde denote that from M_S = +1 reference, while that with tilde is from M_S = -1 reference. Explicit expression of the kernel, $\partial \mathrm{F}_{p\sigma_p q\sigma_q}/\partial \mathrm{P}_{r\sigma_r s\sigma_s}$, with the collinear approximation is given in Eq. (38).*

2.3 Recovery of one-to-one relation between configuration and excitation amplitude

The excitation amplitudes $X^{M_S=0,I}_{ks_2ms_1}$ (k,m = O1,O2) correspond to the type I configurations, see Fig. 2. Unlike the other six types, this type of excitation amplitudes include amplitudes from both M_S = + 1 and −1 components of the mixed reference not from one. Figure 4 shows configurations and the KS determinants, which are labeled as G (ground), D (double), L (left), and R (right) according to the character of the excitation. A subscript added to the label represents the M_S value of the parent component of the reference state. With these notations, the amplitude $X^{M_S=0,I}_{O1s_2O2s_1}$ corresponds to the KS determinants $G_{\pm1}$, $X^{M_S=0,I}_{O2s_2O1s_1}$ to $D_{\pm1}$, $X^{M_S=0,I}_{O1s_2O1s_1}$ to L_{+1} and R_{-1}, and $X^{M_S=0,I}_{O2s_2O2s_1}$ to R_{+1} and L_{-1}. Although $X^{M_S=0,I}_{O1s_2O2s_1}$ and $X^{M_S=0,I}_{O2s_2O1s_1}$ correspond to specific G and D configurations, respectively, the signs of the respective determinants originating from different components of the mixed reference are opposite as shown in Fig. 4a and b, i.e., $G_{+1}=-G_{-1}$, $D_{+1}=-D_{-1}$. On the other hand, $X^{M_S=0,I}_{O1s_2O1s_1}$ corresponds to different configurations L and R originating from $M_S=1$ and –1, respectively, see Fig. 5a. A similar correspondence of configurations for $X^{M_S=0,I}_{O2s_2O2s_1}$ is shown in Fig. 5b.

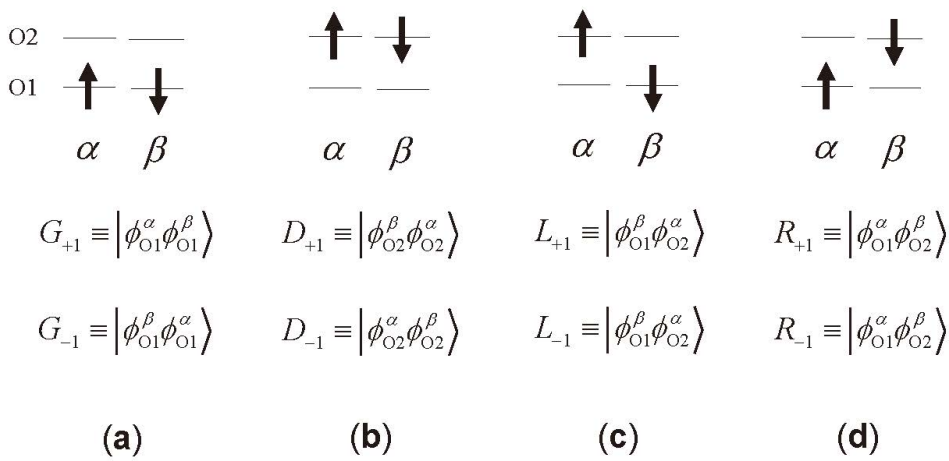

Figure. 4. Type I configurations and notation of their Slater determinants originating from spin flip transitions from the $M_S = +1$ and -1 components of mixed reference. *The subscript at the notation denotes the M_S value of the parent component.*

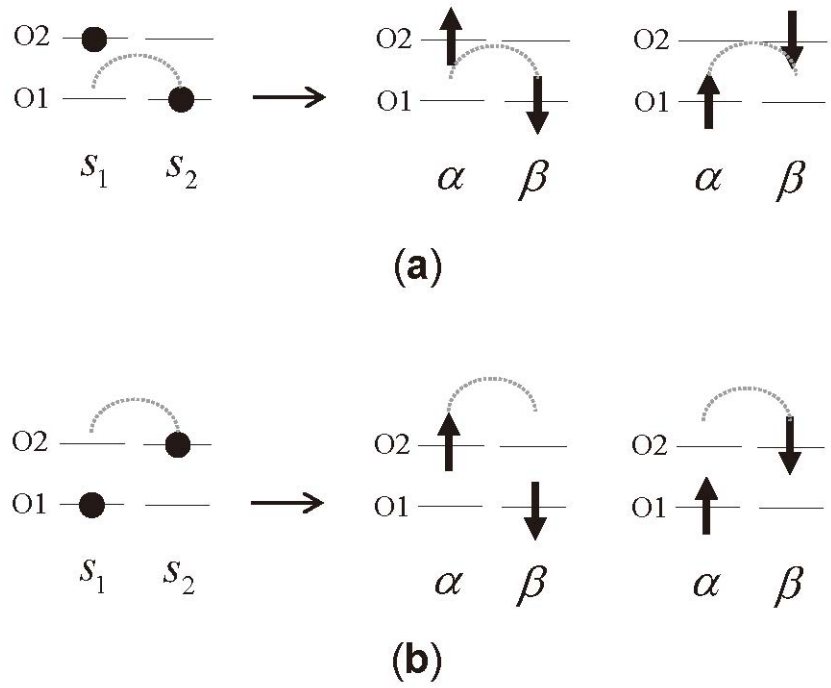

Figure. 5. Connection between one electron transition from the mixed-spin reference and that from the open-shell configuration. *Dotted curves show one-electron spin-flip excitation generating the given configuration.*

To obtain amplitudes corresponding to pure configurations *G, D, L,* and *R*, the respective part of the orbital Hessian matrix $\mathbf{A}$ needs to be modified in such a way as to resolve the sign changes (*G*, *D*) and mixed configurations (*L, R*). Equivalently, the corresponding EOM could be modified with the identical result. Before the modification, let us re-write the affected blocks in the fourth row or column of the $\mathbf{A}$ matrix in Eq. (59) in terms of the individual determinants shown in Fig. 4. The elements $\mathbf{A}_{k4}\,(k=1,2,3)$ in Eq. (59) correspond to the $\alpha \to \beta$ transitions from the $M_S = +1$ component and the elements $\mathbf{A}_{m4}\,(m=5,6,7)$ to the $\beta \to \alpha$ transitions from the $M_S = -1$ component. In terms of the determinants shown in Fig. 4, these elements are represented as

$$\mathbf{A}_{k4} = \left(\mathbf{A}_{kG_{+1}}\mathbf{A}_{kD_{+1}}\mathbf{A}_{kL_{+1}}\mathbf{A}_{kR_{+1}}\right), \qquad k=1,2,3, \tag{61}$$

$$\mathbf{A}_{m4} = \left(\mathbf{A}_{mG_{-1}}\mathbf{A}_{mD_{-1}}\mathbf{A}_{mR_{-1}}\mathbf{A}_{mL_{-1}}\right), \qquad m=5,6,7. \tag{62}$$

These block matrices satisfy the following symmetric relations as

$$\begin{cases} \mathbf{A}_{kG_{+1}} = \mathbf{A}_{(8-k)G_{-1}} \\ \mathbf{A}_{kD_{+1}} = \mathbf{A}_{(8-k)D_{-1}} \\ \mathbf{A}_{kL_{+1}} = \mathbf{A}_{(8-k)R_{-1}} \\ \mathbf{A}_{kR_{+1}} = \mathbf{A}_{(8-k)L_{-1}} \end{cases} \qquad k=1,2,3, \tag{63}$$

The first and second terms of $(\mathbf{A}_{44})_{O1O2,O1O2}$ (see Tab. 3) originate from

the $\alpha \to \beta$ and $\beta \to \alpha$ transitions from the $M_S = +1$ and $M_S = -1$ components, respectively. Hence, the individual contributions to this element can be represented as $A_{G_{+1}G_{+1}}$ and $A_{G_{-1}G_{-1}}$, respectively. With similar notations, the block matrix of the fourth row and column of the $\mathbf{A}$ matrix can be written out as

$$\mathbf{A}_{44} \equiv \begin{pmatrix} A_{GG} & A_{GD} & A_{GL} & A_{GR} \\ & A_{DD} & A_{DL} & A_{DR} \\ & & A_{LL} & A_{LR} \\ & & & A_{RR} \end{pmatrix}$$

$$= \frac{1}{2} \begin{pmatrix} A_{G_{+1}G_{+1}} + A_{G_{-1}G_{-1}} & A_{G_{+1}D_{+1}} + A_{G_{-1}D_{-1}} & A_{G_{+1}L_{+1}} + A_{G_{-1}R_{-1}} & A_{G_{+1}R_{+1}} + A_{G_{-1}L_{-1}} \\ & A_{D_{+1}D_{+1}} + A_{D_{-1}D_{-1}} & A_{D_{+1}L_{+1}} + A_{D_{-1}R_{-1}} & A_{D_{+1}R_{+1}} + A_{D_{-1}L_{-1}} \\ & & A_{L_{+1}L_{+1}} + A_{R_{-1}R_{-1}} & A_{L_{+1}R_{+1}} + A_{R_{-1}L_{-1}} \\ & & & A_{R_{+1}R_{+1}} + A_{L_{-1}L_{-1}} \end{pmatrix} \tag{64}$$

The lower triangular part is not shown in the above equations, because the block matrix $\mathbf{A}_{44}$ is symmetric, $\mathbf{A}_{44} = \mathbf{A}_{44}^T$. Parts of elements satisfy the following symmetric relations as

$$\begin{cases} A_{l_{+1}G_{+1}} = A_{m_{-1}G_{-1}} \\ A_{l_{+1}D_{+1}} = A_{m_{-1}D_{-1}} \\ A_{l_{+1}L_{+1}} = A_{m_{-1}R_{-1}} \\ A_{l_{+1}R_{+1}} = A_{m_{-1}L_{-1}} \end{cases} \qquad (l,m) = \{(G,G),(D,D),(L,R),(R,L)\}. \tag{65}$$

where the symmetry between L_{+1} and R_{-1} and between R_{+1} and L_{-1} is seen.

The Hessian $\mathbf{A}$ matrix can be written out as

$$\mathbf{A}=\begin{pmatrix}
\mathbf{A}_{11} & \mathbf{A}_{12} & \mathbf{A}_{13} & \mathbf{A}_{1G_{+1}} & \mathbf{A}_{1D_{+1}} & \mathbf{A}_{1L_{+1}} & \mathbf{A}_{1R_{+1}} & \mathbf{0} & \mathbf{0} & \mathbf{0} \\
 & \mathbf{A}_{22} & \mathbf{A}_{23} & \mathbf{A}_{2G_{+1}} & \mathbf{A}_{2D_{+1}} & \mathbf{A}_{2L_{+1}} & \mathbf{A}_{2R_{+1}} & \mathbf{0} & \mathbf{0} & \mathbf{0} \\
 & & \mathbf{A}_{33} & \mathbf{A}_{3G_{+1}} & \mathbf{A}_{3D_{+1}} & \mathbf{A}_{3L_{+1}} & \mathbf{A}_{3R_{+1}} & \mathbf{0} & \mathbf{0} & \mathbf{0} \\
 & & & A_{GG} & A_{GD} & A_{GL} & A_{GR} & \mathbf{A}_{G_{-1}3} & \mathbf{A}_{G_{-1}2} & \mathbf{A}_{G_{-1}1} \\
 & & & & A_{DD} & A_{DL} & A_{DR} & \mathbf{A}_{D_{-1}3} & \mathbf{A}_{D_{-1}2} & \mathbf{A}_{D_{-1}1} \\
 & & & & & A_{LL} & A_{LR} & \mathbf{A}_{R_{-1}3} & \mathbf{A}_{R_{-1}2} & \mathbf{A}_{R_{-1}1} \\
 & & & & & & A_{RR} & \mathbf{A}_{L_{-1}3} & \mathbf{A}_{L_{-1}2} & \mathbf{A}_{L_{-1}1} \\
 & & & & & & & \mathbf{A}_{33} & \mathbf{A}_{23} & \mathbf{A}_{13} \\
 & & & & & & & & \mathbf{A}_{22} & \mathbf{A}_{12} \\
 & & & & & & & & & \mathbf{A}_{11}
\end{pmatrix}, \quad (66)$$

where symmetry relations of Eq. (60) were used at $\mathbf{A}_{km}(k,m=5,6,7)$ and the lower triangular part is not shown with the same reason of Eq. (64). The advantage of the new labeling scheme for the matrix elements of $\mathbf{A}$ is that the contributions from $M_S=+1$ and $M_S=-1$ components can now be clearly identified.

With the new notation, amplitudes corresponding to G, D, L and R of Fig. 4 can be easily obtained by exchanging $R_{-1}\leftrightarrow L_{-1}$ in all the elements of Eqs. (64), (65) and (66) with simultaneous sign change of the elements for G_{-1} and D_{-1}; double replacement leaves the sign unchanged. Such an exchange is possible, because, ideally, amplitude and configuration should have one-to-one correspondence. For an

example, let us consider matrix elements of A_{GL} and A_{GR}, i.e., $A_{G_{+1}L_{+1}} + A_{G_{-1}R_{-1}}$ and $A_{G_{+1}R_{+1}} + A_{G_{-1}L_{-1}}$, respectively. As discussed above, one makes a sign change of $A_{G_{-1}L_{-1}}$ and $A_{G_{-1}R_{-1}}$ terms connected with G_{-1}, and exchanges these terms to bring L_{+1} together with L_{-1} and R_{+1} together with R_{-1}. Then, the modified elements become $A_{G_{+1}L_{+1}} - A_{G_{-1}L_{-1}}$ and $A_{G_{+1}R_{+1}} - A_{G_{-1}R_{-1}}$, which are denoted as B_{GL} and B_{GR}, in the following. The Hessian of Eq. (66) becomes modified by applying these discussions. The resulting Hessian matrix $\mathbf{A}_s^{(0)}$ is given by

$$\mathbf{A}_s^{(0)} = \begin{pmatrix}
\mathbf{A}_{11} & \mathbf{A}_{12} & \mathbf{A}_{13} & \mathbf{A}_{1G_{+1}} & \mathbf{A}_{1D_{+1}} & \mathbf{A}_{1L_{+1}} & \mathbf{A}_{1R_{+1}} & \mathbf{0} & \mathbf{0} & \mathbf{0} \\
 & \mathbf{A}_{22} & \mathbf{A}_{23} & \mathbf{A}_{2G_{+1}} & \mathbf{A}_{2D_{+1}} & \mathbf{A}_{2L_{+1}} & \mathbf{A}_{2R_{+1}} & \mathbf{0} & \mathbf{0} & \mathbf{0} \\
 & & \mathbf{A}_{33} & \mathbf{A}_{3G_{+1}} & \mathbf{A}_{3D_{+1}} & \mathbf{A}_{3L_{+1}} & \mathbf{A}_{3R_{+1}} & \mathbf{0} & \mathbf{0} & \mathbf{0} \\
 & & & B_{GG} & B_{GD} & B_{GL} & B_{GR} & -\mathbf{A}_{G_{-1}3} & -\mathbf{A}_{G_{-1}2} & -\mathbf{A}_{G_{-1}1} \\
 & & & & B_{DD} & B_{DL} & B_{DR} & -\mathbf{A}_{D_{-1}3} & -\mathbf{A}_{D_{-1}2} & -\mathbf{A}_{D_{-1}1} \\
 & & & & & B_{LL} & B_{LR} & \mathbf{A}_{L_{-1}3} & \mathbf{A}_{L_{-1}2} & \mathbf{A}_{L_{-1}1} \\
 & & & & & & B_{RR} & \mathbf{A}_{R_{-1}3} & \mathbf{A}_{R_{-1}2} & \mathbf{A}_{R_{-1}1} \\
 & & & & & & & \mathbf{A}_{33} & \mathbf{A}_{23} & \mathbf{A}_{13} \\
 & & & & & & & & \mathbf{A}_{22} & \mathbf{A}_{12} \\
 & & & & & & & & & \mathbf{A}_{11}
\end{pmatrix}, \tag{67}$$

where the superscript (0) in the orbital Hessian matrix do not denote the zeroth-order quantity but will denote Hessian without spin-pairing coupling, and rearranged coupling between type I configurations are

$$\begin{pmatrix} B_{GG} & B_{GD} & B_{GL} & B_{GR} \\ & B_{DD} & B_{DL} & B_{DR} \\ & & B_{LL} & B_{LR} \\ & & & B_{RR} \end{pmatrix}$$

$$= \frac{1}{2}\begin{pmatrix} A_{G_{+1}G_{+1}} + A_{G_{-1}G_{-1}} & A_{G_{+1}D_{+1}} + A_{G_{-1}D_{-1}} & A_{G_{+1}L_{+1}} - A_{G_{-1}L_{-1}} & A_{G_{+1}R_{+1}} - A_{G_{-1}R_{-1}} \\ & A_{D_{+1}D_{+1}} + A_{D_{-1}D_{-1}} & A_{D_{+1}L_{+1}} - A_{D_{-1}L_{-1}} & A_{D_{+1}R_{+1}} - A_{D_{-1}R_{-1}} \\ & & A_{L_{+1}L_{+1}} + A_{L_{-1}L_{-1}} & A_{L_{+1}R_{+1}} + A_{L_{-1}R_{-1}} \\ & & & A_{R_{+1}R_{+1}} + A_{R_{-1}R_{-1}} \end{pmatrix}. \quad (68)$$

As $A_{G_{+1}L_{+1}} = A_{G_{-1}R_{-1}}$ and $A_{G_{+1}R_{+1}} = A_{G_{-1}L_{-1}}$ in Eq. (65), a new relation $B_{GL} = -B_{GR}$ holds. Likewise, new symmetric relations of $B_{DL} = -B_{DR}$ and $B_{LL} = B_{RR}$ also appear. These symmetric relations completely eliminate the spin-contamination of type I in the response states.

In addition, with spin-pairing coupling which will be introduced in subsection 3 of *Spin-pairing coupling*, Hessian matrix $\mathbf{A}_s$ is given by

$$\mathbf{A}_s = \begin{pmatrix} \mathbf{A}_{11} & \mathbf{A}_{12} & \mathbf{A}_{13} & \mathbf{A}_{1G_{+1}} & \mathbf{A}_{1D_{+1}} & \mathbf{A}_{1L_{+1}} & \mathbf{A}_{1R_{+1}} & \mathbf{C}_{13} & \mathbf{C}_{12} & \mathbf{C}_{11} \\ & \mathbf{A}_{22} & \mathbf{A}_{23} & \mathbf{A}_{2G_{+1}} & \mathbf{A}_{2D_{+1}} & \mathbf{A}_{2L_{+1}} & \mathbf{A}_{2R_{+1}} & \mathbf{C}_{23} & \mathbf{C}_{22} & \mathbf{C}_{21} \\ & & \mathbf{A}_{33} & \mathbf{A}_{3G_{+1}} & \mathbf{A}_{3D_{+1}} & \mathbf{A}_{3L_{+1}} & \mathbf{A}_{3R_{+1}} & \mathbf{C}_{33} & \mathbf{C}_{32} & \mathbf{C}_{31} \\ & & & B_{GG} & B_{GD} & B_{GL} & B_{GR} & -\mathbf{A}_{G_{-1}3} & -\mathbf{A}_{G_{-1}2} & -\mathbf{A}_{G_{-1}1} \\ & & & & B_{DD} & B_{DL} & B_{DR} & -\mathbf{A}_{D_{-1}3} & -\mathbf{A}_{D_{-1}2} & -\mathbf{A}_{D_{-1}1} \\ & & & & & B_{LL} & B_{LR} & \mathbf{A}_{L_{-1}3} & \mathbf{A}_{L_{-1}2} & \mathbf{A}_{L_{-1}1} \\ & & & & & & B_{RR} & \mathbf{A}_{R_{-1}3} & \mathbf{A}_{R_{-1}2} & \mathbf{A}_{R_{-1}1} \\ & & & & & & & \mathbf{A}_{33} & \mathbf{A}_{23} & \mathbf{A}_{13} \\ & & & & & & & & \mathbf{A}_{22} & \mathbf{A}_{12} \\ & & & & & & & & & \mathbf{A}_{11} \end{pmatrix}. \quad (69)$$

2.4 Separating matrix equations for singlet and triplet response states

Pure spin configurations are obtained by pairing the respective configurations originating from $M_S = +1$ and -1 references for the type I, II and III (see Fig. 2), which is achieved by a unitary transformation

$$\mathbf{U}' = \frac{1}{\sqrt{2}} \begin{pmatrix} \mathbf{I}_{OC} & \mathbf{0} & \mathbf{0} & \mathbf{0} & \mathbf{0} & \mathbf{0} & \mathbf{0} & \mathbf{0} & \mathbf{0} & \mathbf{I}_{OC} \\ \mathbf{0} & \mathbf{I}_{OV} & \mathbf{0} & \mathbf{0} & \mathbf{0} & \mathbf{0} & \mathbf{0} & \mathbf{0} & \mathbf{I}_{OV} & \mathbf{0} \\ \mathbf{0} & \mathbf{0} & \mathbf{I}_{VC} & \mathbf{0} & \mathbf{0} & \mathbf{0} & \mathbf{0} & \mathbf{I}_{VC} & \mathbf{0} & \mathbf{0} \\ \mathbf{0} & \mathbf{0} & \mathbf{0} & \sqrt{2} & 0 & 0 & 0 & \mathbf{0} & \mathbf{0} & \mathbf{0} \\ \mathbf{0} & \mathbf{0} & \mathbf{0} & 0 & \sqrt{2} & 0 & 0 & \mathbf{0} & \mathbf{0} & \mathbf{0} \\ \mathbf{0} & \mathbf{0} & \mathbf{0} & 0 & 0 & 1 & 1 & \mathbf{0} & \mathbf{0} & \mathbf{0} \\ \mathbf{0} & \mathbf{0} & \mathbf{0} & 0 & 0 & 1 & -1 & \mathbf{0} & \mathbf{0} & \mathbf{0} \\ \mathbf{0} & \mathbf{0} & \mathbf{I}_{VC} & \mathbf{0} & \mathbf{0} & \mathbf{0} & \mathbf{0} & -\mathbf{I}_{VC} & \mathbf{0} & \mathbf{0} \\ \mathbf{0} & \mathbf{I}_{OV} & \mathbf{0} & \mathbf{0} & \mathbf{0} & \mathbf{0} & \mathbf{0} & \mathbf{0} & -\mathbf{I}_{OV} & \mathbf{0} \\ \mathbf{I}_{OC} & \mathbf{0} & \mathbf{0} & \mathbf{0} & \mathbf{0} & \mathbf{0} & \mathbf{0} & \mathbf{0} & \mathbf{0} & -\mathbf{I}_{OC} \end{pmatrix}, \quad (70)$$

with $(\mathbf{I}_{OC})_{ui,wj} = \delta_{uw}\delta_{ij}$, $(\mathbf{I}_{OV})_{av,bz} = \delta_{ab}\delta_{vz}$, $(\mathbf{I}_{VC})_{ai,bj} = \delta_{ab}\delta_{ij}$ and $(\mathbf{I}_{OO})_{uv,wz} = \delta_{uw}\delta_{vz}$.

The rotated amplitude vector by the transformation matrix is given by

$$\mathbf{U}'\mathbf{X}_I = \begin{pmatrix} (\mathbf{X}^{M_S=0,I}_{O_{s_2}C_\alpha} + \mathbf{X}^{M_S=0,I}_{O_{s_2}C_\beta})/\sqrt{2} \\ (\mathbf{X}^{M_S=0,I}_{V_\beta O_{s_1}} + \mathbf{X}^{M_S=0,I}_{V_\alpha O_{s_1}})/\sqrt{2} \\ (\mathbf{X}^{M_S=0,I}_{V_\beta C_\alpha} + \mathbf{X}^{M_S=0,I}_{V_\alpha C_\beta})/\sqrt{2} \\ X^{M_S=0,I}_{G} \\ X^{M_S=0,I}_{D} \\ (X^{M_S=0,I}_{L} + X^{M_S=0,I}_{R})/\sqrt{2} \\ (X^{M_S=0,I}_{L} - X^{M_S=0,I}_{R})/\sqrt{2} \\ (\mathbf{X}^{M_S=0,I}_{V_\beta C_\alpha} - \mathbf{X}^{M_S=0,I}_{V_\alpha C_\beta})/\sqrt{2} \\ (\mathbf{X}^{M_S=0,I}_{V_\beta O_{s_1}} - \mathbf{X}^{M_S=0,I}_{V_\alpha O_{s_1}})/\sqrt{2} \\ (\mathbf{X}^{M_S=0,I}_{O_{s_2}C_\alpha} - \mathbf{X}^{M_S=0,I}_{O_{s_2}C_\beta})/\sqrt{2} \end{pmatrix}. \quad (71)$$

and the orbital Hessian matrix $\mathbf{A}_s^{(0)}$ of Eq. (67) can be split into two blocks with the rotation as

$$\mathbf{A}^{(T)(0)} = \begin{pmatrix} \mathbf{A}_{11} & \mathbf{A}_{12} & \mathbf{A}_{13} & \mathbf{A}_{1L_{+1}} + \mathbf{A}_{1R_{+1}} \\ \mathbf{A}_{21} & \mathbf{A}_{22} & \mathbf{A}_{23} & \mathbf{A}_{2L_{+1}} + \mathbf{A}_{2R_{+1}} \\ \mathbf{A}_{31} & \mathbf{A}_{32} & \mathbf{A}_{33} & \mathbf{A}_{3L_{+1}} + \mathbf{A}_{3R_{+1}} \\ \mathbf{A}_{L_{+1}1} + \mathbf{A}_{R_{+1}1} & \mathbf{A}_{2L_{+1}} + \mathbf{A}_{2R_{+1}} & \mathbf{A}_{L_{+1}3} + \mathbf{A}_{R_{+1}3} & B_{LL} + B_{LR} \end{pmatrix}, \quad (72)$$

$$\mathbf{A}^{(S)(0)} = \begin{pmatrix} B_{GG} & B_{GD} & \sqrt{2}B_{GL} & \sqrt{2}\mathbf{A}_{G_{+1}3} & \sqrt{2}\mathbf{A}_{G_{+1}2} & \sqrt{2}\mathbf{A}_{G_{+1}1} \\ B_{GD} & B_{DD} & \sqrt{2}B_{DL} & \sqrt{2}\mathbf{A}_{D_{+1}3} & \sqrt{2}\mathbf{A}_{D_{+1}2} & \sqrt{2}\mathbf{A}_{D_{+1}1} \\ \sqrt{2}B_{GL} & \sqrt{2}B_{DL} & B_{LL} - B_{LR} & \mathbf{A}_{L_{+1}3} - \mathbf{A}_{R_{+1}3} & \mathbf{A}_{L_{+1}2} - \mathbf{A}_{R_{+1}2} & \mathbf{A}_{L_{+1}1} - \mathbf{A}_{R_{+1}1} \\ \sqrt{2}\mathbf{A}_{3G_{+1}} & \sqrt{2}\mathbf{A}_{3D_{+1}} & \mathbf{A}_{3L_{+1}} - \mathbf{A}_{3R_{+1}} & \mathbf{A}_{33} & \mathbf{A}_{23} & \mathbf{A}_{13} \\ \sqrt{2}\mathbf{A}_{2G_{+1}} & \sqrt{2}\mathbf{A}_{2D_{+1}} & \mathbf{A}_{2L_{+1}} - \mathbf{A}_{2R_{+1}} & \mathbf{A}_{23} & \mathbf{A}_{22} & \mathbf{A}_{12} \\ \sqrt{2}\mathbf{A}_{1G_{+1}} & \sqrt{2}\mathbf{A}_{1D_{+1}} & \mathbf{A}_{1L_{+1}} - \mathbf{A}_{1R_{+1}} & \mathbf{A}_{13} & \mathbf{A}_{12} & \mathbf{A}_{11} \end{pmatrix}. \quad (73)$$

Hence, two matrix equations

$$\mathbf{A}^{(T)(0)}\mathbf{X}_I^{(T)(0)} = \Omega_{(T)(0)}^I \mathbf{X}_I^{(T)(0)}, \quad (74)$$

$$\mathbf{A}^{(S)(0)}\mathbf{X}_I^{(S)(0)} = \Omega_{(S)(0)}^I \mathbf{X}_I^{(S)(0)}, \quad (75)$$

are obtained, for the triplet (T) and singlet (S) state amplitudes. In these equations, the excitation amplitude vectors are

$$\mathbf{X}_I^{(T)(0)} \equiv \begin{pmatrix} \mathbf{X}_{\mathrm{CO}}^{(T)(0),I} \\ \mathbf{X}_{\mathrm{OV}}^{(T)(0),I} \\ \mathbf{X}_{\mathrm{CV}}^{(T)(0),I} \\ X_{\mathrm{OOT}}^{(T)(0),I} \end{pmatrix} = \begin{pmatrix} (\mathbf{X}_{\mathrm{Os_2C}\alpha}^{M_S=0,I} + \mathbf{X}_{\mathrm{Os_2C}\beta}^{M_S=0,I})/\sqrt{2} \\ (\mathbf{X}_{\mathrm{V}_\beta\mathrm{O}s_1}^{M_S=0,I} + \mathbf{X}_{\mathrm{V}_\alpha\mathrm{O}s_1}^{M_S=0,I})/\sqrt{2} \\ (\mathbf{X}_{\mathrm{V}_\beta\mathrm{C}_\alpha}^{M_S=0,I} + \mathbf{X}_{\mathrm{V}_\alpha\mathrm{C}_\beta}^{M_S=0,I})/\sqrt{2} \\ (X_{\mathrm{L}}^{M_S=0,I} + X_{\mathrm{R}}^{M_S=0,I})/\sqrt{2} \end{pmatrix}, \quad (76)$$

$$\mathbf{X}_I^{(S)(0)} \equiv \begin{pmatrix} X_{\mathrm{G}}^{(S)(0),I} \\ X_{\mathrm{D}}^{(S)(0),I} \\ X_{\mathrm{OOS}}^{(S)(0),I} \\ \mathbf{X}_{\mathrm{CV}}^{(S)(0),I} \\ \mathbf{X}_{\mathrm{OV}}^{(S)(0),I} \\ \mathbf{X}_{\mathrm{CO}}^{(S)(0),I} \end{pmatrix} = \begin{pmatrix} X_{\mathrm{G}}^{M_S=0,I} \\ X_{\mathrm{D}}^{M_S=0,I} \\ (X_{\mathrm{L}}^{M_S=0,I} - X_{\mathrm{R}}^{M_S=0,I})/\sqrt{2} \\ (\mathbf{X}_{\mathrm{V}_\beta\mathrm{C}_\alpha}^{M_S=0,I} - \mathbf{X}_{\mathrm{V}_\alpha\mathrm{C}_\beta}^{M_S=0,I})/\sqrt{2} \\ (\mathbf{X}_{\mathrm{V}_\beta\mathrm{O}_{s_1}}^{M_S=0,I} - \mathbf{X}_{\mathrm{V}_\alpha\mathrm{O}_{s_1}}^{M_S=0,I})/\sqrt{2} \\ (\mathbf{X}_{\mathrm{O}_{s_2}\mathrm{C}_\alpha}^{M_S=0,I} - \mathbf{X}_{\mathrm{O}_{s_2}\mathrm{C}_\beta}^{M_S=0,I})/\sqrt{2} \end{pmatrix}. \quad (77)$$

Here also, the superscript (0) do not denote the zeroth-order quantity but will denote quantity without spin-pairing coupling. The new response equations (74) and (75) yield spin-adapted excited states, where a complete decontamination of the type I, II and type III configurations is achieved. Hence, clean separation of triplet and singlet states is achieved in MRSF-TDDFT; which is an advantage before the standard SF-TDDFT formalism.

For the type IV configurations, only one missing configuration (out of five) is recovered in MRSF-TDDFT and spin-adaptation of this type of configurations remains incomplete. However, contribution of these configurations into the low lying excited states is expected to be small and the resulting spin contamination insignificant.

Likewise, rotation of the Hessian matrix $\mathbf{A}_s$ of Eq. (69), which can be split into two blocks

$$\mathbf{A}^{(T)} = \begin{pmatrix} \mathbf{A}_{11}+\mathbf{C}_{11} & \mathbf{A}_{12}+\mathbf{C}_{12} & \mathbf{A}_{13}+\mathbf{C}_{13} & \mathbf{A}_{1L_{+1}}+\mathbf{A}_{1R_{+1}} \\ \mathbf{A}_{12}+\mathbf{C}_{12} & \mathbf{A}_{22}+\mathbf{C}_{22} & \mathbf{A}_{23}+\mathbf{C}_{23} & \mathbf{A}_{2L_{+1}}+\mathbf{A}_{2R_{+1}} \\ \mathbf{A}_{13}+\mathbf{C}_{13} & \mathbf{A}_{23}+\mathbf{C}_{23} & \mathbf{A}_{33}+\mathbf{C}_{33} & \mathbf{A}_{3L_{+1}}+\mathbf{A}_{3R_{+1}} \\ \mathbf{A}_{L_{+1}1}+\mathbf{A}_{R_{+1}1} & \mathbf{A}_{2L_{+1}}+\mathbf{A}_{2R_{+1}} & \mathbf{A}_{L_{+1}3}+\mathbf{A}_{R_{+1}3} & B_{LL}+B_{LR} \end{pmatrix}, \qquad (78)$$

$$\mathbf{A}^{(S)} = \begin{pmatrix} B_{GG} & B_{GD} & \sqrt{2}B_{GL} & \sqrt{2}\mathbf{A}_{G_{+1}3} & \sqrt{2}\mathbf{A}_{G_{+1}2} & \sqrt{2}\mathbf{A}_{G_{+1}1} \\ B_{GD} & B_{DD} & \sqrt{2}B_{DL} & \sqrt{2}\mathbf{A}_{D_{+1}3} & \sqrt{2}\mathbf{A}_{D_{+1}2} & \sqrt{2}\mathbf{A}_{D_{+1}1} \\ \sqrt{2}B_{GL} & \sqrt{2}B_{DL} & B_{LL}-B_{LR} & \mathbf{A}_{L_{+1}3}-\mathbf{A}_{R_{+1}3} & \mathbf{A}_{L_{+1}2}-\mathbf{A}_{R_{+1}2} & \mathbf{A}_{L_{+1}1}-\mathbf{A}_{R_{+1}1} \\ \sqrt{2}\mathbf{A}_{3G_{+1}} & \sqrt{2}\mathbf{A}_{3D_{+1}} & \mathbf{A}_{3L_{+1}}-\mathbf{A}_{3R_{+1}} & \mathbf{A}_{33}-\mathbf{C}_{33} & \mathbf{A}_{23}-\mathbf{C}_{23} & \mathbf{A}_{13}-\mathbf{C}_{13} \\ \sqrt{2}\mathbf{A}_{2G_{+1}} & \sqrt{2}\mathbf{A}_{2D_{+1}} & \mathbf{A}_{2L_{+1}}-\mathbf{A}_{2R_{+1}} & \mathbf{A}_{23}-\mathbf{C}_{23} & \mathbf{A}_{22}-\mathbf{C}_{22} & \mathbf{A}_{12}-\mathbf{C}_{12} \\ \sqrt{2}\mathbf{A}_{1G_{+1}} & \sqrt{2}\mathbf{A}_{1D_{+1}} & \mathbf{A}_{1L_{+1}}-\mathbf{A}_{1R_{+1}} & \mathbf{A}_{13}-\mathbf{C}_{13} & \mathbf{A}_{12}-\mathbf{C}_{12} & \mathbf{A}_{11}-\mathbf{C}_{11} \end{pmatrix}, \qquad (79)$$

leads to two sets of response equations

$$\mathbf{A}^{(T)}\mathbf{X}_I^{(T)} = \Omega_{(T)}^I \mathbf{X}_I^{(T)}, \qquad (80)$$

$$\mathbf{A}^{(S)}\mathbf{X}_I^{(S)} = \Omega_{(S)}^I \mathbf{X}_I^{(S)}, \qquad (81)$$

2.5 Expectation value of S^2 operator for response states of MRSF-TDDFT

It has been a common practice that the spin-contamination of TDDFT is measured by the operation of $\mathbf{S}^2$ on a wave function of noninteracting system. The $\mathbf{S}^2$ operator is represented as

$$\mathbf{S}^2 = S_z(S_z+1)+S_-S_+, \quad \text{with} \qquad (82)$$

$$S_z = \sum_m s_z(m), \tag{83}$$

$$S_\pm = \sum_m s_\pm(m), \tag{84}$$

where $s_z(m)$, $s_+(m)$, and $s_-(m)$ are the one-electron operators of the spin z-component, spin raising and lowering operators for the mth electron, respectively. In the second quantization, the $S_\pm$ operators are

$$S_- = \sum_p a^\dagger_{p\beta} a_{p\alpha}, \tag{85}$$

$$S_+ = \sum_q a^\dagger_{q\alpha} a_{q\beta}, \tag{86}$$

where the p and q indices are running over all the MOs and the $a^\dagger_{p\sigma_p}$, $a_{p\sigma_p}$ ($\sigma_p = \alpha, \beta$) are the creation and annihilation operators of electron in the $\phi_p^{\sigma_p}$ orbital. Therefore, the last term of Eq. (82) can be written as

$$S_- S_+ = \sum_{p,q} a^\dagger_{p\beta} a_{p\alpha} a^\dagger_{q\alpha} a_{q\beta}. \tag{87}$$

With the help of the anti-commutation relations, the above equation is re-written as

$$S_- S_+ = \sum_p a^\dagger_{p\beta} a_{p\beta} - \sum_{p,q} a^\dagger_{p\beta} a^\dagger_{q\alpha} a_{p\alpha} a_{q\beta}. \tag{88}$$

The second term on the right hand side of above equation can be split as

$$S_- S_+ = \sum_p a^\dagger_{p\beta} a_{p\beta} - \sum_p a^\dagger_{p\beta} a^\dagger_{p\alpha} a_{p\alpha} a_{p\beta} - \sum_{\substack{p,q \\ p \neq q}} a^\dagger_{p\beta} a^\dagger_{q\alpha} a_{p\alpha} a_{q\beta}. \tag{89}$$

The three terms on right hand side of Eq. (89) correspond to the operators of the number of electrons in the β-spin MOs, in the doubly occupied MOs, and in the open-shell configurations with two singly occupied MOs, respectively. The MR-SF-TDDFT wavefunction for an excited state with $M_S = 0$ is

$$\begin{aligned}\Psi^{(S)} = & X_G^{M_S=0,I}\Psi_{\mathrm{O1}\beta\mathrm{O2}\alpha}^{M_S=+1} + X_D^{M_S=0,I}\Psi_{\mathrm{O2}\beta\mathrm{O1}\alpha}^{M_S=+1} + X_L^{M_S=0,I}\Psi_{\mathrm{O1}\beta\mathrm{O1}\alpha}^{M_S=+1} + X_R^{M_S=0,I}\Psi_{\mathrm{O2}\beta\mathrm{O2}\alpha}^{M_S=+1} \\ & + \sum_{ui}\left(X_{us_2i\alpha}^{M_S=0,I}\Psi_{u\beta i\alpha}^{M_S=+1} + X_{us_2i\beta}^{M_S=0,I}\Psi_{u\alpha i\beta}^{M_S=-1} \right) + \sum_{aw}\left(X_{a\beta ws_1}^{M_S=0,I}\Psi_{a\beta w\alpha}^{M_S=+1} + X_{a\alpha ws_1}^{M_S=0,I}\Psi_{a\alpha w\beta}^{M_S=-1} \right) \\ & + \sum_{ai}\left(X_{a\beta i\alpha}^{M_S=0,I}\Psi_{a\beta i\alpha}^{M_S=+1} + X_{a\alpha i\beta}^{M_S=0,I}\Psi_{a\alpha i\beta}^{M_S=-1} \right)\end{aligned} \tag{90}$$

where $\Psi_{p\beta q\alpha}^{M_S=+1}$ and $\Psi_{p\alpha q\beta}^{M_S=-1}$ are the determinants obtained by the spin-flip transitions from the $M_S = +1$ and $M_S = -1$ components of the mixed reference state, respectively. The first four terms on the right hand side of Eq. (90) correspond to the type I configurations, see Fig. 2, while 5th, 6th, 7th terms represent the type II, III, IV, respectively. Using Ψ_I the expectation value of $\mathbf{S}^2$ becomes

$$\left\langle \Psi_I \left| \mathbf{S}^2 \right| \Psi_I \right\rangle = \left\langle \Psi_I \left| S_z(S_z+1) \right| \Psi_I \right\rangle + \left\langle \Psi_I \left| S_- S_+ \right| \Psi_I \right\rangle. \tag{91}$$

where the first term on the right hand side vanishes, since $M_S = 0$, and the second term is given by

$$\begin{aligned}\left\langle \Psi_I \left| S_- S_+ \right| \Psi_I \right\rangle = & 1 - \left(X_G^{M_S=0,I} \right)^2 - \left(X_D^{M_S=0,I} \right)^2 + 2X_L^{M_S=0,I} X_R^{M_S=0,I} \\ & + 2\Big(\sum_{us} X_{us_2i\alpha}^{M_S=0,I} X_{us_2i\beta}^{M_S=0,I} + \sum_{aw} X_{a\beta ws_1}^{M_S=0,I} X_{a\alpha ws_1}^{M_S=0,I} + \sum_{ai} X_{a\beta i\alpha}^{M_S=0,I} X_{a\alpha i\beta}^{M_S=0,I} \Big).\end{aligned} \tag{92}$$

Magnitudes of two amplitudes for each pair which is $(X_L^{M_S=0,I}, X_R^{M_S=0,I})$, $(X_{Os_2C\alpha}^{M_S=0,I}, X_{Os_2C\beta}^{M_S=0,I})$, $(X_{V\beta Os_1}^{M_S=0,I}, X_{V\alpha Os_1}^{M_S=0,I})$, or $(X_{V\beta C\alpha}^{M_S=0,I}, X_{V\alpha C\beta}^{M_S=0,I})$ are same, while those sign are different and same for singlet and triplet response states, respectively. Thus, with the orthonormal condition, the expectation values of $\mathbf{S}^2$ for singlet and triplet response states are always 0 and 2, respectively. This shows that MRSF-TDDFT eliminates spin contamination of SF-TDDFT for singlet and triplet response states. As discussed in the beginning of this section, there is still quintet mixing for C→V configurations but it is minor contribution for low-lying excited states.

2.6 Dimensional transformation matrix

The different singlet and triplet response dimensions of MRSF-TDDFT as compared to SF-TDDFT could introduce complications to the subsequent derivations and potentially require a major modification to the existing SF-TDDFT code. Therefore, in this subsection, we introduce dimensional-transformation $U_{pq}^{(S)}$ and $U_{pq}^{(T)}$ matrices, which cause the singlet and triplet response dimensions of MRSF-TDDFT to be equal to that of SF-TDDFT. With these transformation matrices,

the expanded X vectors, which have the same dimension of SF-TDDFT, can be represented as $U_{pq}^{(S)} X_{pq}^{(S)(0)}$ and $U_{pq}^{(T)} X_{pq}^{(T)(0)}$ for the singlet and triplet response spaces, respectively. For example, the expanded X vectors of G and D configurations for the singlet and triplet spaces, respectively, are defined as:

$$U_{pq}^{(S)G} X_{G}^{(S)(0)} \equiv \delta_{pO2}\delta_{qO1} X_{G}^{(S)(0)}, \tag{93a}$$

$$U_{pq}^{(S)D} X_{D}^{(S)(0)} \equiv \delta_{pO1}\delta_{qO2} X_{D}^{(S)(0)}, \tag{93b}$$

$$U_{pq}^{(T)G} X_{G}^{(T)(0)} \equiv 0, \tag{94a}$$

$$U_{pq}^{(T)D} X_{D}^{(T)(0)} \equiv 0. \tag{94b}$$

Likewise, the expanded X vectors of OOS and OOT configurations for the singlet and triplet spaces, respectively, are defined as:

$$U_{pq}^{OOS} X_{OOS}^{(S)(0)} \equiv \frac{1}{\sqrt{2}}\left(\delta_{pO1}\delta_{qO1} - \delta_{pO2}\delta_{qO2}\right) X_{OOS}^{(S)(0)}, \tag{95}$$

$$U_{pq}^{OOT} X_{OOT}^{(T)(0)} \equiv \frac{1}{\sqrt{2}}\left(\delta_{pO1}\delta_{qO1} + \delta_{pO2}\delta_{qO2}\right) X_{OOT}^{(T)(0)}. \tag{96}$$

Note that the one-dimensional excitation amplitudes of $X_{OOS}^{(S)(0)}$ and $X_{OOT}^{(T)(0)}$ are represented as two-dimensional excitation amplitudes of ($U_{O1O1}^{(S)OO} X_{OOS}^{(S)(0)}$, $U_{O2O2}^{(S)OO} X_{OOS}^{(S)(0)}$) and ($U_{O1O1}^{(T)OO} X_{OOT}^{(T)(0)}$, $U_{O2O2}^{(T)OO} X_{OOT}^{(T)(0)}$), respectively. As compared to the OO type, the U_{pq}^{COm}, U_{pq}^{OmV}, and U_{pq}^{CV} are defined without changing their dimensions as:

$$U_{pq}^{COm} X_{pq}^{(k)(0)} \equiv \delta_{p<O1}\delta_{qOm} X_{pq}^{(k)(0)}, \tag{97}$$

$$U_{pq}^{OmV} X_{pq}^{(k)(0)} \equiv \delta_{pOm} \delta_{q>O2} X_{pq}^{(k)(0)}, \tag{98}$$

$$U_{pq}^{CV} X_{pq}^{(k)(0)} \equiv \delta_{p<O1} \delta_{q>O2} X_{pq}^{(k)(0)}, \tag{99}$$

where $m = 1, 2$, $k = S, T$, and

$$\delta_{p<O1} = 1 \text{ for } p < O1, \ \delta_{p<O1} = 0 \text{ for } p \geq O1, \tag{100a}$$

$$\delta_{q>O2} = 1 \text{ for } q > O2, \ \delta_{q>O2} = 0 \text{ for } q \leq O2. \tag{100b}$$

As a result, the expanded dimensions of both singlet and triplet response spaces are equal to $n_{occ}^{\alpha} n_{vir}^{\beta}$ of SF-TDDFT. With the help of these transformation matrices, the expanded single and triplet response spaces can be elegantly defined, respectively, as:

$$U_{pq}^{(S)} \equiv U_{pq}^{(S)G} + U_{pq}^{(S)D} + U_{pq}^{OOS} + U_{pq}^{CO1} + U_{pq}^{CO2} + U_{pq}^{O1V} + U_{pq}^{O2V} + U_{pq}^{CV}, \tag{101a}$$

$$U_{pq}^{(T)} \equiv U_{pq}^{(T)G} + U_{pq}^{(T)D} + U_{pq}^{OOT} + U_{pq}^{CO1} + U_{pq}^{CO2} + U_{pq}^{O1V} + U_{pq}^{O2V} + U_{pq}^{CV}. \tag{101b}$$

With the collinear approximation, the singlet and triplet orbital Hessians of Eqs. (72) and (73) can be succinctly represented with a single form of:

$$A_{pq,rs}^{(k)(0)} = U_{pq}^{(k)} \left\{ \delta_{pr} F_{qs\beta} - \delta_{qs} F_{pr\alpha} - c_H \left(pr \middle| sq \right) \right\} U_{rs}^{(k)}, \tag{102}$$

where $k = S, T$ and the zeroth-order Fock matrix from $M_S = +1$ is represented with more concise notation as $F_{pq\sigma} = F_{p\sigma_p q\sigma_q}^{(0)}$ and all Fock matrices from $M_S = -1$, $\tilde{F}_{p\sigma_p q\sigma_q}^{(0)}$, is converted to that from $M_S = +1$. The singlet and triplet response equations can be represented as:

$$A^{(k)(0)}_{pq,rs} X^{(k)(0)}_{rs} = \Omega_{(k)(0)} X^{(k)(0)}_{pq}, \quad (103)$$

the $\Omega_{(S)(0)}$ and $\Omega_{(T)(0)}$ are their eigenvalues or excitation energies from the reference.

3. Spin-pairing coupling

Because no coupling occurs between the responses originating from the two different references of the MR-RDM, a posteriori coupling was introduced as

$$A'_{pq,rs} = c_{SP} \left\langle \Psi^{M_S=+1}_{p\alpha q\beta} \middle| \hat{H} \middle| \Psi^{M_S=-1}_{r\beta s\alpha} \right\rangle, \quad (104)$$

where $\left\langle \Psi^{M_S=+1}_{p\alpha q\beta} \right|$ and $\left| \Psi^{M_S=-1}_{r\beta s\alpha} \right\rangle$ are the bra and ket vectors for configurations originating from the $M_S = +1$ and $M_S = -1$ components of the mixed reference state, respectively. The pairing-strength coefficient, c_{SP}, is adjustable depending on situations or a specific molecule. The best pairing strength may be able to be determined by benchmarking calculations. However, by default one can use the pairing strength with the same value of HF exchange mixing coefficient, i.e., $c_{SP} = c_{HF}$. After defining a sign function for the singlet and triplet states as

$$sgn(k) = +1, \quad \text{if} \quad k = S, \quad (105a)$$

$$sgn(k) = -1, \quad \text{if} \quad k = T, \quad (105b)$$

the two types of couplings can be defined by:

$$H_{pq,rs}^{(k)\text{intra}} \equiv sgn(k)c_H \left(ps|rq \right), \tag{106a}$$

$$H_{pq,rs}^{(k)\text{inter}} \equiv sgn(k)c_H \left\{ \left(pq|rs \right) - \left(pr|sq \right) \right\}, \tag{106b}$$

where $k = S,T$. With these, the spin-pairing coupling in Eq. (104) for the singlet and triplet response equations in Eq. (74) and (75), respectively, are represented as:

$$\begin{aligned} A'^{(k)}_{pq,rs} &= H^{(k)\text{intra}}_{p\underline{q},r\underline{s}} (U^{CO1}_{pq} - U^{CO2}_{pq})(U^{CO1}_{rs} - U^{CO2}_{rs}) + H^{(k)\text{intra}}_{\underline{pq},\underline{rs}} (U^{O1V}_{pq} - U^{O2V}_{pq})(U^{O1V}_{rs} - U^{O2V}_{rs}) \\ &+ H^{(k)\text{inter}}_{pq,rs} (U^{CO1}_{pq} U^{O2V}_{rs} + U^{CO2}_{pq} U^{O1V}_{rs} + U^{O1V}_{pq} U^{CO2}_{rs} + U^{O2V}_{pq} U^{CO1}_{rs}) \end{aligned} \tag{107}$$

Note that the underline notation used in the indices of the coupling $H^{(k)\text{intra}}_{pq,rs}$ in Eq. (107) is defined as:

$$\underline{p} \equiv O2, \quad \text{if} \quad p = O1, \tag{108a}$$

$$\underline{p} \equiv O1, \quad \text{if} \quad p = O2. \tag{108b}$$

As a result, the orbital Hessians for the singlet and triplet responses with the spin-pairing coupling can be simply given by:

$$A^{(k)}_{pq,rs} = A^{(k)(0)}_{pq,rs} + A'^{(k)}_{pq,rs}. \tag{109}$$

It should be noted that even with the couplings, the excitation amplitudes of singlet ($X^{(S)}_{pq}$) and triplet configurations ($X^{(T)}_{pq}$) are completely decoupled from each other. In addition, the response spaces can be expanded with the same dimensional-transformation

$U_{pq}^{(S)}$ and $U_{pq}^{(T)}$ matrices in Eq. (101a) and (101b). Finally, the singlet and triplet response equations with the spin-pairing coupling are given by:

$$A_{pq,rs}^{(k)} X_{pq}^{(k)} = \Omega_{(k)} X_{pq}^{(k)}, \tag{110}$$

where $k = S, T$ and the $\Omega_{(S)}$ and $\Omega_{(T)}$ are their eigenvalues or excitation energies.

ANALYTIC ENERGY GRADIENT OF MIXED-REFERENCE SPIN-FLIP TDDFT

An analytic gradient with respect to nuclear coordinates represents the essential quantity for the vast majority of quantum mechanical applications such as geometry optimization, reaction path following, and molecular dynamics simulations. In addition, gradients of excited states are crucial in the emerging field of nonadiabatic dynamics. The analytic energy gradient of LR- and SF-TDDFT is formulated by using the Lagrangian formalism.[46, 49] Likewise, that of MRSF-TDDFT can be obtained with similar way[50] which will be describing in this section. In the first subsection of *Lagrangian*, the Lagrangians of both singlet and triplet response states are defined with two new Lagrange multipliers W and Z. These two multipliers can be determined by orbital stationary condition described by subsections 2 and 3, respectively. With the determined multipliers satisfying orbital stationary conditions, analytic energy gradient can be represented by concise form which will be derived in the last subsection 4.

1. Lagrangian

The reference of MRSF-TDDFT is optimized by variational conditions for the restricted open-shell Kohn-Sham MOs in the Guest-Saunders canonicalization.[51]

$$\bar{F}_{pq} = \bar{F}_{pq\alpha} + \bar{F}_{pq\beta}, \tag{111}$$

with

$$\bar{F}_{pq\alpha} = \begin{pmatrix} F_{ij\alpha}/2 & 0 & F_{ib\alpha}/2 \\ 0 & F_{xy\alpha}/2 & F_{xb\alpha} \\ F_{aj\alpha}/2 & F_{ay\alpha} & F_{ab\alpha}/2 \end{pmatrix}, \tag{112}$$

$$\bar{F}_{pq\beta} = \begin{pmatrix} F_{ij\beta}/2 & F_{iy\beta} & F_{ib\beta}/2 \\ F_{xj\beta} & F_{xy\beta}/2 & 0 \\ F_{aj\beta}/2 & 0 & F_{ab\beta}/2 \end{pmatrix}. \tag{113}$$

The off-diagonal blocks represent the variational conditions, i.e., rotations between C-O, C-V, and O-V orbitals that go to zero.

MRSF-TDDFT yields two independent Lagrangian for singlet ($k = S$) and triplet response states ($k = T$) as:

$$L^{(k)}[\mathbf{X}^{(k)}, \Omega_{(k)}, \mathbf{C}, \mathbf{Z}^{(k)}, \mathbf{W}^{(k)}] = G[\mathbf{X}^{(k)}, \Omega_{(k)}] + 2\sum_{ia\sigma} Z^{(k)}_{ia\sigma} \bar{F}_{ia\sigma} + \sum_{ix\sigma} Z^{(k)}_{ix\sigma} \bar{F}_{ix\sigma}$$
$$+ \sum_{xa\sigma} Z^{(k)}_{xa\sigma} \bar{F}_{xa\sigma} - 2\sum_{p \le q} \sum_{\sigma} W^{(k)}_{pq\sigma} (S_{pq\sigma} - \delta_{pq}), \tag{114}$$

where the vector $\mathbf{C}$ and $S_{pq\sigma}$ are the MO coefficients and MO overlap integral, respectively, and the $\mathbf{Z}^{(k)}$ and $\mathbf{W}^{(k)}$ vectors are undetermined Lagrange multipliers. The first term on the right-hand

side is:

$$G[\mathbf{X}^{(k)},\Omega_{(k)}] = \sum_{pr}^{C,OO,V}\sum_{qs} X_{pq}^{(k)} A_{pq,rs}^{(k)} X_{rs}^{(k)} - \Omega_{(k)}\left(\sum_{p}^{C,OO,V}\sum_{q} X_{pq}^{(k)} X_{pq}^{(k)} - 1\right). \quad (115)$$

It is noteworthy that only the $G[\mathbf{X}^{(k)},\Omega_{(k)}]$ term differs in SF- and MRSF-TDDFT except for the undetermined Lagrange-multipliers $\mathbf{Z}^{(k)}$ and $\mathbf{W}^{(k)}$.

2. Orbital stationary condition I (Coupled perturbed Hartree-Fock equation): Lagrange multiplizer Z

Two independent sets of orbital stationary conditions for singlet ($k = S$) and triplet response states ($k = T$) are defined, respectively, as

$$\sum_{\mu} \frac{\partial L^{(k)}}{\partial c_{\mu t\alpha}} c_{\mu u\alpha} + \sum_{\mu} \frac{\partial L^{(k)}}{\partial c_{\mu t\beta}} c_{\mu u\beta} = 0. \quad (116)$$

From this condition, the following $\mathbf{Z}^{(k)}$-vector equation can be derived as

$$\sum_{r}^{C,OO,V}\sum_{s} \overline{J}_{pq,rs} \overline{Z}_{rs}^{(k)} = -\overline{R}_{pq}^{(k)}, \quad p \in C,O \quad q \in O,V, \quad (117)$$

where the unique spin-independent $\overline{\mathbf{Z}}^{(k)}$ vector (with the bar symbol) is introduced as:

$$\overline{Z}_{ix}^{(k)} = Z_{ix\beta}^{(k)}, \quad (118a)$$

$$\overline{Z}_{xa}^{(k)} = Z_{xa\alpha}^{(k)}, \quad (118b)$$

$$\bar{Z}_{ia}^{(k)} = Z_{ia\alpha}^{(k)} = Z_{ia\beta}^{(k)}, \quad \text{otherwise, 0.} \tag{118c}$$

The orbital Hessian $\bar{J}_{pq,rs}$ of MRSF-TDDFT takes the identical forms of SF-TDDFT[46] as:

$$\bar{J}_{ix,jy} = (ix|jy) - \frac{c_H}{2}[(iy|jx) + (ij|xy)] + f_{ix\beta,jy\beta}^{xc} - \frac{1}{2}F_{ij\beta}\delta_{xy} + \frac{1}{2}F_{xy\beta}\delta_{ij}, \tag{119a}$$

$$\bar{J}_{ia,jy} = 2(ia|jy) - \frac{c_H}{2}[(iy|ja) + (ij|ya)] + f_{ia\alpha,jy\beta}^{xc} + f_{ia\beta,jy\beta}^{xc} + \frac{1}{2}F_{ya\beta}\delta_{ij}, \tag{119b}$$

$$\bar{J}_{xa,jy} = (xa|jy) + f_{xa\alpha,jy\beta}^{xc} - \frac{1}{2}F_{ja\alpha}\delta_{xy}, \tag{119c}$$

$$\bar{J}_{ia,jb} = 4(ia|jb) - c_H[(ib|ja) + (ij|ab)] + f_{ia\alpha,jb\alpha}^{xc} + f_{ia\alpha,jb\beta}^{xc} + f_{ia\beta,jb\alpha}^{xc} + f_{ia\beta,jb\beta}^{xc} + (\epsilon_a - \epsilon_i)\delta_{ij}\delta_{ab}, \tag{119d}$$

$$\bar{J}_{xa,jb} = 2(xa|jb) - c_H[(xb|ja) + (jx|ab)] + f_{xa\alpha,jb\alpha}^{xc} + f_{xa\alpha,jb\beta}^{xc} - \frac{1}{2}F_{jx\alpha}\delta_{ab}, \tag{119e}$$

$$\bar{J}_{xa,yb} = (xa|yb) - \frac{1}{c_H}[(xb|ya) + (xy|ab)] + f_{xa\alpha,yb\alpha}^{xc} - \frac{1}{2}F_{xy\alpha}\delta_{ab} + \frac{1}{2}F_{ab\alpha}\delta_{xy}, \tag{119f}$$

where $f_{pq\sigma,rs\tau}^{xc}$ represents the matrix elements of the second functional derivatives of the exchange-correlation functional with respect to the electron density. The spin-state-specific $\bar{R}_{pq}^{(k)}$ on the right-hand side of Eq. (7) for the singlet ($k = S$) and triplet states ($k = T$) are given by:

$$\bar{R}_{ix}^{(k)} = \frac{1}{2}H_{ix\beta}^{+}[\mathbf{T}^{(k)}] + H_{ix\alpha}[\mathbf{X}^{(k)}, \mathbf{X}^{(k)}] - H_{xi\alpha}[\mathbf{X}^{(k)}, \mathbf{X}^{(k)}] - H_{xi\beta}[\mathbf{X}^{(k)}, \mathbf{X}^{(k)}], \tag{120a}$$

$$\bar{R}_{xa}^{(k)} = \frac{1}{2}H_{xa\alpha}^{+}[\mathbf{T}^{(k)}] + H_{xa\alpha}[\mathbf{X}^{(k)}, \mathbf{X}^{(k)}] + H_{xa\beta}[\mathbf{X}^{(k)}, \mathbf{X}^{(k)}] - H_{ax\beta}[\mathbf{X}^{(k)}, \mathbf{X}^{(k)}], \tag{120b}$$

$$\bar{R}_{ia}^{(k)} = \frac{1}{2}(H_{ia\alpha}^{+}[\mathbf{T}^{(k)}] + H_{ia\beta}^{+}[\mathbf{T}^{(k)}]) + H_{ia\alpha}[\mathbf{X}^{(k)}, \mathbf{X}^{(k)}] - H_{ai\beta}[\mathbf{X}^{(k)}, \mathbf{X}^{(k)}], \tag{120c}$$

where

$$H_{pq\sigma}^{+}[V] \equiv \sum_{rs\tau}\{2\left(pq|rs\right) + 2f_{pq\sigma,rs\tau}^{xc} - c_H\delta_{\sigma\tau}[\left(ps|rq\right) + \left(pr|sq\right)]\}V_{rs\tau}, \tag{121}$$

with

$$T_{pr\alpha}^{(k)} \equiv -\sum_{q}^{O,V} U_{pq}^{(k)} X_{pq}^{(k)} U_{rq}^{(k)} X_{rq}^{(k)}, \quad p,r \in C,O, \tag{122a}$$

$$T_{qs\beta}^{(k)} \equiv \sum_{p}^{C,O} U_{pq}^{(k)} X_{pq}^{(k)} U_{ps}^{(k)} X_{ps}^{(k)}, \quad q,s \in O,V. \tag{122b}$$

And the $H_{tu\sigma}[\mathbf{X}^{(k)}, \mathbf{X}^{(k)}]$ of Eq. (120) is defined as

$$H_{tu\sigma}[\mathbf{X}^{(k)}, \mathbf{X}^{(k)}] \equiv H_{tu\sigma}^{(0)}[\mathbf{X}^{(k)}, \mathbf{X}^{(k)}] + \sum_{xy} H_{tu\sigma}^{intra}[\mathbf{X}_{Cx}^{(k)}, \mathbf{X}_{Cy}^{(k)}] + \sum_{xy} H_{tu\sigma}^{intra}[\mathbf{X}_{xV}^{(k)}, \mathbf{X}_{yV}^{(k)}]$$

$$+ \sum_{x} H_{tu\sigma}^{inter}[\mathbf{X}_{Cx}^{(k)}, \mathbf{X}_{\underline{x}V}^{(k)}] + \sum_{x} H_{tu\sigma}^{inter}[\mathbf{X}_{xV}^{(k)}, \mathbf{X}_{C\underline{x}}^{(k)}], \tag{123}$$

where

$$H_{tu\alpha}^{(0)}[\mathbf{X}^{(k)}, \mathbf{X}^{(k)}] \equiv \sum_{r}^{C,O} \sum_{qs}^{O,V} U_{tq}^{(k)} X_{tq}^{(k)} \{\delta_{ur} F_{qs\beta} - \delta_{qs} F_{ur\alpha} - c_H \left(ur|sq\right)\} U_{rs}^{(k)} X_{rs}^{(k)}, \tag{124a}$$

$$H_{tu\beta}^{(0)}[\mathbf{X}^{(k)}, \mathbf{X}^{(k)}] \equiv \sum_{pr}^{C,O} \sum_{s}^{O,V} U_{pt}^{(k)} X_{pt}^{(k)} \{\delta_{pr} F_{us\beta} - \delta_{us} F_{pr\alpha} - c_H \left(pr|su\right)\} U_{rs}^{(k)} X_{rs}^{(k)}, \tag{124b}$$

and

$$H_{tu\alpha}^{intra}[\mathbf{X}_{Cx}^{(k)}, \mathbf{X}_{Cy}^{(k)}] \equiv (-1)^{1-\delta_{xy}} \sum_{r}^{C} \sum_{qs}^{O} U_{tq}^{Cx} X_{tq}^{(k)} H_{u\underline{q},r\underline{s}}^{(k)intra} U_{rs}^{Cy} X_{rs}^{(k)}, \tag{125a}$$

$$H_{tu\alpha}^{intra}[\mathbf{X}_{xV}^{(k)}, \mathbf{X}_{yV}^{(k)}] \equiv (-1)^{1-\delta_{xy}} \sum_{r}^{O} \sum_{qs}^{V} U_{\underline{t}q}^{xV} X_{\underline{t}q}^{(k)} H_{uq,\underline{r}s}^{(k)intra} U_{rs}^{yV} X_{rs}^{(k)}, \tag{125b}$$

$$H_{tu\alpha}^{inter}[\mathbf{X}_{Cx}^{(k)}, \mathbf{X}_{yV}^{(k)}] \equiv \sum_{rq}^{O} \sum_{s}^{V} U_{tq}^{Cx} X_{tq}^{(k)} H_{uq,rs}^{(k)inter} U_{rs}^{yV} X_{rs}^{(k)}, \tag{125c}$$

$$H^{inter}_{tu\alpha}[\mathbf{X}^{(k)}_{xV},\mathbf{X}^{(k)}_{Cy}] \equiv \sum_{r}^{C}\sum_{s}^{O}\sum_{q}^{V} U^{xV}_{tq} X^{(k)}_{tq} H^{(k)inter}_{uq,rs} U^{Cy}_{rs} X^{(k)}_{rs}, \tag{125d}$$

$$H^{intra}_{tu\beta}[\mathbf{X}^{(k)}_{Cx},\mathbf{X}^{(k)}_{Cy}] \equiv (-1)^{1-\delta_{xy}} \sum_{pr}^{C}\sum_{s}^{O} U^{Cx}_{p\underline{t}} X^{(k)}_{p\underline{t}} H^{(k)intra}_{pu,r\underline{s}} U^{Cy}_{rs} X^{(k)}_{rs}, \tag{125e}$$

$$H^{intra}_{tu\beta}[\mathbf{X}^{(k)}_{xV},\mathbf{X}^{(k)}_{yV}] \equiv (-1)^{1-\delta_{xy}} \sum_{pr}^{O}\sum_{s}^{V} U^{xV}_{pt} X^{(k)}_{pt} H^{(k)intra}_{\underline{pu},\underline{rs}} U^{yV}_{rs} X^{(k)}_{rs}, \tag{125f}$$

$$H^{inter}_{tu\beta}[\mathbf{X}^{(k)}_{Cx},\mathbf{X}^{(k)}_{yV}] \equiv \sum_{p}^{C}\sum_{r}^{O}\sum_{s}^{V} U^{Cx}_{pt} X^{(k)}_{pt} H^{(k)inter}_{pu,rs} U^{yV}_{rs} X^{(k)}_{rs}, \tag{125g}$$

$$H^{inter}_{tu\beta}[\mathbf{X}^{(k)}_{xV},\mathbf{X}^{(k)}_{Cy}] \equiv \sum_{r}^{C}\sum_{pr}^{O} U^{xV}_{pt} X^{(k)}_{pt} H^{(k)inter}_{pu,rs} U^{Cy}_{rs} X^{(k)}_{rs}. \tag{125h}$$

Four terms on the right-hand side of Eq. (123) except for the first term are derived from the spin-pairing coupling in Eq. (107). Without these terms, all equations for the $\mathbf{Z}^{(k)}$-vector equation are almost same as those of SF-TDDFT.[46] Only the difference is using the expanded excitation amplitudes, $U^{(k)}_{pq} X^{(k)}_{pq}$, in MRSF-TDDFT. This is great advantage since one can simply utilize the same existing routines for SF-TDDFT.

3. Orbital stationary condition II: Lagrange multiplizer W

After $\mathbf{Z}^{(k)}$ vector is determined by solving Eq. (117), the relaxed difference density matrix $\mathbf{P}^{(k)}$ can thus be calculated as:

$$P^{(k)}_{pq\sigma} = T^{(k)}_{pq\sigma} + Z^{(k)}_{pq\sigma}. \tag{126}$$

If we define the spin-state-specific $\bar{W}_{pq}^{(k)}$ as

$$\bar{W}_{pq}^{(k)} \equiv W_{pq\alpha}^{(k)} + W_{pq\beta}^{(k)}, \tag{127}$$

the other Lagrange multiplier $\bar{W}_{pq}^{(k)}$ can be obtained by:

$$\bar{W}_{ix}^{(k)} = H_{xi\alpha}[\mathbf{X}^{(k)}, \mathbf{X}^{(k)}] + H_{xi\beta}[\mathbf{X}^{(k)}, \mathbf{X}^{(k)}] + F_{xi\alpha}[\mathbf{X}^{(k)}, \mathbf{X}^{(k)}] + \frac{1}{2} H_{ix\alpha}^{+}[\mathbf{P}^{(k)}]$$

$$+ \frac{1}{2} \sum_{j} F_{ij\beta} \bar{Z}_{jx}^{(k)} + \frac{1}{2} \sum_{a} F_{ia\alpha} \bar{Z}_{xa}^{(k)}, \tag{128a}$$

$$\bar{W}_{ia}^{(k)} = H_{ai\beta}[\mathbf{X}^{(k)}, \mathbf{X}^{(k)}] + \epsilon_i \bar{Z}_{ia}^{(k)} + \frac{1}{2} \sum_{x} F_{ix\alpha} \bar{Z}_{xa}^{(k)}, \tag{128b}$$

$$\bar{W}_{xa}^{(k)} = H_{ax\beta}[\mathbf{X}^{(k)}, \mathbf{X}^{(k)}] + F_{ax\beta}[\mathbf{X}^{(k)}, \mathbf{X}^{(k)}] + \frac{1}{2} \sum_{y} F_{xy\alpha} \bar{Z}_{ya}^{(k)} + \frac{1}{2} \sum_{i} F_{ix\alpha} \bar{Z}_{ia}^{(k)}, \tag{128c}$$

$$\bar{W}_{ij}^{(k)} \left(1 + \delta_{ij}\right) = H_{ij\alpha}[\mathbf{X}^{(k)}, \mathbf{X}^{(k)}] + F_{ij\alpha}[\mathbf{X}^{(k)}, \mathbf{X}^{(k)}] + \frac{1}{2} \left(H_{ij\alpha}^{+}[\mathbf{P}^{(k)}] + H_{ij\beta}^{+}[\mathbf{P}^{(k)}] \right), \; i \le j \tag{128d}$$

$$\bar{W}_{xy}^{(k)} \left(1 + \delta_{xy}\right) = H_{xy\alpha}[\mathbf{X}^{(k)}, \mathbf{X}^{(k)}] + H_{xy\beta}[\mathbf{X}^{(k)}, \mathbf{X}^{(k)}] + F_{ij\alpha}[\mathbf{X}^{(k)}, \mathbf{X}^{(k)}] + F_{ij\beta}[\mathbf{X}^{(k)}, \mathbf{X}^{(k)}]$$

$$+ \frac{1}{2} H_{xy\alpha}^{+}[\mathbf{P}^{(k)}], \; x \le y \tag{128e}$$

$$\bar{W}_{ab}^{(k)} \left(1 + \delta_{ab}\right) = H_{ab\alpha}[\mathbf{X}^{(k)}, \mathbf{X}^{(k)}] + F_{ab\alpha}[\mathbf{X}^{(k)}, \mathbf{X}^{(k)}], \quad a \le b, \tag{128f}$$

where

$$F_{tu\alpha}[\mathbf{X}^{(k)}, \mathbf{X}^{(k)}] = -X_{tq}^{(k)} F_{qs\beta} X_{us}^{(k)}, \tag{129a}$$

$$F_{tu\beta}[\mathbf{X}^{(k)}, \mathbf{X}^{(k)}] = X_{pt}^{(k)} F_{pr\alpha} X_{ru}^{(k)}. \tag{129b}$$

Also in this case, form of equations are exactly same as those of SF-TDDFT[46] without four terms originated from spin-pairing coupling in Eq. (107).

4. Analytic energy gradient with respect to the nuclear coordinate

From the stationary condition of Lagrangian for a nuclear coordinate (ξ) of

$$\frac{\partial L^{(k)}}{\partial \xi} = 0, \tag{130}$$

the analytic gradient of the excitation energy ($\Omega^{\xi}_{(k)}$) can be obtained by:

$$\Omega^{\xi}_{(k)} = \sum_{\mu\nu\sigma} h^{\xi}_{\mu\nu} P^{(k)}_{\mu\nu\sigma} - \sum_{\mu\nu\sigma} S^{\xi}_{\mu\nu} W^{(k)}_{\mu\nu\sigma} + \sum_{\mu\nu\sigma,\kappa\lambda\tau} (\mu\nu\,|\,\kappa\lambda)^{\xi}\, \Gamma^{(k)}_{\mu\nu\sigma,\kappa\lambda\tau}, \tag{131}$$

where the superscript ξ denote the derivative with respect to the nuclear coordinate. $h^{\xi}_{\mu\nu}$ and $(\mu\nu\,|\,\kappa\lambda)^{\xi}$ are the derivatives of one- and two-electron integrals in AO basis. $S^{\xi}_{\mu\nu}$ is the derivative of AO overlap integral. $P^{(k)}_{\mu\nu\sigma}$ and $W^{(k)}_{\mu\nu\sigma}$ are

$$P^{(k)}_{\mu\nu\alpha} \equiv \sum_{pq}^{C,O} c_{\mu p\alpha} P^{(k)}_{pq\alpha} c_{\nu q\alpha}, \tag{132a}$$

$$P^{(k)}_{\mu\nu\beta} \equiv \sum_{pq}^{O,V} c_{\mu p\beta} P^{(k)}_{pq\beta} c_{\nu q\beta}, \tag{132b}$$

$$W^{(k)}_{\mu\nu\alpha} \equiv \sum_{p\le q} c_{\mu p\alpha} W^{(k)}_{pq\alpha} c_{\nu q\alpha}, \tag{133a}$$

$$W^{(k)}_{\mu\nu\beta} \equiv \sum_{p\le q} c_{\mu p\beta} W^{(k)}_{pq\beta} c_{\nu q\beta}. \tag{133b}$$

In addition, $\Gamma^{(k)}_{\mu\nu\sigma,\kappa\lambda\tau}$ are given by

$$\Gamma^{(k)}_{\mu\nu\sigma,\kappa\lambda\tau} = \frac{1}{2}[2P^{(k)}_{\mu\nu\sigma}D_{\kappa\lambda\tau} - c_H\delta_{\sigma\tau}(P^{(k)}_{\mu\kappa\sigma}D_{\nu\lambda\sigma} + P^{(k)}_{\mu\lambda\sigma}D_{\nu\kappa\sigma}) - c_H\delta_{\sigma\alpha}\delta_{\tau\beta}(X^{(k)}_{\mu\lambda}X^{(k)}_{\nu\kappa} + X^{(k)}_{\mu\kappa}X^{(k)}_{\nu\lambda})]$$

$$+sgn(k)c_H\delta_{\sigma\alpha}\delta_{\tau\beta}\times[\{(X^{intra}_{O1V})^{(k)}_{\mu\lambda} - (X^{intra}_{O2V})^{(k)}_{\mu\lambda}\}\{(X^{intra}_{O1V})^{(k)}_{\kappa\nu} - (X^{intra}_{O2V})^{(k)}_{\kappa\nu}\}$$

$$+\{(X^{intra}_{CO1})^{(k)}_{\mu\lambda} - (X^{intra}_{CO2})^{(k)}_{\mu\lambda}\}\{(X^{intra}_{CO1})^{(k)}_{\kappa\nu} - (X^{intra}_{CO2})^{(k)}_{\kappa\nu}\}$$

$$+(X^{inter}_{CO1})^{(k)}_{\mu\nu}(X^{inter}_{O2V})^{(k)}_{\kappa\lambda} + (X^{inter}_{CO2})^{(k)}_{\mu\nu}(X^{inter}_{O1V})^{(k)}_{\kappa\lambda}$$

$$+(X^{inter}_{O2V})^{(k)}_{\mu\nu}(X^{inter}_{CO1})^{(k)}_{\kappa\lambda} + (X^{inter}_{O1V})^{(k)}_{\mu\nu}(X^{inter}_{CO2})^{(k)}_{\kappa\lambda}$$

$$-(X^{inter}_{CO1})^{(k)}_{\mu\lambda}(X^{inter}_{O2V})^{(k)}_{\nu\kappa} - (X^{inter}_{CO2})^{(k)}_{\mu\lambda}(X^{inter}_{O1V})^{(k)}_{\nu\kappa}$$

$$-(X^{inter}_{O2V})^{(k)}_{\mu\lambda}(X^{inter}_{CO1})^{(k)}_{\nu\kappa} - (X^{inter}_{O1V})^{(k)}_{\mu\lambda}(X^{inter}_{CO2})^{(k)}_{\nu\kappa}], \qquad (134)$$

where

$$D_{\mu\nu\alpha} \equiv \sum_{p}^{C,O} c_{\mu p\alpha}c_{\nu p\alpha}, \qquad (135a)$$

$$D_{\mu\nu\beta} \equiv \sum_{p}^{C} c_{\mu p\beta}c_{\nu p\beta}, \qquad (135b)$$

$$X^{(k)}_{\mu\nu} \equiv \sum_{p}^{C,O}\sum_{q}^{O,V} c_{\mu p\alpha}U^{(k)}_{pq}X^{(k)}_{pq}c_{\nu q\beta}, \qquad (136)$$

and

$$(X^{intra}_{OmV})^{(k)}_{\mu\nu} \equiv \sum_{p}^{O}\sum_{q}^{V} c_{\mu \underline{p}\alpha}U^{OmV}_{pq}X^{(k)}_{pq}c_{\nu q\beta}, \qquad (137a)$$

$$(X^{intra}_{COm})^{(k)}_{\mu\nu} \equiv \sum_{p}^{C}\sum_{q}^{O} c_{\mu p\alpha}U^{COm}_{pq}X^{(k)}_{pq}c_{\nu \underline{q}\beta}, \qquad (137b)$$

$$(X^{inter}_{OmV})^{(k)}_{\mu\nu} \equiv \sum_{p}^{O}\sum_{q}^{V} c_{\mu p\alpha}U^{OmV}_{pq}X^{(k)}_{pq}c_{\nu q\beta}, \qquad (137c)$$

$$(X_{COm}^{inter})_{\mu\nu}^{(k)} \equiv \sum_{p}^{C}\sum_{q}^{O} c_{\mu p\alpha} U_{pq}^{COm} X_{pq}^{(k)} c_{\nu q\beta}. \quad (137d)$$

Finally, the gradient of the ground state energy is given by:

$$E^{\xi} = \sum_{\mu\nu\sigma} h_{\mu\nu}^{\xi} D_{\mu\nu\sigma} - \sum_{\mu\nu\sigma} S_{\mu\nu}^{\xi} W'_{\mu\nu\sigma} + \sum_{\mu\nu\sigma,\kappa\lambda\tau} (\mu\nu \mid \kappa\lambda)^{\xi} \Gamma'_{\mu\nu\sigma,\kappa\lambda\tau}, \quad (138)$$

where

$$\Gamma'_{\mu\nu\sigma,\kappa\lambda\tau} = \frac{1}{2}(D_{\mu\nu\sigma} D_{\kappa\lambda\tau} - c_H \delta_{\sigma\tau} D_{\mu\lambda\sigma} D_{\nu\kappa\sigma}). \quad (139)$$

$$W'_{\mu\nu\sigma} = \sum_{p,q} c_{\mu p\sigma} F_{pq\sigma} c_{\nu q\sigma} \quad (140)$$

The gradient of excited response states can be obtained by adding the gradient of excitation energy in Eq. (131) and that of ground energy in Eq. (138). The second term on the right-hand side of Eq. (134) is derived from the spin-pairing coupling in Eq. (107). Without this term, all equations for the energy gradient are almost same as those of SF-TDDFT.[46] Similarly, only the difference is using the expanded excitation amplitudes, $U_{pq}^{(k)} X_{pq}^{(k)}$, in MRSF-TDDFT. In the same manner, one can simply utilize the same existing routines for SF-TDDFT.

NUMERICAL RESULTS

In this section, it is investigated that how spin-contamination and spin-pairing coupling affects various calculations containing 1. Vertical excitation energy, 2. Singlet-triplet energy gap, 3. Geometry-optimization structure, 4. Adiabatic excitation energy, 5. Minimum energy conical intersection, 6. Non-adiabatic coupling matrix elements, and 7. Non-adiabatic molecular dynamics.

MRSF-, MRSF(0)-, SF-TDDFT, and MRSF-CIS are utilized for these calculations. The MRSF(0)-TDDFT is a MRSF-TDDFT without the spin-pairing coupling and MRSF-CIS is a MRSF-TDDFT using 100% HF exchange. All calculations are performed by a local development version of the GAMESS-US program.[52]

The differences between MRSF(0)- and SF-TDDFT can specifically represent the pure spin-contamination effect of SF-TDDFT. Also, the effects of spin-pairing coupling to geometry can be understood from the differences between MRSF- and MRSF(0)-TDDFT.

1. Vertical excitation energy

1.1 P excited state of Be atom

Be atom has the ^{1}S ground state arising in the configuration $1s^2 2s^2$. The low-lying excited states of Be are the $^3P_{x,y,z}$ and the $^1P_{x,y,z}$ states arising in the configuration $1s^2 2s^1 2p_k^1$, $k=x,y,z$. The SF-TDDFT and the MR-SF-TDDFT calculations use the ^3P_z state ($1s^2 2s^1 2p_z^1$) as the reference state. With this choice of reference, the $X_L^{M_S=0,I}$ and $X_R^{M_S=0,I}$ amplitudes generate the ^1P_z and ^3P_z states, while the rest of the P states are produced by the $\mathbf{X}^I_{V_\beta O_\alpha}$ and $\mathbf{X}^I_{V_\alpha O_\beta}$ amplitudes.

The results of the calculations are collected in Tab. 4. SF-TDDFT, MRSF-TDDFT(0) and MRSF-TDDFT, yield nearly identical energy for the ^{1}S ground electronic state since there is little spin-contamination in the SF-TDDFT. The collinear SF-TDDFT method yields relatively minor spin-contamination of the ^1P_z and ^3P_z components, for which the excitation amplitudes arise in the O→O excitation (type I in Fig. 2). However, the $^3P_{x,y}$ components, which are described by the amplitudes arising in the OV excitation (type II in Fig. 2), are strongly spin-contaminated; $\langle \mathbf{S}^2 \rangle$ =1.0, which is typical for mixtures of the true

singlet and triplet states. As a result, there are absences of $^1P_{x,y}$ components. Strictly, one cannot say the strongly spin-contaminated states as neither singlet nor triplet states. Hence, an erroneous energy splitting between the (x,y) components and z component of the ^3P and ^1P multiplets is predicted by SF-TDDFT; 0.811 eV and 1.247 eV, respectively.

Although the removal of the spin-contamination by MRSF-TDDFT(0) does not improve the energies of the multiplet components, the $^1P_{x,y}$ and $^3P_{x,y}$ can now be distinguished. The use of the pairing strengths in MRSF-TDDFT lifts the degeneracy of these components of the ^1P and ^3P multiplets, see the fourth column in Tab. 4. The magnitude of the splitting between the components of the same multiplet with the non-zero pairings is considerably reduced as compared to SF-TDDFT; the $^3P_{x,y}$ and ^3P_z splitting is now 0.233 eV and the $^1P_{x,y}$ and ^1P_z splitting is reduced to 0.223 eV. It can be expected that the residual splitting between the (x,y) and z components can be further reduced by considering more accurate expressions for the pairing strengths than simple Eq. (104) used here.

To understand the origin of the residual splitting, calculations with 100% HF exchange instead of the XC functional (labeled MRSF-CIS in Tab.

4) were performed. The use of the self-interaction free HF exchange completely eliminates the erroneous splitting between the $^3P_{x,y}$ and ^3P_z components and reduces the $^1P_{x,y}$–^1P_z splitting to only 0.09 eV. This indicates that the bulk of the splitting between the multiplet components may be caused by the effect of the self-interaction error of the density functional. The remaining tiny splitting between the components of the ^1P multiplet are probably caused by the incompleteness of the mixed reference.

Not only for Be atom but also for other examples, MRSF-TDDFT properly splits an unphysical state of SF-TDDFT (half-singlet and half-triplet mixed state) into correct singlet and triplet states. A posteriori spin-pairing coupling is expected to improve the split states.

State	SF-TDDFT	MRSF-TDDFT(0)	MRSF-TDDFT	MRSF-CIS
^1S	-14.651 (0.00)	-14.651 (0.00)	-14.651 (0.00)	-14.584 (0.00)
^3P_z	2.877 (1.98)	2.899 (2.00)	2.900 (2.00)	2.107 (2.00)
$^3P_{x,y}$	3.688 (1.00)	3.688 (2.00)	2.667 (2.00)	2.107 (2.00)
^1P_z	4.935 (0.02)	4.913 (0.00)	4.913 (0.00)	6.042 (0.00)
$^1P_{x,y}$		3.688 (0.00)	4.690 (0.00)	5.952 (0.00)

Table 4. Ground state total energies (Hartree) and excitation energies (eV) for Be atom. *MRSF-TDDFT(0) denote MRSF-TDDFT without spin-pairing coupling, and MRSF-CIS denote using 100% HF exchange within the MRSF-TDDFT formalism. The BHHLYP functional and 6-31G basis set are utilized for these calculations. The expectation value of* S^2 *is given in parentheses.*

1.2 Singlet valence excited state of molecule

Benchmark calculations for the singlet valence excited states with organic molecules of Thiel set[53] were performed. Vertical excitation energies to Franck-Condon excited states are calculated by MRSF- and SF-TDDFT with cc-pVTZ basis set.[54] Mean absolute errors (MAE) in unit of eV for the benchmark calculations by MRSF-, SF-, and LR-TDDFT are tabulated in Tab. 5 compared against the TBE-2 reference.[55] In MRSF-TDDFT, sets of MAE with different the pairing-strength coefficient c_{SP} are tabulated.

As the c_{SP} coefficient increases from 0.3 to 0.9 the MAE values somewhat rise. This is related to the fact that the vertical excitation energies also rise, although weakly, as c_{SP} changes. Note, the SF-TDDFT MAE values can be considered as those obtained from MRSF-TDDFT at c_{SP}=0, due to the fact that MRSF-TDDFT is similar to SF-TDDFT when the pairing-strength is neglected (c_{SP}=0). Thus, one can say that there is a minimum for the dependence of MAE on c_{SP}. In other word, there is a minimum value of MAE at a particular value(s) of the c_{SP} coefficient. For the B3LYP, PBE0, and BHHLYP this minimum is at the following values of c_{SP}: 0.4-0.5, 0.3-0.5, and 0.0-0.3, correspondingly. This means that overall MRSF-TDDFT outperforms

SF-TDDFT.

LR-TDDFT gives better MAE than MRSF- and SF-TDDFT for every xc functional in this calculations. This can be understandable. Since the vertical excitation energy is calculated at the optimized structure in the S_0 ground state, the reference state of LR-TDDFT (*i.e.*, closed-shell singlet state) describes the geometry better than that of MRSF- and SF-TDDFT (*i.e.*, open-shell triplet state). Better reference could give better linear response of density, which lead to give better vertical excitation energy.

Although the vertical excitation energy is important, the main focus of SF- and MRSF-TDDFT is on describing conical intersections and single-bond breaking/twisted systems. Therefore, we can conclude that the slightly large 0.5 ~ 0.6 MAE at the Franck-Condon region can be allowed for many other advantages around conical intersections and avoided crossing points.

Table 5. Mean absolute errors MAE (in eV) for the vertical excitation energies computed at MRSF-, SF-, and LR-TDDFT level of theory compared against the TBE-2 reference. *Four different xc functionals and the cc-pVTZ basis set are utilized for this benchmark calculations. In MRSF-TDDFT, sets of MAE with different the pairing-strength coefficient* c_{SP} *are given.*

	B3LYP	PBE0	BHHLYP	M08-SO
c_{SP}		MRSF-TDDFT		
0.3	0.58	0.51	0.53	0.50
0.4	0.58	0.50	0.54	0.51
0.5	0.58	0.50	0.55	0.52
0.6	0.58	0.51	0.57	0.54
0.7	0.59	0.51	0.60	0.57
0.8	0.60	0.53	0.63	0.59
0.9	0.61	0.54	0.65	0.62
		SF-TDDFT		
	0.65	0.57	0.53	0.51
		LR-TDDFT		
	0.30	0.28	0.53	0.34

2. Singlet-triplet energy gap

Singlet-triplet energy gap is an important chemical property to study intersystem crossing or singlet fission. We have performed MRSF- and LR-TDDFT calculations for the singlet-triplet (ST) gaps in a series of molecules. For the majority of the molecules, adiabatic ST gaps were calculated, except c-C_4H_4, C_3H_6, br-C_7H_{14}, ln-C_7H_{14}, C_2H_4, butadiene, and hexatriene for which vertical ST gaps were calculated. 6-31G(d) basis set is utilized for all calculations with several other functionals; D18X, B3LYP, PBE0, BHHLYP and M08-HX. Here, a functional D18X functional stands for a new hybrid functional consisting 0.15 Becke + 0.75 Hartree-Fock exchange and Lee-Yang-Parr correlation, which yield the best performance for MRSF-TDDFT.

Figure 6a and 6b show absolute errors of the ST gaps with respect to experimental results for MRSF- and LR-TDDFT, respectively. For small molecules from NH to PH_2^+, the best agreement with the experimental ST gaps is obtained with the use of the D18X functional. The use of lower fraction of the HF exchange resulted in greater errors. For molecules of medium size, it were the M08-HX and BHHLYP functionals that showed the best agreement with the experimental ST gaps.

On the other hand, with LR-TDDFT, the best agreement with the experiment is delivered by M08-HX. For the medium-sized molecules all functionals give the deviations from the experiment strongly exceeding 0.36 eV with large values for absolute errors.

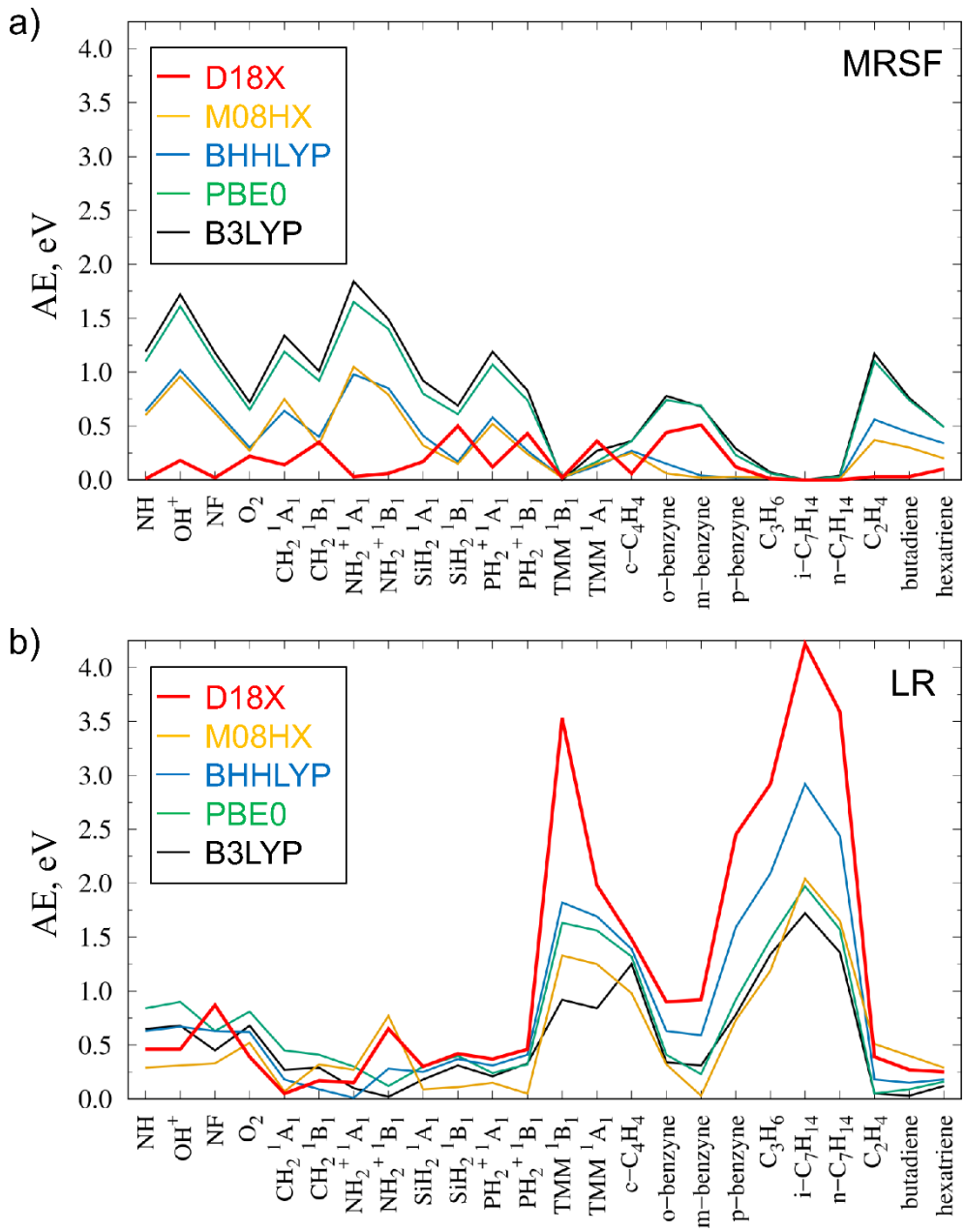

Figure 6. Comparison of the absolute errors (AE) of singlet-triplet energy gaps for the organic molecules. *6-31G(d) basis set is utilized for all calculations.*

3. Geometry-optimization structure

In this subsection, it is investigated that how spin-contamination and spin-pairing coupling affects the optimized geometries of ground and excited states. All geometries were obtained by using the analytic gradients of MRSF-, MRSF(0)-, and SF-TDDFT. The BHHLYP[56-58] collinear XC kernel combined with the 6-31G (d) basis set[59] were adopted for TDDFT calculations. In order to measure accuracy of these geometries, geometry optimizations with the equation-of-motion coupled-cluster singles and doubles (EOM-CCSD)[60, 61] were also performed as a benchmarks level of theory with the same basis set. Geometries of 8 organic molecules are optimized for different states, which leads 20 different geometries (8 for S_0 state, 8 for S_1 state, and 4 for S_2 state). All the structures were optimized with the default threshold of 10^{-4} a.u./bohr and the default integration grid for DFT (nrad = 96, nleb = 302) and TDDFT (nrad = 48, nleb = 110). All minimum points are confirmed by numerical calculations of the Hessian.

After aligning all geometries obtained by different methods by using vmd, geometric RMSDs of SF-, MRSF(0)- and MRSF-TDDFT with respect to the reference geometry of EOM-CCSD are calculated.

$$\mathrm{RMSD} = \sqrt{\frac{1}{N}\sum_{m=1}^{N}\left\|\mathbf{R}_M - \mathbf{R}_{\text{EOM-CCSD}}\right\|^2}. \qquad (141)$$

Here, N is the number of atoms for a molecule and $\mathbf{R}_M$ is the geometry vector of an optimized molecule by the M method (where M =SF-, MRSF(0)-, or MRSF-TDDFT). The double vertical bar denotes the Euclidean norm. Each RMSD is represented as a point in Fig. 7 along the $\langle \mathbf{S}^2 \rangle$ value of SF-TDDFT.

The spin contamination resulting from missing configurations for the S_0 states is rare. Thus, RMSDs of the S_0 state are accumulated around 0.0 ~ 0.1 of the $\langle \mathbf{S}^2 \rangle$ values. At the same time, their geometric RMSDs against EOM-CCSD turned out to be small. The predicted results with $\langle \mathbf{S}^2 \rangle$ values of 0.1 ~ 0.7 are coming from the type I (O→O). Even for excited states composed of the spin-complete type I (O→O) configurations of SF-TDDFT shown in Fig. 1, considerable spin contamination appears due to the asymmetric nature of SF-TDDFT. Both MRSF(0)- and MRSF-TDDFT well improve the geometric RMSDs compared to those of SF-TDDFT. However, in the cases of cyclopentadiene (S_1), propanamide (S_1), formamide (S_1), and acetamide (S_1), MRSF-TDDFT is slightly inferior to MRSF(0)-TDDFT. While, the MRSF-TDDFT in particular significantly improves RMSDs with $\langle \mathbf{S}^2 \rangle > 0.8$ which are from the type II (C→O) and type III (O→V).

Overall, the average RMSD of MRSF-TDDFT as represented by horizontal black line is smaller than that of MRSF(0)-TDDFT in blue line. The improved prediction accuracy of MRSF-TDDFT can justify the introduction of a posteriori coupling.

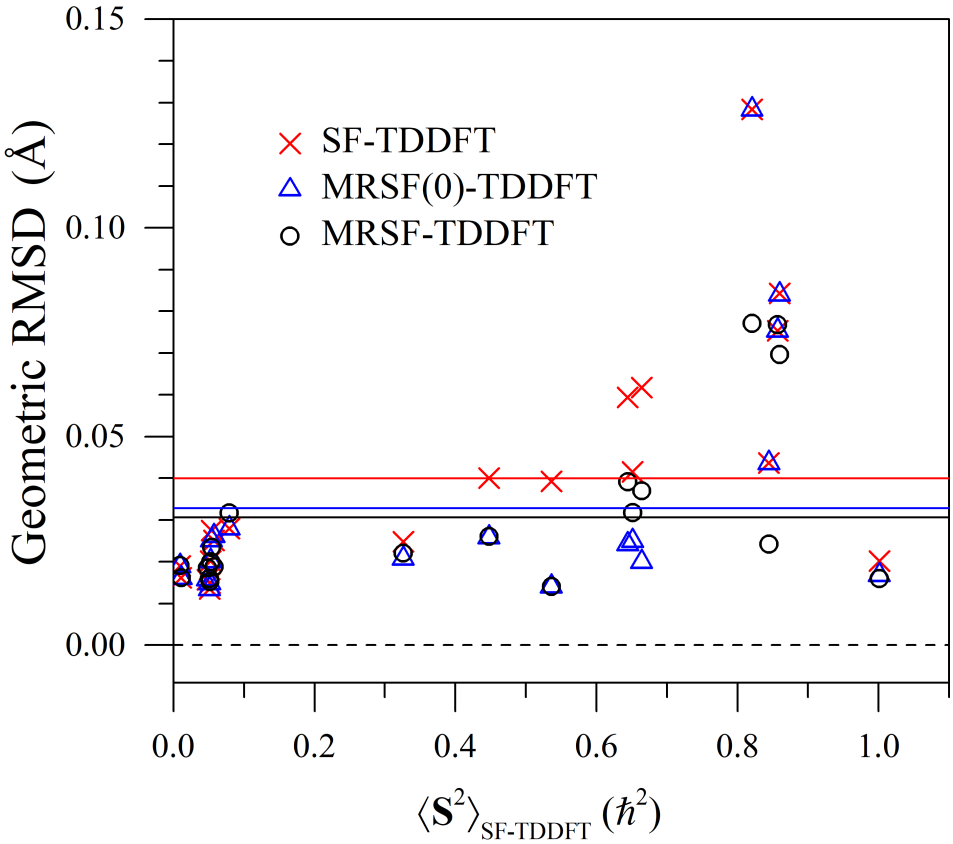

Figure 7. Geometric RMSDs of SF-, MRSF(0)- and MRSF-TDDFT with respect to the reference geometry of EOM-CCSD. *Each point denotes the RMSD for an optimized structure for 8 organic molecules. There are 20 points (8 for S_0, 8 for S_1, and 4 for S_2 optimized structures) The x-axis represents the expectation value of S^2 operator for SF-TDDFT. The red, blue and black horizontal lines represent the average values of SF-, MRSF(0)- and MRSF-TDDFT, respectively.*

4. Adiabatic excitation energy

In this subsection, adiabatic excitation energies (AEEs) were calculated with the optimized structures obtained in previous subsection. Then, the AEEs by SF-, MRSF(0)-, MRSF-TDDFT are compared to those by EOM-CCSD and the magnitude of differences are presented in Fig. 8 in unit of eV with the same x-axis as Fig. 7.

In the case of AEEs, the MRSF-TDDFT performs extremely well to the degree that many of predicted AEEs are nearly identical to those of EOM-CCSD, which is also seen from the average AEE differences as presented by the black horizontal line. The improved prediction accuracy of MRSF-TDDFT can justify the introduction of a posteriori coupling.

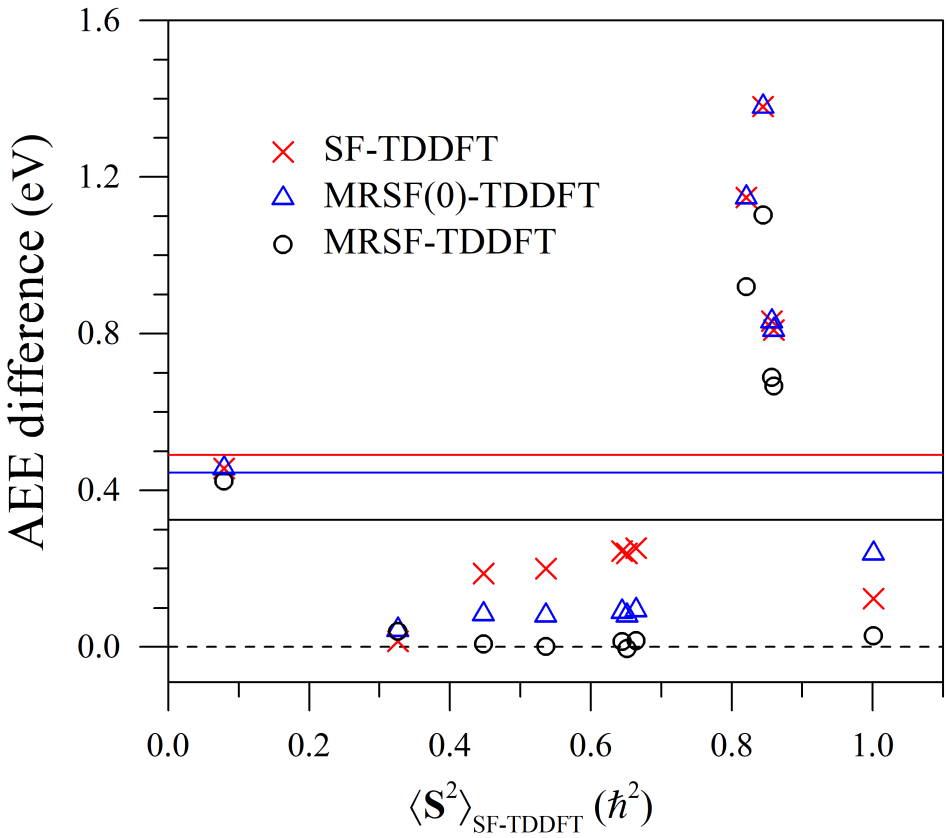

Figure 8. Magnitudes of AEE differences of SF-, MRSF(0)- and MRSF-TDDFT with respect to the reference AEE of EOM-CCSD in eV. *Each point denotes the AEE difference for the same set of Fig. 7. Thus, there are 12 points (8 for AEE(S_1-S_0) and 4 for AEE(S_2-S_0)) The x-axis and horizontal lines represent same as Fig. 7.*

5. Conical intersection

5.1 Minimum energy conical intersection of PSB3

The penta-2,4-dieniminium cation (PSB3) is an important model system for vision used to test the ability of methods to correctly describe topology of the conical intersections between the S_0 and S_1 states.[28, 29, 62-64] While LR-TDDFT fails to produce the conical intersections correctly,[27-29, 65] SF-TDDFT does this correctly.[28, 46, 65] However, $\langle \mathbf{S}^2 \rangle$ of S_0 and S_1 at the MECI geometry of SF-TDDFT are 0.31 and 0.36, respectively.[42]

The MECI geometries of MRSF- and MRSF(0)-TDDFT also can be obtained and the spin contamination is eliminated. Geometric RMSDs of MRSF- and MRSF(0)-, SF-TDDFT with respect to MRCISD are 0.077, 0.165 and 0.240 in unit of Å, respectively. The MECI geometries are aligned and presented in Fig. 9.

As clearly seen in the RMSDs as well as in Fig. 9, the geometric improvement between SF- and MRSF(0)-TDDFT is seen, which is purely from spin contamination. The geometry is further improved in MRSF-TDDFT with a posteriori coupling.

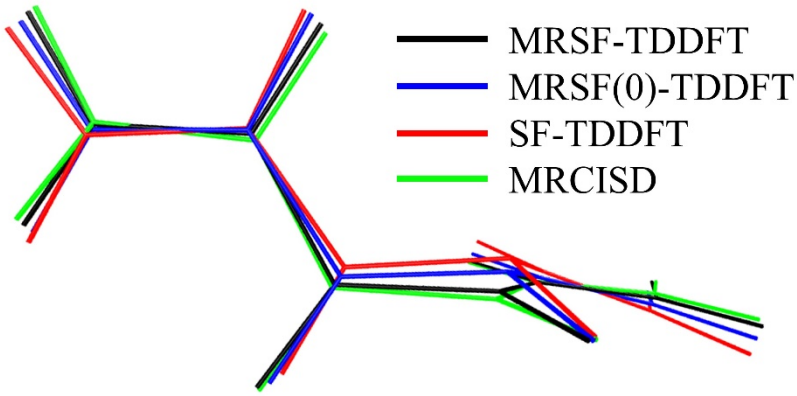

Figure 9. Aligned MECI geometry for the PSB3 molecule optimized by MRSF-, MRSF(0)-, SF-TDDFT, and MR-CISD. *The geometric RMSDs of MRSF- and MRSF(0)-, SF-TDDFT with respect to MRCISD are 0.077, 0.165 and 0.240 in Å, respectively.*

5.2 Topology of conical intersection for PSB3

In describing non-adiabatic process, the importance of the topology of the conical intersection has been emphasized from the early stage of study.[66-68] The conical intersection topology of PSB3 molecule has been studied by Gozem et al.[28] and Huix-Rotllant et al..[29] They reported that multi-reference methods (CASSCF and MRCISD) yield double cone topology (*i.e.*, conical intersection), while a linear S_1/S_0 crossing is obtained by the LR-TDDFT (*i.e.*, linear intersection). In addition, SF-TDDFT provided a correct topology even though there is a spin-contamination.

This topology was able to be measured by calculating difference of energies between S_1 and S_0 states in a circular loop around the conical intersection for each method. The double cone topology should provide non-zero energy difference anywhere in the loop, while the linear topology yield two zero points in the loop.

We performed the loop calculation with the MRSF-TDDFT shown in Fig. 10. MRSF-TDDFT predict the non-zero energy difference round the loop; hence, the correct double cone topology is reproduced by the method.

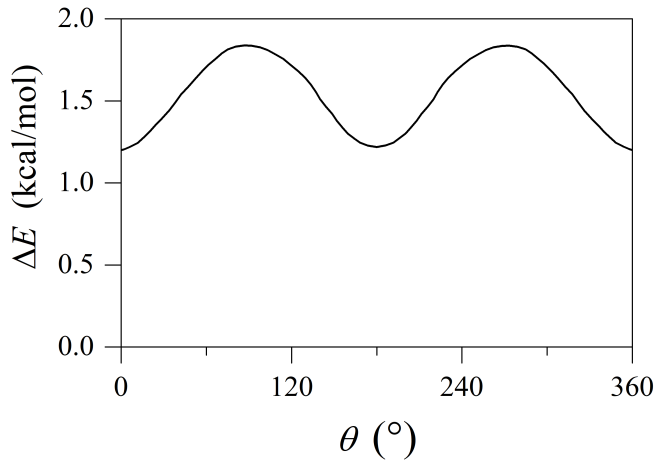

Figure 10. Energy difference between S_1 and S_0 states calculated a loop around the conical intersection of PSB3 molecule with MRSF-TDDFT.

6. Non-adiabatic coupling term

6.1 Numerical non-adiabatic coupling term

The Tully's fewest-switches trajectory-surface-hopping (TSH) method is one of the most popular semi-classical methods to study excited state dynamics with radiationless vibronic transition. In TSH method,[69] nuclear wave packets are described by ensembles of independent classical trajectories. Each trajectory is propagated on a single adiabatic PES, and it is allowed to hop to other adiabatic PESs at every time step according to hopping probabilities. The hopping probabilities between different electronic states depend on the nonadiabatic coupling term (NACT). The NACT can be obtained numerically by the finite difference approximation in terms of overlap integrals (OIs) between wave functions at different time steps as

$$\left\langle \Psi_I(t-\Delta/2)\middle|\frac{\partial}{\partial t}\middle|\Psi_J(t-\Delta/2)\right\rangle$$

$$\cong \frac{1}{2\Delta}\left(\left\langle \Psi_I(t-\Delta)\middle|\Psi'_J(t)\right\rangle - \left\langle \Psi_I(t)\middle|\Psi'_J(t-\Delta)\right\rangle\right). \qquad (142)$$

Here, the notation prime is introduced to emphasize that the state is in a different time-step t as opposed to $t-\Delta$. In this subsection, the time variable will be omitted with the notation prime.

The OIs between wave functions at different time steps are represented as a function of products OIs between MOs at different time steps.

$$\langle \Psi_I | \Psi'_J \rangle = f\left(\varepsilon_{i_1 i_2 \cdots i_M} \langle \phi_1 | \phi'_{i_1} \rangle \langle \phi_2 | \phi'_{i_2} \rangle \cdots \langle \phi_M | \phi'_{i_M} \rangle \right) \tag{143}$$

where $\varepsilon_{i_1 i_2 \cdots i_M}$ is the Levi-Civita symbol which is the sign of a permutation of the natural number.

6.2 Fast overlap evaluations with truncation

If one multiplies an unit parameter λ, *i.e.*, λ=1, to each OI between MOs, $\langle \phi_m | \phi'_{i_m} \rangle$, only when the index is different $m \neq i_m$, the OIs between the wave function can be represented as ascending order of the parameter λ as

$$\langle \Psi_I | \Psi'_J \rangle = \sum_{m=0}^{M} A_m \lambda^m. \tag{144}$$

Although the MOs at consecutive time steps are formally nonorthogonal, they become nearly orthogonal as time-step size Δ becomes zero. Thus, OIs between MOs, i.e., $\langle \phi_m | \phi'_{i_m} \rangle$ become nearly the Kronecker delta function δ_{m,i_m}. When using a time step smaller

than change of the wave function, especially in the non-adiabatic molecular dynamics simulation, one can truncate the series depending on an order of the parameter λ.[70]

The computing times for calculating an OI between wave functions are obtained with different the truncation order from 0 to 2 and without the truncation. Here, wave functions of SF-TDDFT are utilized and size of basis set M is varying. The ratio of the computing times with respect to the time with the zeroth order is shown in Fig. 11.

The truncation up to the second and the zeroth order gives four and five orders improvements of system size compared to the calculation without truncation, which is enormous time reduction for the OI calculation.

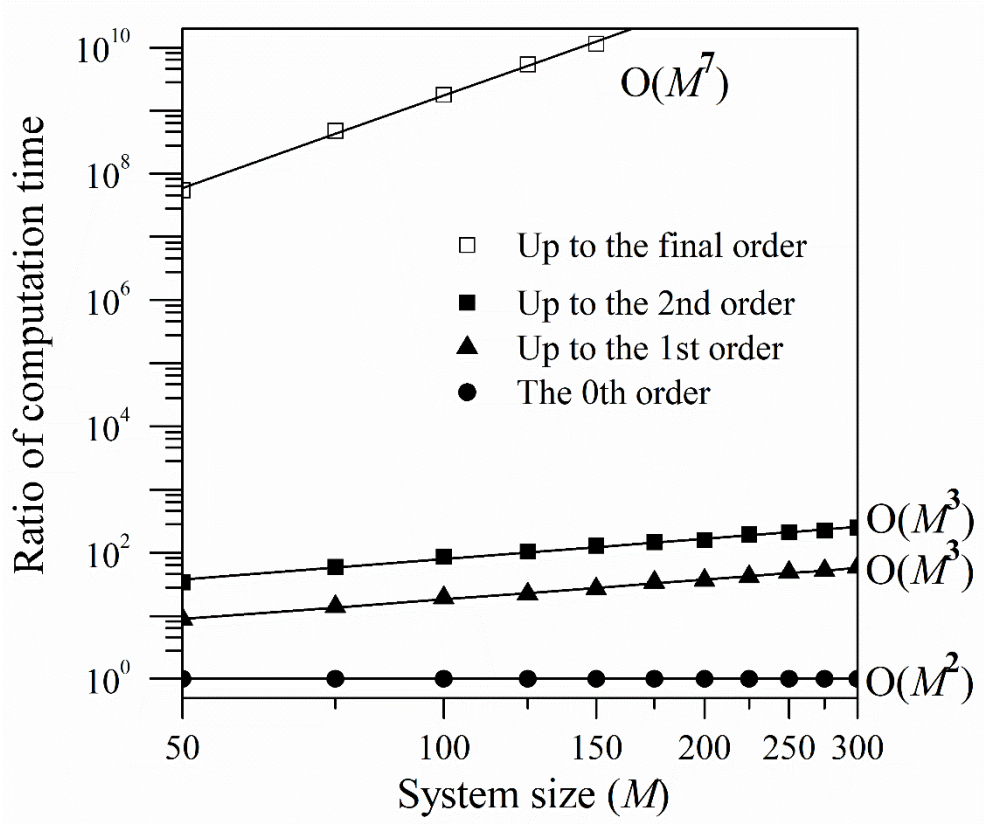

Figure 11. Ratios of computation times for evaluating OIs varying the truncation order with respect to the time with the lowest truncation order. *Both x- and y-axis are represented in log scale. From the slopes one can obtain the computational order of system size.*

6.3 Accuracy of truncation

In order to investigate accuracies of the truncated OI in actual calculations, the NACTs near three different conical interactions were studied. They are twisted-pyramidalized, H-migrated ethylene, and twisted-pyramidalized stilbene. The BHHLYP[56-58] functional in combination with 6-31G(d) basis set[59] was utilized. NACTs between S_1 and S_0 states for the three different conical intersections and for three different time-step sizes are tabulated in the third column of Tab. 6. NACTs errors with the truncation of OIs are tabulated in the fourth, the fifth, the sixth columns. Those are calculated with truncated OIs up to the 0th, 1st, 2nd order of the λ. All NACT values even with non-truncated OIs are subjected to the finite difference approximation, therefore any differences below 10^{-7} are meaningless. In the table, when the error magnitudes become smaller than 10^{-7}, we simply specify them as $< 10^{-7}$.

It can be expected that the NACT errors with truncated OIs up to the 0th, 1st, 2nd order of λ are nearly on the zeroth, the first, and the second order of the time-step size, respectively. This expectation is supported by results for which the error magnitudes with OIs up to the 2nd order is always under 10^{-7}, and those up to the 1st order yield

similar dependencies in the finite difference approximation. On the other hand, those up to the 0th order are one or two orders larger than others, and slightly larger than those of the finite difference approximation. Nevertheless, these are still highly accurate compared to the absolute NACT values. In general, it can be concluded that the truncated OIs up to the 1st and 2nd order do not introduce additional errors to the NACT. On the other hand, although the truncated OIs with only 0th order adds error higher by one order of magnitude, it is still capable of producing accurate values compared to the absolute NACT.

Molecule	Δ (fs)	NACT (a.u.)	NACT with truncation – NACT (a.u.)		
		w/o truncation	0th	1st	2nd
Twisted ethylene	0.1	0.2361078	2.8×10^{-6}	$< 10^{-7}$	$< 10^{-7}$
	0.2	0.1199419	2.5×10^{-6}	$< 10^{-7}$	$< 10^{-7}$
	0.5	0.0480514	4.5×10^{-6}	-6.0×10^{-7}	$< 10^{-7}$
H-migrated Ethylene	0.1	0.0885232	4.8×10^{-6}	$< 10^{-7}$	$< 10^{-7}$
	0.2	0.1156795	3.0×10^{-6}	$< 10^{-7}$	$< 10^{-7}$
	0.5	0.0472909	5.4×10^{-6}	$< 10^{-7}$	$< 10^{-7}$
Twisted stilbene	0.1	0.0105009	4.7×10^{-6}	-1.2×10^{-7}	$< 10^{-7}$
	0.2	0.0092561	5.2×10^{-6}	-1.1×10^{-7}	$< 10^{-7}$
	0.5	0.0085117	9.9×10^{-6}	-2.1×10^{-7}	$< 10^{-7}$

Table 6. Errors of nonadiabatic coupling term (NACT) with the truncated overlap integrals. *NACTs (a.u.) between S_1 and S_0 states for three different conical intersections and for three different time-step sizes (Δ) are in the third column. NACTs error (a.u.) with the truncation of OIs are in the fourth, the fifth, the sixth columns. Those are calculated with truncated OIs up to the 0th, 1st, 2nd order of the λ. In all calculations, the NACTs were calculated between the given geometries and propagated geometries by velocity-Verlet algorithm with its gradient of the first excited state. "$< 10^{-7}$" denotes that the magnitude of difference is lower than 1.0×10^{-7}.*

7. Non-adiabatic molecular dynamic

7.1 Photoisomerization and photocyclization of cis-stilbene

The photoisomerization mechanism has been examined considerable experimental and theoretical studies. As a prototypical model system, 1,2-diphenylethylene (stilbene) has been intensively studied. From early experimental research, the quantum yield for the photoreaction of the excitation on the S_1 state of *cis*-stilbene have been reported to be 10% for DHP, 35% for *trans*-stilbene and 55 % for *cis*-stilbene. Figure 12[71] illustrate a schematic diagram for the excited (S_1) *cis*-stilbene dynamics based on previous mechanism studies. The three branching points are well known represented by **A**, **B** and **C**, respectively in Fig. 12. The S_1 *cis*-stilbene branch into two channels at the **A** point, which are referred as *cis*-*trans* (photoisomerization) and *cis*-DHP (photocyclization) channels. As much as 70% of S_1 *cis*-stilbene head to *cis*-*trans* channel.[72, 73] At the **B** branching point, half of them yield S_0 *trans*-stilbene, and the other half convert to S_0 *cis*-stilbene.[74-77] Meanwhile, the remaining 30% of S_1 *cis*-stilbene head to the *cis*-DHP channel, and one-third yield S_0 DHP while the other two-thirds become S_0 *cis*-stilbene at the **C** point.[78]

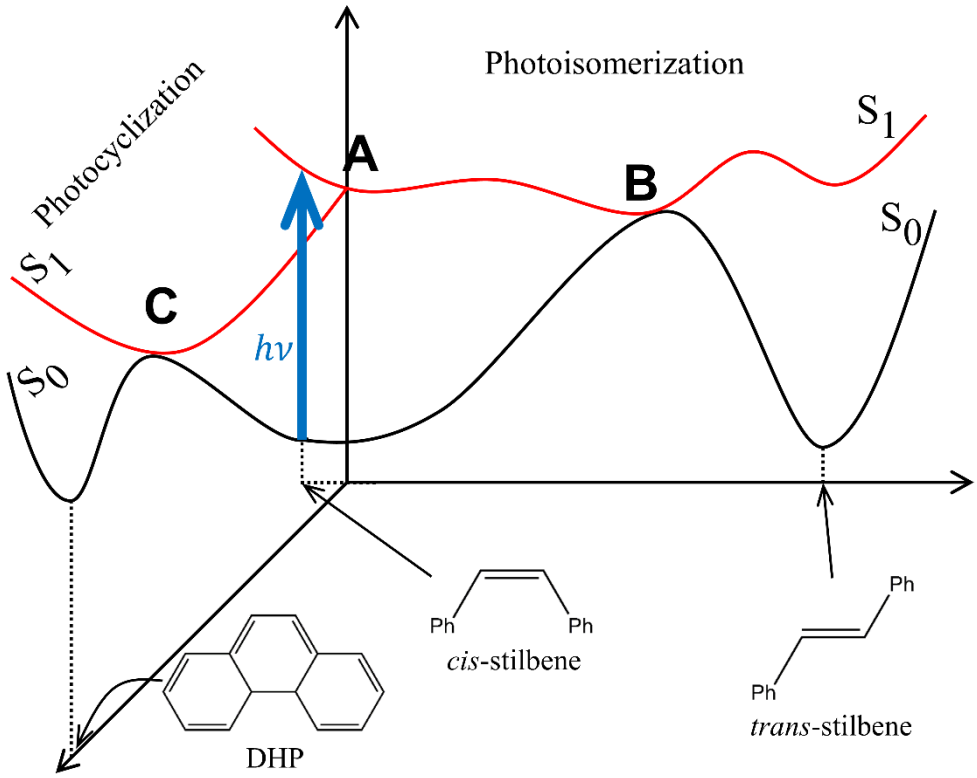

Figure 12. Schematic diagram of cis-stilbene photodynamics. *Three branching points A, B, and C are presented on the schematic potential energy diagram.*

7.2 Branching ratio and Quantum yield

Nonadiabatic molecular dynamics simulations for the ππ* excited *cis*-stilbene have been performed for 2 ps using SF- or MRSF(0)-TDDFT [50] with the TSH method.[69] Two sets of 50 trajectories are simulated for the methods with initial geometries randomly chosen from a 30 ps ground-state simulation of *cis*-stilbene. Full vibrational degrees of freedom have been explored with 0.5 fs time step divided into sub-time steps of 5.0×10^{-5} fs. The BHHLYP hybrid functional[56-58] with 6-31G(d) basis set[59] has been utilized for all calculations. The nonadiabatic coupling terms (NACT) are numerically calculated with finite difference method and with truncated overlap integrals[70] as described in previous subsection 5 of *Non-adiabatic coupling term*.

First, we could obtain branching ratios at three branching points **A**, **B** and **C** and quantum yield for both sets of calculations, and these are tabulated in Tabs. 7 and 8. Error bars for all values denote the 90% confidence interval obtained by the bootstrapping.

Branching ratios of the MRSF-TDDFT at branching points **B** and **C** are well agree with those of experimental results except for slight

discrepancy at a branching point **A** as 70/30 for experiment and 60(±9)/40(±9) for MRSF-TDDFT. On the other hand, the branching ratios at **A** and **C** for SF-TDDFT are well agree, while the branching ratios at **B** have quite large discrepancy as 50/50 for experiment and 74(±10)/26(±10) for SF-TDDFT.

For the final quantum yields of *cis*-, *trans*-stilbene and DHP in Tab. 8, all values with MRSF-TDDFT are well agree with those of experiments as 56(±9)/32(±8)/12(±6) for MRSF-TDDFT and 55/35/10 for experiments. On the other hand, SF-TDDFT underestimates quantum yield of *cis*-stilbene and overestimates that of *trans*-stilbene as 36(±9)/50(±9) for SF-TDDFT and 55/35 for experiments. In NAMD with LR-TDDFT,[79] it cannot yield DHP product at all, and that of *cis*-stilbene is overestimated as 66(±3) for LR-TDDFT and 55 for an experiment.

	A		B		C	
	cis-*trans*	*cis*-DHP	*trans*	*cis*	DHP	*Cis*
MRSF-TDDFT	60(±9)	40(±9)	53(±12)	47(±12)	25(±12)	75(±12)
SF-TDDFT	68(±9)	32(±9)	74(±10)	26(±10)	44(±16)	56(±16)
Experiment	70	30	50	50	33	67

Table 7. Branching ratio (%) at three branching points during non-adiabatic molecular dynamics of *cis*-stilbene. *Values in parentheses denote the 90% confidence interval obtained by the bootstrapping*

	cis	*trans*	DHP
MRSF-TDDFT	56 (± 9)	32 (± 8)	12 (± 6)
SF-TDDFT	36 (± 9)	50 (± 9)	14 (± 6)
LR-TDDFT	66 (± 3)	34 (± 3)	0
Experiment	55	35	10

Table 8. Quantum yields (%) of $\pi\pi^*$ excited *cis*-stilbene. *Values in parentheses denote the 90% confidence interval obtained by the bootstrapping*

7.3 Dynamics in the branching point

Further understanding about the branching ratio is investigated with two dimensional histogram shown in Fig. 13. The *x*-axis is a bond length (R) between two carbons in which a new single bond is formed in DHP product, and the *y*-axis is a dihedral angle ($D_{C=C}$) between two bonds which connect the centered double bond and two phenyl rings. The histograms for all 50 trajectories in the excited states are presented in a and b for MRSF- and SF-TDDFT, respectively. The histograms for 30 and 34 trajectories headed to the *cis-trans* channel in the ground state is presented in c and d for MRSF- and SF-TDDFT with points where hopping from S_1 to S_0 occur. Likewise, the ground state histograms for 20 and 16 trajectories headed to *cis*-DHP channel are shown in e and f for MRSF- and SF-TDDFT, respectively with the hopping points.

A clear discrepancy between S_1 state histograms for MRSF- and SF-TDDFT is seen. The **A** branching point is highly populated, while both **A** and **B** points are highly populated in SF-TDDFT. It represent trajectories hopping from S_1 to S_0 quite fast not to reside around **B** points for MRSF-TDDFT. Since a difference between MRSF(0)- and SF-TDDFT is the absence or presence of spin contamination, it is

expected that the difference come from spin contamination problem of SF-TDDFT. Figure 14 shows averaged $\langle S^2 \rangle$ value of SF-TDDFT in the excited state. Overall region for **A** and **B** points has 0.2 ~ 0.4 of $\langle S^2 \rangle$ value, which is not negligible spin contamination.

Around branching point **B** (*cis*-*trans*), surface hoppings appear in broad region of the histogram. It is seen that trajectories hopping with relatively small R and $D_{C=C}$ become *cis*-stilbene, while these become *trans*-stilbene in the other case. In MRSF-TDDFT, more trajectories are hopping with relatively small R and $D_{C=C}$ compared to those of SF-TDDFT. It lead to good agreement of branching ratio of MRSF-TDDFT, while overestimate *trans*-stilbene branching ratio of SF-TDDFT as 74(±10) for SF-TDDFT and 50 for experiment.

Branching ratios at branching point **C** (*cis*-DHP) for both MRSF- and SF-TDDFT are agree with experiment results shown in Tab. 7. However, a difference between distributions of hopping points for two methods are seen. Surface hoppings appear in narrow region of the histogram for MRSF-TDDFT, while these are relatively scattered for SF-TDDFT. In SF-TDDFT, there are a few hoppings with R less than 1.7 angstrom, which lead to DHP product. In Fig. 14, there is severe spin contamination where $\langle S^2 \rangle > 0.4$. Although the branching ratio of

SF-TDDFT is agree with experiment result, these are seemed to be problematic hoppings.

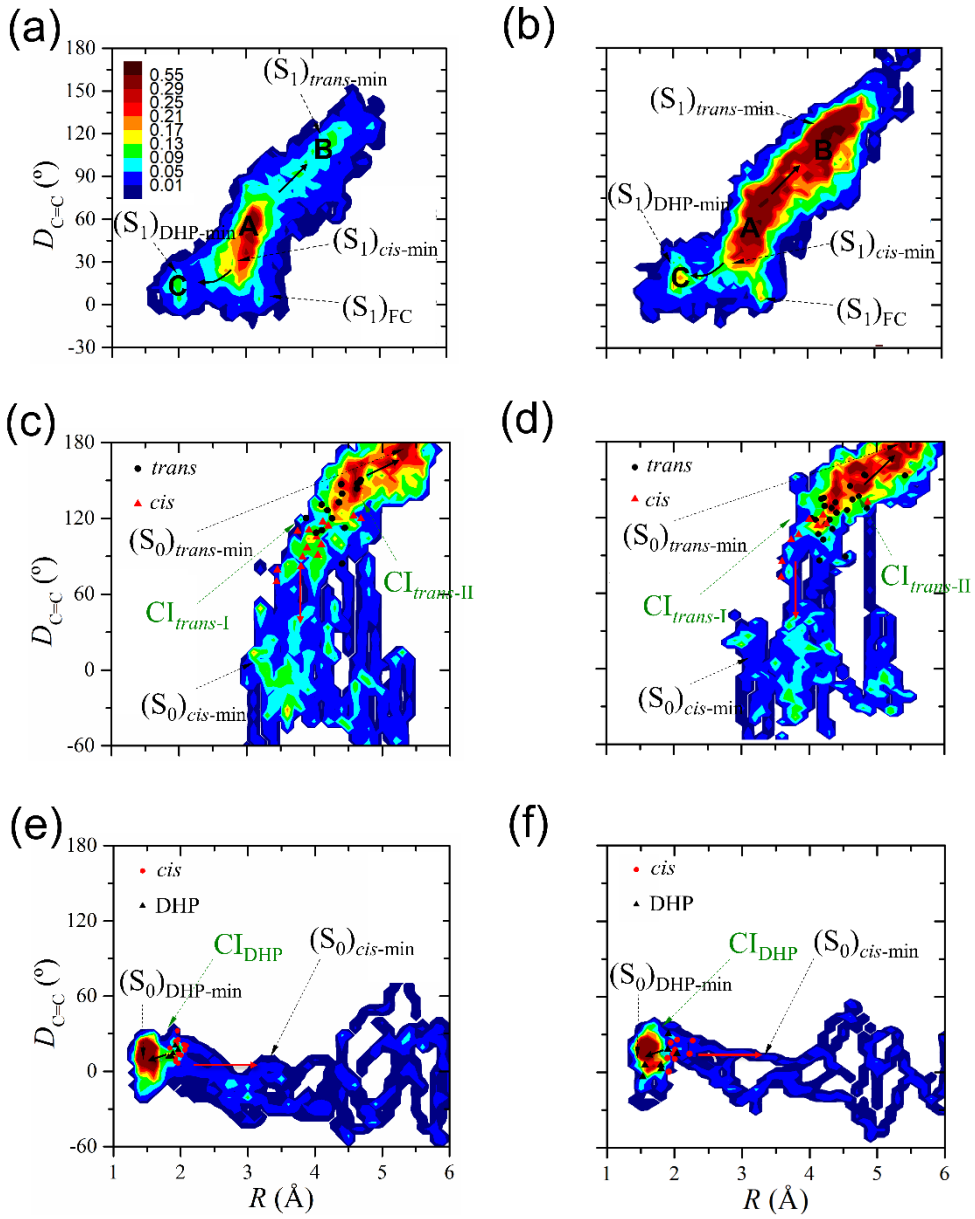

Figure 13. Two-dimensional histogram of *cis*-stilbene NAMD dynamics simulation. *The histograms for 50 trajectories in excited states are presented in a and b, The geometric RMSDs of MRSF- and MRSF(0)-, SF-TDDFT with respect to MRCISD are 0.077, 0.165 and 0.240 in Å, respectively.*

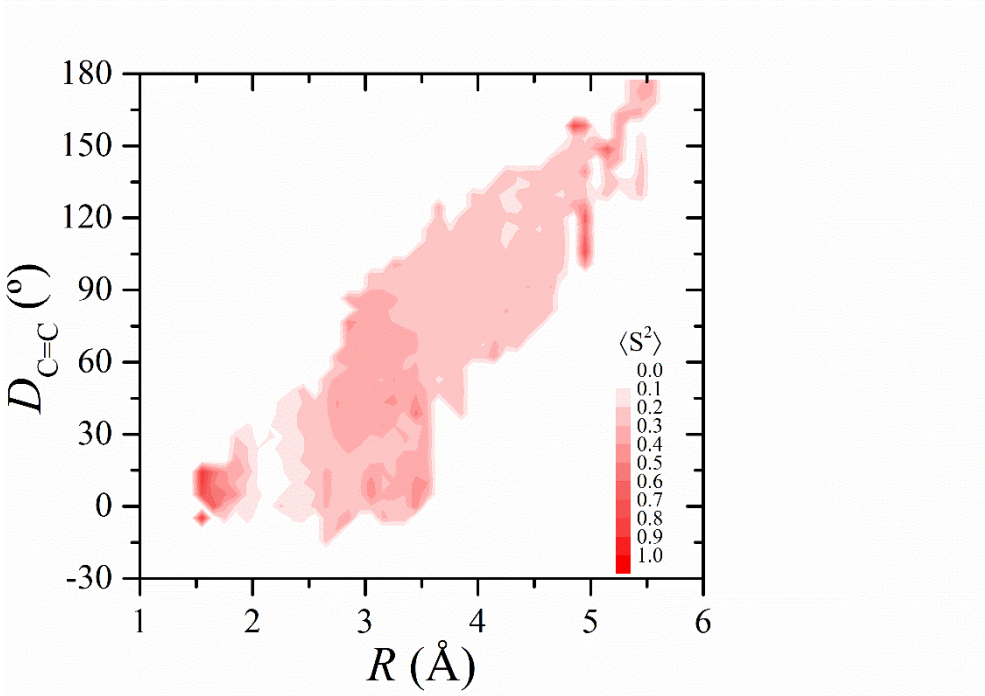

Figure 14. Averaged <S^2> value of SF-TDDFT for 50 trajectories in excited states.

CONCLUSION

A new method in the context of collinear spin-flip linear response TDDFT is proposed, which employs an equiensemble of the $M_S = +1$ and $M_S = -1$ components of the triplet state as a (mixed) reference state. The TD-KS equation with the mixed state can be solved within linear response formalism by the use of spinor-like open-shell orbitals. It is a novel attempt to add configurations within the realm of TDDFT.

The resulting MRSF-TDDFT has several advantages over the conventional collinear SF-TDDFT. MRSF-TDDFT gives more accurate results than SF-TDDFT by eliminating the spin contamination of the response states of SF-TDDFT. The accuracy of MRSF-TDDFT has been tested and verified in various calculations. The spin contaminated P state of Be atom for SF-TDDFT properly splits into singlet (^{1}P) and triplet states (^{3}P). A posteriori coupling is shown to be improve degeneracy of the P states. In the vertical excitation energy calculations to Franck-Condon states for organic molecules, results of MRSF-TDDFT give slightly better than those of SF-TDDFT compared to reference results of the theoretical best estimate (TBE-2). For the structures and adiabatic excitation energies obtained from geometry optimization of organic molecules, MRSF(0)-TDDFT results are closer

than SF-TDDFT results compared to the EOM-CCSD results. It is shown that MRSF-TDDFT results (with a posteriori coupling) further improve the results. Comparing MRCISD calculation, MRSF(0)-TDDFT is also superior than SF-TDDFT in calculations for the minimum energy conical intersection of PSB3 molecule, which is the important model system in vision. Likewise, a posteriori coupling improves the result. Apart from the accuracy of MRSF-TDDFT, we propose a truncation method to calculate non-adiabatic coupling which drastically reduce computation time while maintaining greatly high accuracy. Using this non-adiabatic coupling term, non-adiabatic molecular dynamics of *cis*-stilbene molecules were able to be performed by SF- and MRSF(0)-TDDFT. Both methods are superior than LR-TDDFT since the methods produced a DHP product which LR-TDDFT could not produce. The SF-TDDFT yield a non-negligible amount of spin-contamination throughout the dynamics simulations and the MRSF(0)-TDDFT could completely eliminate the spin contamination. Branching ratio and quantum yield of MRSF(0)-TDDFT is more closer to the experimental value than those of SF-TDDFT. Not only for the accuracy but clear separation of singlet and triplet response states considerably simplify the means by which excited states are identified, especially in ``black-box''-type applications, such as automatic geometry optimization, reaction path following, and

molecular dynamics simulations.

From these reasons it is highly expected that MRSF-TDDFT yield improved results than SF-TDDFT by eliminating spin contamination problem in general cases. Therefore, we can conclude that MRSF-TDDFT has advantages over SF-TDDFT in terms of both practicality and accuracy.

REFERENCES

1. G. J. Hedley, A. Ruseckas, and I. D. W. Samuel, *Light harvesting for organic photovoltaics.* 2016. **117**, pp. 796-837.
2. A. Japahuge and T. Zeng, *Theoretical studies of singlet fission: searching for materials and exploring mechanisms.* 2018. **83**, pp. 146-182.
3. D. Roke, S. J. Wezenberg, and B. L. Feringa, *Molecular rotary motors: Unidirectional motion around double bonds.* 2018. **115**, pp. 9423-9431.
4. M. E. Casida, C. Jamorski, F. Bohr, J. G. Guan, and D. R. Salahub, *Nonlinear Optical Materials: Theory and Modeling*. 1996, pp. 145-163, American Chemical Society, Division of Computers in Chemistry.
5. M. E. Casida, *Recent advances in density functional methods*. Vol. 1. 1995: World Scientific, pp. 155-192.
6. M. E. Casida and M. Huix-Rotllant, *Progress in time-dependent density-functional theory.* 2012. **63**, pp. 287-323.
7. E. Runge and E. K. U. Gross, *Density-functional theory for time-dependent systems.* 1984. **52**, p. 997.
8. K. Burke, J. Werschnik, and E. K. U. Gross, *Time-dependent density functional theory: Past, present, and future.* 2005. **123**,

p. 062206.

9. M. A. L. Marques, N. T. Maitra, F. M. S. Nogueira, E. K. U. Gross, and A. Rubio, *Fundamentals of time-dependent density functional theory*. Vol. 837. 2012: Springer Science & Business Media.

10. N. T. Maitra, *Perspective: Fundamental aspects of time-dependent density functional theory.* 2016. **144**, p. 220901.

11. P. Hohenberg and W. Kohn, *Inhomogeneous electron gas.* 1964. **136**, p. B864.

12. W. Kohn and L. J. Sham, *Self-consistent equations including exchange and correlation effects.* 1965. **140**, p. A1133.

13. R. McWeeny, *Methods of molecular quantum mechanics*. 1992: Academic press, pp. 438-442.

14. F. Zahariev and M. S. Gordon, *Nonlinear response time-dependent density functional theory combined with the effective fragment potential method.* 2014. **140**, p. 18A523.

15. A. Dreuw, J. L. Weisman, and M. Head-Gordon, *Long-range charge-transfer excited states in time-dependent density functional theory require non-local exchange.* 2003. **119**, pp. 2943-2946.

16. A. Dreuw and M. Head-Gordon, *Single-reference ab initio*

methods for the calculation of excited states of large molecules. 2005. **105**, pp. 4009-4037.

17. P. Dev, S. Agrawal, and N. J. English, *Determining the appropriate exchange-correlation functional for time-dependent density functional theory studies of charge-transfer excitations in organic dyes.* 2012. **136**, p. 224301.

18. N. T. Maitra, *Undoing static correlation: Long-range charge transfer in time-dependent density-functional theory.* 2005. **122**, p. 234104.

19. E. J. Baerends, O. V. Gritsenko, and R. van Meer, *The Kohn-Sham gap, the fundamental gap and the optical gap: the physical meaning of occupied and virtual Kohn-Sham orbital energies.* 2013. **15**, pp. 16408-16425.

20. R. J. Cave, F. Zhang, N. T. Maitra, and K. Burke, *A dressed TDDFT treatment of the 21Ag states of butadiene and hexatriene.* 2004. **389**, pp. 39-42.

21. Neugebauer, E. J. Baerends, and M. Nooijen, *Vibronic coupling and double excitations in linear response time-dependent density functional calculations: Dipole-allowed states of N 2.* 2004. **121**, pp. 6155-6166.

22. N. T. Maitra, F. Zhang, R. J. Cave, and K. Burke, *Double excitations within time-dependent density functional theory*

linear response. 2004. **120**, pp. 5932-5937.

23. M. E. Casida and M. Huix-Rotllant, *Density-functional methods for excited states*. Topics in Current Chemistry, ed. N. Ferré, M. Filatov, and M. Huix-Rotllant. Vol. 368. 2016, Heidelberg: Springer.

24. F. Aryasetiawan, O. Gunnarsson, and A. Rubio, *Excitation energies from time-dependent density-functional formalism for small systems.* 2002. **57**, p. 683.

25. M. Filatov, *Density-functional methods for excited states*. Topics in Current Chemistry, ed. N. Ferré, M. Filatov, and M. Huix-Rotllant. Vol. 368. 2016, Heidelberg: Springer, pp. 97-124

26. B. G. Levine, C. Ko, J. Quenneville, and T. J. Martínez, *Conical intersections and double excitations in time-dependent density functional theory.* 2006. **104**, pp. 1039-1051.

27. M. Huix-Rotllant, M. Filatov, S. Gozem, I. Schapiro, M. Olivucci, and N. Ferré, *Assessment of density functional theory for describing the correlation effects on the ground and excited state potential energy surfaces of a retinal chromophore model.* 2013. **9**, pp. 3917-3932.

28. S. Gozem, F. Melaccio, A. Valentini, M. Filatov, M. Huix-Rotllant, N. Ferré, L. M. Frutos, C. Angeli, A. I. Krylov, A. A. Granovsky,

R. Lindh, and M. Olivucci, *Shape of multireference, equation-of-motion coupled-cluster, and density functional theory potential energy surfaces at a conical intersection.* 2014. **10**, pp. 3074-3084.

29. M. Huix-Rotllant, A. Nikiforov, W. Thiel, and M. Filatov, *Density-functional methods for excited states*. Topics in Current Chemistry, ed. N. Ferré, M. Filatov, and M. Huix-Rotllant. Vol. 368. 2016, Heidelberg: Springer, pp. 445-476.

30. A. I. Krylov, *Size-consistent wave functions for bond-breaking: the equation-of-motion spin-flip model.* 2001. **338**, pp. 375-384.

31. Y. Shao, M. Head-Gordon, and A. I. Krylov, *The spin-flip approach within time-dependent density functional theory: Theory and applications to diradicals.* 2003. **118**, pp. 4807-4818.

32. Z. Li and W. Liu, *Theoretical and numerical assessments of spin-flip time-dependent density functional theory.* 2012. **136**, p. 024107.

33. J. S. Sears, C. D. Sherrill, and A. I. Krylov, *A spin-complete version of the spin-flip approach to bond breaking: What is the impact of obtaining spin eigenfunctions?* 2003. **118**, pp. 9084-

9094.

34. D. Casanova and M. Head-Gordon, *The spin-flip extended single excitation configuration interaction method.* 2008. **129**, p. 064104.

35. T. Tsuchimochi, *Spin-flip configuration interaction singles with exact spin-projection: Theory and applications to strongly correlated systems.* 2015. **143**, p. 144114.

36. X. Zhang and J. M. Herbert, *Spin-flip, tensor equation-of-motion configuration interaction with a density-functional correction: A spin-complete method for exploring excited-state potential energy surfaces.* 2015. **143**, p. 234107.

37. J. Mato and M. S. Gordon, *A general spin-complete spin-flip configuration interaction method.* 2018. **20**, pp. 2615-2626.

38. M. E. Casida, *Propagator corrections to adiabatic time-dependent density-functional theory linear response theory.* 2005. **122**, p. 054111.

39. W. Liu and Y. Xiao, *Relativistic time-dependent density functional theories.* 2018. **47**, pp. 4481-4509.

40. Z. Li and W. Liu, *Spin-adapted open-shell random phase approximation and time-dependent density functional theory. I. Theory.* 2010. **133**, p. 064106.

41. Z. Li, W. Liu, Y. Zhang, and B. Suo, *Spin-adapted open-shell*

time-dependent density functional theory. II. Theory and pilot application. 2011. **134**, p. 134101.

42. S. Lee, M. Filatov, S. Lee, and C. H. Choi, *Eliminating spin-contamination of spin-flip time dependent density functional theory within linear response formalism by the use of zeroth-order mixed-reference (MR) reduced density matrix.* 2018. **149**, p. 104101.

43. A. K. Kerman and S. E. Koonin, *Hamiltonian formulation of time-dependent variational principles for the many-body system.* 1976. **100**, pp. 332-358.

44. I. E. Tamm, *Relativistic interaction of elementary particles.* 1945. **9**, p. 449.

45. S. M. Dancoff, *Non-adiabatic meson theory of nuclear forces.* 1950. **78**, p. 382.

46. N. Minezawa and M. S. Gordon, *Optimizing Conical Intersections by Spin- Flip Density Functional Theory: Application to Ethylene.* 2009. **113**, pp. 12749-12753.

47. M. Filatov, *Spin-restricted ensemble-referenced Kohn-Sham method: basic principles and application to strongly correlated ground and excited states of molecules.* 2015. **5**, pp. 146-167.

48. M. Filatov, T. J. Martínez, and K. S. Kim, *Description of ground and excited electronic states by ensemble density functional*

method with extended active space. 2017. **147**, p. 064104.

49. F. Furche and R. Ahlrichs, *Adiabatic time-dependent density functional methods for excited state properties.* 2002. **117**, pp. 7433-7447.

50. S. Lee, E. E. Kim, H. Nakata, S. Lee, and C. H. Choi, *Efficient implementations of analytic energy gradient for mixed-reference spin-flip time-dependent density functional theory (MRSF-TDDFT).* **150**, p. 184111.

51. M. F. Guest and V. R. Saunders, *On methods for converging open-shell Hartree-Fock wave-functions.* 1974. **28**, pp. 819-828.

52. M. W. Schmidt, K. K. Baldridge, J. A. Boatz, S. T. Elbert, M. S. Gordon, J. H. Jensen, S. Koseki, N. Matsunaga, K. A. Nguyen, S. Su, T. L. Windus, M. Dupuis, and J. A. Montgomery, *General atomic and molecular electronic structure system.* 1993. **14**, pp. 1347-1363.

53. M. R. Silva-Junior, M. Schreiber, S. P. A. Sauer, and W. Thiel, *Benchmarks for electronically excited states: Time-dependent density functional theory and density functional theory based multireference configuration interaction.* 2008. **129**, p. 104103.

54. T. H. Dunning Jr., *Gaussian basis sets for use in correlated*

molecular calculations. I. The atoms boron through neon and hydrogen. 1989. **90**, pp. 1007-1023.

55. M. Schreiber, M. R. Silva-Junior, S. P. A. Sauer, and W. Thiel, *Benchmarks for electronically excited states: CASPT2, CC2, CCSD, and CC3.* 2008. **128**, p. 134110.

56. A. D. Becke, *Density-functional exchange-energy approximation with correct asymptotic behavior.* 1988. **38**, p. 3098.

57. C. Lee, W. Yang, and R. G. Parr, *Development of the Colle-Salvetti correlation-energy formula into a functional of the electron density.* 1988. **37**, p. 785.

58. A. D. Becke, *Density-functional thermochemistry. III. The role of exact exchange.* 1993. **98**, pp. 5648-5652.

59. R. Krishnan, J. S. Binkley, R. Seeger, and J. A. Pople, *Self-consistent molecular orbital methods. XX. A basis set for correlated wave functions.* 1980. **72**, pp. 650-654.

60. H. J. Monkhorst, *Calculation of properties with the coupled-cluster method.* 1977. **12**, pp. 421-432.

61. H. Koch, H. J. A. Jensen, P. Jorgensen, and T. Helgaker, *Excitation energies from the coupled cluster singles and doubles linear response function (CCSDLR). Applications to Be, CH+, CO, and H2O.* 1990. **93**, pp. 3345-3350.

62. S. Gozem, M. Huntress, I. Schapiro, R. Lindh, A. A. Granovsky, C. Angeli, and M. Olivucci, *Dynamic electron correlation effects on the ground state potential energy surface of a retinal chromophore model.* 2012. **8**, pp. 4069-4080.

63. S. Gozem, F. Melaccio, R. Lindh, A. I. Krylov, A. A. Granovsky, C. Angeli, and M. Olivucci, *Mapping the excited state potential energy surface of a retinal chromophore model with multireference and equation-of-motion coupled-cluster methods.* 2013. **9**, pp. 4495-4506.

64. A. Zen, E. Coccia, S. Gozem, M. Olivucci, and L. Guidoni, *Quantum monte carlo treatment of the charge transfer and diradical electronic character in a retinal chromophore minimal model.* 2015. **11**, pp. 992-1005.

65. A. Nikiforov, J. A. Gamez, W. Thiel, M. Huix-Rotllant, and M. Filatov, *Assessment of approximate computational methods for conical intersections and branching plane vectors in organic molecules.* 2014. **141**, p. 124122.

66. C. Zener, Containing Papers of a Mathematical and P. Character, *Non-adiabatic crossing of energy levels.* 1932. **137**, pp. 696-702.

67. D. R. Yarkony, *Diabolical conical intersections.* 1996. **68**, p. 985.

68. S. Klein, M. J. Bearpark, B. R. Smith, M. A. Robb, M. Olivucci, and F. Bernardi, *Mixed stateon the fly'non-adiabatic dynamics: the role of the conical intersection topology.* 1998. **292**, pp. 259-266.

69. J. C. Tully, *Molecular dynamics with electronic transitions.* 1990. **93**, pp. 1061-1071.

70. S. Lee, E. Kim, S. Lee, and C. H. Choi, *Fast Overlap Evaluations for Nonadiabatic Molecular Dynamics Simulations: Applications to SF-TDDFT and TDDFT.* 2019. **15**, pp. 882-891.

71. J. H. Frederick, Y. Fujiwara, J. H. Penn, K. Yoshihara, and H. Petek, *Models for stilbene photoisomerization: experimental and theoretical studies of the excited-state dynamics of 1, 2-diphenylcycloalkenes.* 1991. **95**, pp. 2845-2858.

72. J. Saltiel, *Perdeuteriostilbene. The role of phantom states in the cis-trans photoisomerization of stilbenes.* 1967. **89**, pp. 1036-1037.

73. F. E. Doany, R. M. Hochstrasser, B. I. Greene, and R. R. Millard, *Femtosecond-resolved ground-state recovery of cis-stilbene in solution.* 1985. **118**, pp. 1-5.

74. S. Malkin and E. Fischer, *Temperature Dependence of Photoisomerization. III. 1 Direct and Sensitized Photoisomerization of Stilbenes.* 1964. **68**, pp. 1153-1163.

75. D. Gegiou, K. A. Muszkat, and E. Fischer, *Temperature dependence of photoisomerization. V. Effect of substituents on the photoisomerization of stilbenes and azobenzenes.* 1968. **90**, pp. 3907-3918.

76. S. Sharafy and K. A. Muszkat, *Viscosity dependence of fluorescence quantum yields.* 1971. **93**, pp. 4119-4125.

77. J. Saltiel, AI Marinari, D. W. L. Chang, J. C. Mitchener, and E. D. Megarity, *Trans-cis photoisomerization of the stilbenes and a reexamination of the positional dependence of the heavy-atom effect.* 1979. **101**, pp. 2982-2996.

78. H. Petek, K. Yoshihara, Y. Fujiwara, Z. Lin, J. H. Penn, and J. H. Frederick, *Is the nonradiative decay of S1 cis-stilbene due to the dihydrophenanthrene isomerization channel? Suggestive evidence from photophysical measurements on 1, 2-diphenylcycloalkenes.* 1990. **94**, pp. 7539-7543.

79. A. J. Neukirch, L. C. Shamberger, E. Abad, B. J. Haycock, H. Wang, J. Ortega, O. V. Prezhdo, and J. P. Lewis, *Nonadiabatic ensemble simulations of cis-stilbene and cis-azobenzene photoisomerization.* 2013. **10**, pp. 14-23.

ABSTRACT IN KOREAN (국문초록)

혼합참조 스핀젖힘 시간의존 밀도범함수 이론(MRSF-TDDFT)이 제안됐다. 이 새로운 양자화학 계산 방법은 잘 알려진 시간의존 Kohn-Sham 방정식의 선형응답 이론에 혼합참조라는 새로운 개념을 도입해 유도된다. 혼합참조는 삼중항의 두 구성요소(M_S=+1, -1)를 결합한 참조상태로, 혼합참조로부터 나오는 선형응답은 기존 SF-TDDFT 방법이 만들지 못해 문제가 됐던 전자구성을 TDDFT 이론 내에서 생성한다. MRSF-TDDFT의 핵 좌표에 대한 응답상태의 에너지 기울기 수식이 유도됐고, 프로그램화 됐다. 새로운 방법의 에너지 그리고 에너지 기울기에 대한 계산 요구량은 기존 SF-TDDFT 의 요구량과 거의 동일하다. 새롭게 제안 된 MRSF-TDDFT 방법은 기존 SF-TDDFT에 비해 실용성과 정확성 측면에서 장점이 있다. 응답상태들을 단일항 또는 삼중항 상태로 완전히 분리해냄으로써, 기존 SF-TDDFT의 응답상태들의 스핀오염문제를 제거한다. 따라서, 특정 응답상태에 대한 자동 구조 최적화, 반응 경로 추적 또는 분자 동력학 시뮬레이션과 같은 "블랙 박스(black-box)" 유형의 응용에서 필수적인 응답 상태의 식별을 상당히 단순화한다. 또한, MRSF-TDDFT의 정확성은 수직 여기 에너지, 단열 여기 에너지, 구조최적화된 구조, 최소 에너지 원뿔 교차점, 비단열 상호작용 항 및 비단열 분자 동력학 시뮬레이션과 같은 다양한 방법으로 시험되고 검증되었다. 따라서, MRSF-TDDFT 방법은 광화학 반응 연구에 유망한 양자화학 계산방법으로 기대된다.